On the influence of storm parameters on extreme surge events at the Dutch coast

MSc thesis
in Civil Engineering and Management

Niels-Jasper van den Berg

On the influence of storm parameters on extreme surge events at the Dutch coast

MSc thesis
in Civil Engineering and Management
Faculty of Engineering Technology
University of Twente

Student:	Niels-Jasper van den Berg BSc.
Location and date:	Nijmegen, August 19, 2013
Thesis defense date:	August 27, 2013
Graduation supervisor:	Prof.dr. S.J.M.H. Hulscher
Daily supervisor:	Dr.ir. P.C. Roos
External supervisors:	Dr.ir. M. van Ledden (Royal HaskoningDHV)
	Ir. W. de Jong (Royal HaskoningDHV)

UNIVERSITY OF TWENTE.

Royal HaskoningDHV
Enhancing Society Together

Abstract

A storm surge is the rise in water level due to a storm. Storm surges are a threat for low-lying areas near coasts. In the Netherlands, storm surges are input for design conditions of coastal protection. The allowed change of failure per year is incorporated into Dutch law. For the densely-populated Randstad region, represented by a measurement station by Hoek van Holland, this chance is $1 \cdot 10^{-4}$ year^{-1}. Associated water levels are determined by extrapolation of measurements because data for extreme conditions are not available. This method entails large uncertainties.

A result of the currently used approach is lack of insight into the coupling between the storm and the storm surge. In addition, little is known about the duration and course of extreme surges. These data are important for dune and dike design. The time that the water level remains at about the maximum surge level is the most determinative factor for the amount of dune erosion in the entire development of the water level during the storm surge. A quick decline of the water level can result in dike failure, for example by piping, failure of revetments on the top layer due to overpressure and sliding of the outer slope.

This thesis focuses on the properties of storms causing extreme surges at Hoek van Holland, by modeling surges with an idealized coupled meteorological-hydrodynamical model. Six storm characteristics (storm parameters) are used as model input. The meteorological part of the model is an analytical parametrical model, based on the Holland model. The hydrodynamical model is forced by the meteorological model and numerically solves the non-linear depth-averaged shallow water equations in a one-dimensional domain. The model domain is a one-dimensional transect from the edge of the continental shelf between Scotland and Norway to Hoek van Holland. Output is given in water levels at Hoek van Holland.

The meteorological model is validated with rather good results, but some outliers are indicated. The coupled model is calibrated using data of 21

historical storms. Results of the calibrated model are good when focusing on peak surge levels. The surge duration however is underestimated but the model. Probability distributions for the six storm parameters, based on an earlier analysis of historical data, are used as input for Monte Carlo analysis. Return periods for each modeled surge are determined using the methodology of Gringorten.

The computed surge level (including tide) with a statistical return period of 10,000 years is 6 m, compared to 5.10 m according to the hydraulic boundary conditions determined by the Dutch government. For low return periods, calculated surges exceed observed surges. The average duration of computed surges with a return period of 10,000 year is more or less two hours larger than the design conditions accepted under Dutch law. The storms causing extreme surges differ from average storms in a high radius to maximum winds and large atmospheric pressure gradients, represented by a pressure shape factor. To a lesser extent, these storms have lower central pressures and move more slowly than average storms.

The present study reveals possible errors in the analysis of historical data mentioned before. Further research should therefore focus on improvement of these data. The determination of probability distributions is also open for discussion. The currently used one-dimensional model could be extended to two or three dimensions to improve results.

Preface

This report represents my Master's thesis and it marks the end of my study in Civil Engineering and Management at the University of Twente. Research has been carried out at Royal HaskoningDHV. The objective of this research is gaining insight in the relation between atmospheric processes (forcing) and storm surges (response) on the North Sea, by setting up and using an idealized model.

The past six months I lived like a nomad for science and the safety of the Dutch people, by dealing with a new methodology to predict extreme water levels at our coasts. I lived in Peize, Utrecht, Nijmegen, Huissen and finally Utrecht again; and worked in Rotterdam, Amersfoort and Nijmegen. I enjoyed studying a subject which brought together two topics which interest me for a long time: meteorology and hydrodynamics. It was a great time!

I would like to thank Mathijs for his enthusiasm for both MATLAB and the developed model, and Wiebe for his helicopter view on the topics I was dealing with. I wish to extend my gratitude to all the people from Royal HaskoningDHV I was working with and with whom I discussed my progress. Suzanne and Pieter, your remote assistance and focus on the scientific quality of this thesis is really appreciated. Kevin, Jelmer, Nienke and Stijn, thank you for staying temporary at your places. Finally I would like to thank my family and friends for their support.

Niels-Jasper van den Berg
Nijmegen, August 19, 2013

Contents

Abstract **i**

Preface **iii**

1 Introduction **1**
1.1 Storm surges 1
1.2 Surges as input for design conditions 2
1.3 Research objective 3
1.4 Research questions 4
1.5 Methodology 4
1.6 Report outline 5

2 The processes of storm surges on the North Sea **7**
2.1 Meteorological processes 7
2.2 Hydrodynamical processes 10
2.3 Conclusions 14

3 Model setup **15**
3.1 Model outline 16
3.2 Meteorological model 18
3.3 Hydrodynamical model 25
3.4 Conclusions 30

4 Model validation, calibration & assessing model sensitivity **31**
4.1 Historical data 31
4.2 Validation of the meteorological model 33
4.3 Calibration of the coupled model 35
4.4 Assessing model sensitivity 42
4.5 Conclusions 46

5 Monte Carlo analysis **49**
5.1 Computation of extreme surges 49
5.2 Analysis of surges with different return periods 53
5.3 Duration of $1 \cdot 10^{-4}$ year^{-1} surges 56
5.4 Conclusions 62

6 Discussion **63**
6.1 One dimensional hydrodynamical model 63
6.2 Storm parameter values 67
6.3 Methodology of Gringorten 69
6.4 Excluding tide 70
6.5 Simplicity of the storm field 70
6.6 Conclusions 71

7 Conclusions and recommendations **73**
7.1 Conclusions 73
7.2 Recommendations 76

Bibliography **78**

Appendices

A List of frequently used symbols **85**

B Solution method of the hydrodynamical model **87**

C Testing of the hydrodynamical model **93**

D Validation of the meteorological model **99**

E Calibration results for surge courses **105**

F Sensitivity analysis **109**

G Storm parameter distributions of different types of surges **117**

H New storm parameter values **123**

Chapter 1

Introduction

Storm surges are of great interest for the low-lying parts of the Netherlands. The objective of this study is to gain insight into extreme water levels at our coasts. Better understanding of the underlying processes of extreme water levels is expected to result in improvement of coastal protection.

This chapter will introduce the phenomenon of storm surges and will explain how storm surges are used to design coastal protection in the Netherlands. Shortcomings in the currently used method to determine design conditions result in the objective of this research. Research questions and a research plan are presented next. Finally an outline of this report is given.

1.1 Storm surges

A storm surge is the rise in water level due to a storm. It is the non-tidal residual of excess sea levels. Surges are mainly forced by wind and low atmospheric pressure (Pugh, 1987). An effect of storm surges is the possible flooding of low-lying land. Coastal areas and flood planes contain often fertile soils and are generally densely populated, which increases the economical risk of a storm surge (Hinton et al., 2007). A second effect is the occurrence of strong currents, which can affect oil rigs and pipelines (Pugh, 1987). A well-known example of a storm surge is the one of January 1953, which caused large floods in Southern England and the Netherlands. More than 2100 people in total fell victim in Netherlands, Belgium and the United Kingdom (Gerritsen, 2005).

1.2 Surges as input for design conditions

The 1953 disaster was reason for the Minister of Transport, Public Works and Water Management of the Netherlands to form the Delta committee. This committee proposed measures against the devastating effects of surges and recommended to give each set of dikes (*'dijkring'* in Dutch) a certain norm (Deltacommisie, 1960). This norm determines in a statistical sense the exceedence frequency of water levels. For the Randstad region, this norm is once per 10,000 years (probability of $1 \cdot 10^{-4}$ year^{-1}) (Ministerie van Verkeer en Waterstaat, 2007). This advice was followed by the government and today the safety of the Dutch coasts is enacted by law. Water levels (the sum of high tides and storm surge set-up), corresponding to that norm, are calculated for nine places along the coast. These water levels are called basic water levels. These water levels are part of the hydraulic boundary conditions, which are used to design flood defenses.

All basic water levels of the Dutch coast are based on the basic water level of Hoek van Holland. This water level is determined by extrapolation of historical water levels, by using non-parametric (or distribution-free) inferential statistical methods (Dillingh et al., 1993). The basic water levels have been determined for the year 1985 (Dillingh et al., 1993). To use them today, the levels are adjusted for relative sea level rise. For Hoek van Holland, the basic water level of 1985 is 5.00 m +NAP, and the adjusted level is 5.10 m +NAP for today (Ministerie van Verkeer en Waterstaat, 2007). To determine the basic water level for the other eight places, two methods are used: extrapolation of historical data and numerical modeling of storm surges. The numerical models used to determine the basic water levels are made in the WAQUA software package (Gerritsen et al., 2005). A weighted average of the two results determine the basic water levels.

This current approach entails a large uncertainty (the standard deviation of the basic water level for Hoek van Holland is 0.90 m (Dillingh et al., 1993)). Another aspect to keep in mind of this method is that the characteristics of the governing storm are not known and are thus not incorporated. Therefore, the duration and course of extreme surges are not known, but are important for dune and dike design. The time that the water level remains at about the maximum surge level is the most determinative factor for the amount of dune erosion in the entire development of the water level during the storm surge (Steetzel et al., 2007). In the Netherlands, dune safety is assessed by calculating the amount of sand which will be eroded during a normative event with a constant peak surge level of 5 hours. Uncertainty

in peak surge duration is incorporated by adding 10% to the total amount of dune erosion (Gautier & Groeneweg, 2012). A quick decline of the water level can result in dike failure, for example by piping, failure of revetments on the top layer due to overpressure and sliding of the outer slope (Deltares & Witteveen+Bos, 2010). A normative surge course of an extreme surge event is used for Dutch dike design, described in Section 5.3.1.

A relatively new approach to determine the basic water levels is to use statistical extrapolation of storm parameters to model extreme storms. Storm parameters describe the characteristics of a storm, such as central pressure, size, propagation speed and location. Parametric models use these parameters to describe the wind field and the pressure field of a storm. These wind fields and pressure fields can force hydrodynamical models. This way, the effects of these storms on the water level along the coast can be determined in a process-based manner. This approach is proposed by Bijl (1997) and first steps on this topic have been made by De Jong (2012). De Jong developed a joint probability method to determine the extreme water levels for the Dutch coast by means of a parametric model.

1.3 Research objective

The current methods to determine design conditions for coastal protection at Hoek van Holland are not based on the underlying forcing processes of storm surges. Instead, they are only based on observations of the effects of atmospheric forcing (i.e. observed storm surges). Information of storms which force these surges is not included. A result of this approach is lack of insight into the coupling between the storm and the storm surge. In this research, storms and related surges will be modeled using statistical extrapolated storm parameters. Focus is on the properties of storms causing extreme surges at Hoek van Holland as well as on surge heights and surge duration. The research objective is:

> *"To gain more insight into the influence of the storm parameters on extreme surge events at the Dutch coast through idealized process-based modeling of the meteorological-hydrodynamic behavior of the North Sea."*

1.4 Research questions

The research objective will be achieved by answering the following research questions:

1) What are relevant physical processes that need to be included in a model to predict storm surge events at the Dutch coast?
2) How can we formulate a coupled idealized process-based meteorological-hydrodynamical model suitable for the prediction of storm surge events at the Dutch coast?
3) How accurate does the model describe the storm surge characteristics (surge height and surge duration) of surges in the North Sea and which parameters of the model have a strong influence on these characteristics?
4) What are the governing storm parameters affecting the storm surge characteristics for extreme conditions?

1.5 Methodology

In order to achieve the research objective and to answer the research questions, the following methodology is used:

- An overview of all meteorological and hydrodynamical processes which contribute to storm surges will be given. This overview is obtained from literature. A selection of these processes, which will be incorporated in the model, will be made.
- The selected meteorological processes will be used to apply a parametric process-based analytical meteorological model. The model of Holland (1980) is used to describe an atmospheric pressure field. Movement of the storm is implemented using methods often used in literature. This model uses six storm parameters as input. Model output is atmospheric pressure and both wind speed and wind direction. The model is build in MATLAB.
- Next, a one-dimensional depth averaged idealized hydrodynamical numerical model, based on the selected hydrodynamical processes, is built and tested. Output from the meteorological model serves as model input for this hydrodynamical model. The hydrodynamical model computes water levels at Hoek van Holland. The advantage of a one-dimensional model is the short computation time, which later

allows us to conduct an extensive Monte Carlo analysis. This hydrodynamical model is build in MATLAB as well.

- The meteorological model will be validated in a qualitative way using historical data. These data are obtained from work of (De Jong, 2012). Next, the coupled meteorological-hydrodynamical model will be calibrated using the same historical data. This is done using Generalized Reduced Gradient non-linear optimization techniques of the Excel software package. Model properties will be assessed by performing a sensitivity analysis.
- Probability distributions of the storm parameters are used as input for Monte Carlo analysis. These probability distributions are given by De Jong (2012) and are based on the historical data. A dataset of 1,000,000 surges will be produced and the return period of each surge will be determined.
- Properties of storms causing extreme surges are investigated by comparing storm parameter values of these storms with averaged values. This is done by presenting histograms of the distributions of input parameter values.
- The duration of surges with return periods of 10,000 years is investigated and compared with the duration as given by the hydraulic boundary conditions, by presenting hydrographs. The differences in storms causing long and short surges is analyzed as well. This is done by comparing histograms of storm parameter values.

1.6 Report outline

The outline of this report is as follows:

Chapter 2: The processes of storm surges at the North Sea In this chapter processes which contribute to storm surges are described. A selection is made of processes which are incorporated into the model. This chapter answers the first research question.

Chapter 3: Model setup This chapter covers the building and testing of the model. The second research question is answered in this chapter.

Chapter 4: Model validation, calibration & sensitivity analysis This chapter addresses the third research question.

Chapter 5: Monte Carlo analysis This chapter covers a Monte Carlo analysis which is used to compute extreme surges. The storm parameter values of the associated storms are investigated. Surge duration is analyzed as well. This answers the last research question.

Chapter 6: Discussion This chapter contains discussion about the limitations of the one-dimensional approach. Also model input and the exclusion of tides is discussed.

Chapter 7: Conclusions and recommendations This final chapter covers final conclusions. Answers to all research questions are summarized. Finally, recommendations for further research are presented.

Chapter 2

The processes of storm surges on the North Sea

Storm surges are driven by meteorological processes. These processes bring the water of the seas into motion. The motion of water is described by hydrodynamical processes. In this chapter, all relevant meteorological and hydrodynamical processes of storm surges will be discussed; first the meteorological processes, second the hydrodynamical processes. Next, a selection is made of the processes which will be incorporated in this study. The first research question (stated in section 1.4) is answered in this chapter.

2.1 Meteorological processes

First, the life course of a storm is discussed. A pressure field develops during this life course. Pressure gradients cause winds. This process is discussed next. Finally, a selection of incorporated processes is made.

2.1.1 The life course of a depression

A temperature gradient exists between the equator and the poles, as a result of differences in radiation balances on the Earth. This horizontal temperature gradient results in a pressure gradient which in turn results, in combination with the Coriolis force and gravity, in a thermal wind shear. This shear is called the jet stream, it is located around the mid latitudes and it is heading eastwards. The temperature differences around the Earth have a second effect; the formation of Hadley cells. Hadley cells emerge in areas of high pressure at the poles and around the tropic, and areas of low pressure

at the equator and at mid latitudes (near the jet stream). Because air is moving from areas of high pressure towards areas of low pressure, air from the tropics and the poles collide at the mid latitudes and at the equator. The collision at the mid latitudes is called the polar front (Gill, 1982).

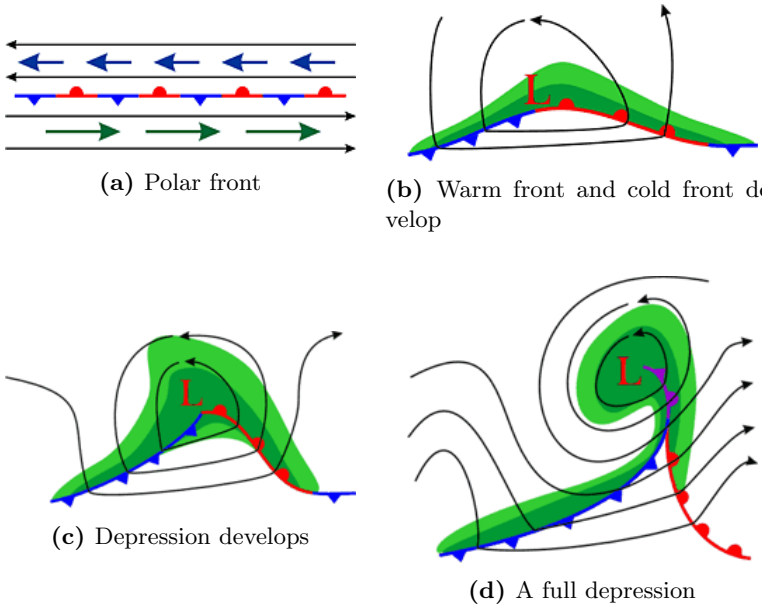

(a) Polar front

(b) Warm front and cold front develop

(c) Depression develops

(d) A full depression

Figure 2.1: Stages of the development of a depression (National Oceanic and Atmospheric Administration, 2012) on the Northern Hemisphere. Cold air is denoted by dark blue arrows, warm air by dark green arrows (Figure 2.1a). The blue lines with triangles represent a cold front, the red lines with semicircles represent a warm front. The black lines denote isobars and wind direction is given by the small black arrows. The green colored areas denote precipitation.

At the polar front, small disturbances can form a wave in the front (Figure. 2.1a). Cold air is moving towards the south (a cold front) and warm air is moving towards the north (a warm front) (Figure. 2.1b). Warm air is moved upwards by the more dense cold air, where the warm air cools down. Because cold air can contain less moisture, condensation and precipitation starts to occur. The condensation of water releases heat and this intensifies the process of the rising of warm moist air. At the surface, a local area of low pressure occurs and the system becomes a depression (Figure. 2.1c). This kind of depression is called an extra-tropical storm. The cold front west of the depression is moving faster than the warm front and near the depression the fronts collide and form an occlusion front. This cuts off the supply of warm air and slowly the depression will dissipate (Figure. 2.1d) (National Oceanic and Atmospheric Administration, 2012). The atmospheric pressure

will increase with further distance from the depression center. The shape of the atmospheric pressure field is quite irregular, especially close to the fronts.

Because depressions occur near the jet stream, they are moved by the jet stream eastwards. Most of the Dutch severe storms relevant for high storm surges are coming North of Scotland and are heading south-east over the North Sea towards the Netherlands or Denmark (Wieringa & Rijkoort, 1983). In reality, storms are often more complex than described here. More than one cold and warm front can occur. It also possible that multiple depressions act together as one storm.

2.1.2 Wind

The atmospheric pressure gradients, induced by the depression and surrounding ambient pressure, cause air to move. When neglecting friction, the curved pressure gradient around the depression is in balance with the Coriolis acceleration and the centripetal acceleration. This results in a wind following the isobars (imaginary lines connecting points of equal pressure) around the low-pressure area, counter-clockwise in the Northern Hemisphere and clockwise on the Southern hemisphere. This flow is called gradient flow. The gradient wind will circle around the depression, following the isobars, without ever reaching its center.

Friction becomes more important near the Earth's and Ocean's surface (Gill, 1982). Due to friction, the wind direction will turn a small angle (typical values of about 20° (Gill, 1982)) counter-clockwise from the isobars in the direction of the pressure-low. The depression will hereby slowly be filled with the influx of wind. A second effect of friction is reduction of the wind speed.

The movement of a storm has a strong influence on the wind. When wind direction and the direction of movement of the depression are the same, wind speeds increases. For the North Sea, this is often the case with a north-westerly storm. Due to irregular shape of the pressure field near the fronts, wind direction changes when a front passes. The pressure field and wind direction of a real storm are shown in Figure. 2.2.

2.1.3 Selection of processes

Storm surges are driven by the meteorological processes of a depression or multiple depressions. The complexity of multiple depressions per storm is circumvented by taking only one depression per storm into account. This

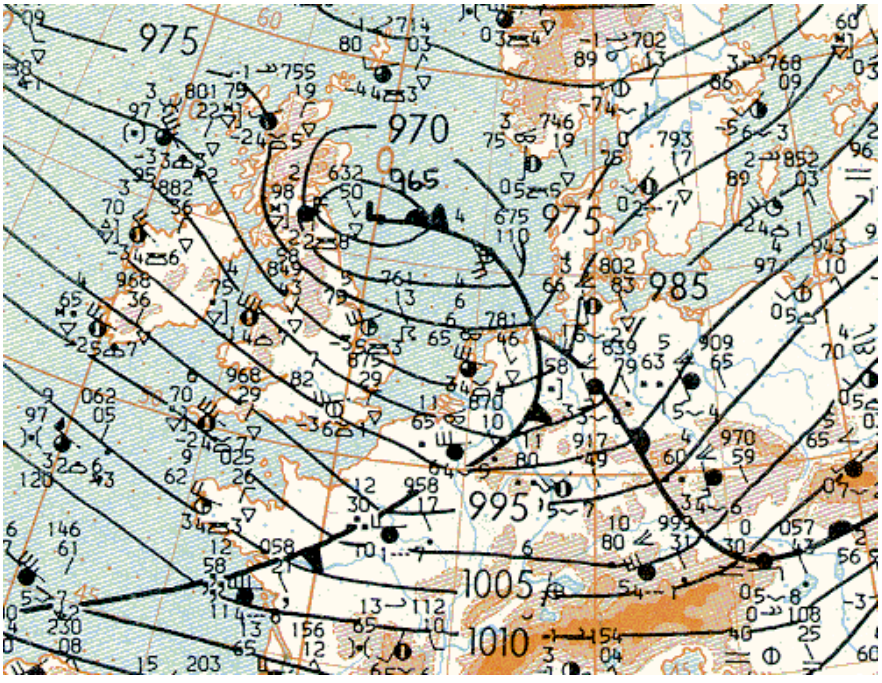

Figure 2.2: Weather map of 14 January 1984, 12:00 GMT (Deutschen Wetterdienstes, 1984).

will cause possible errors in model results which is discussed in Chapter 6. The depression has a life course which will not be incorporated in the model, because it is assumed that the storms are fully developed and do not change while passing the North Sea. In reality, storms can increase and decrease in force while passing. These effects roughly cancel each other out, so this model choice has no major consequences and it also reduces the amount of model input. On the other hand, the pressure field of the depression and the movement of the depression are implemented. All wind processes are incorporated: gradient wind, the effect of friction on wind speed and direction and the influence of the depression movement on wind.

2.2 Hydrodynamical processes

The hydrodynamical processes of storm surges described in this section are divided into three categories: 1) external influences, which force a storm surge; 2) internal processes, which describe the motion of currents and 3) other processes. Finally, a selection is made of incorporated hydrodynamical processes.

2.2.1 External influences

A storm surge is mainly driven by 1) reduced atmospheric pressure and 2) wind. Other factors also contribute to the forcing of a storm surge, like 3) buoyancy differences, 4) storm-driven rainfall and 5) waves.

Reduced atmospheric pressure influences the water level. A local area of low atmospheric pressure will cause the water level to rise compared to the surrounding regions. This is called the inverted barometer effect (Proudman, 1953). The atmospheric pressure in a depression can be as low as 960 mbar, compared to an ambient pressure of 1 atmosphere (1013 mbar). The inverted barometer effect of such a depression will force the water level to rise 0.53 m.

Wind exerts a horizontal stress on the sea surface in two ways: by pressure differences across irregularities (waves) and by viscous stresses. Viscous stress is acting on the surface due to frictional contact between the surface of the ocean and the wind. Because the irregularities are small enough, the associated stress is often added to the viscous stress and is called wind stress (Proudman, 1953). The wind stress brings the water into motion. This results in piling up of the water at closed boundaries. A second effect of wind is wave generation.

Buoyancy differences are caused by, among others, salinity and temperature differences of the water. Local regions of more dense water tend to sink whereas less dense water tends to move upwards. Sources of density differences are fresh water inputs like precipitation and rivers. Shelf seas, such a the North Sea, are often well-mixed due to tides and storms, especially during the winter season (Brown et al., 1999). In these well-mixed seas, the associated sea level changes are of much lower magnitude and have a much longer time scale than the scale of a storm surge (Slobbe et al., 2012).

Storm-driven rainfall can cause a temporary increase of the water level, especially in tidal rivers and estuaries where rivers contribute to the input of rainwater (Orton et al., 2012). The depressions forcing a storm surge often bring heavy precipitation.

Waves are generated by the wind of the depression. Waves increase the height of a storm surge by so called wave radiation stresses, caused when waves approach shallow water. A second effect of waves is the increase of bottom stress due to increasing near-bed velocity. A last

effect is an increase of surface stress due to the increased roughness of the ocean surface (Bode & Hardy, 1997).

2.2.2 Internal processes

The motion of currents can be described by the Navier Stokes equations, a set of nonlinear partial differential equations. The Navier Stokes equations arise from applying Newton's second law (the net force on an object is equal to the rate of change of momentum) to a fluid. Forces on the water mass are pressure gradients and viscous forces. The terms are 1) acceleration, 2) advection, 3) Coriolis acceleration, 4) pressure gradients, 5) vertical shear 6) horizontal mixing of momentum and 7) stresses. These terms will be described here. Wind stress is already discussed in the previous paragraph, so only bottom stress will be addressed.

Acceleration is the change in velocity over time.

Advection is the transport of momentum through the domain.

Coriolis acceleration is a result of a force which acts perpendicular to the direction of moving objects, like water. It is caused by the rotation of the Earth. In the Northern Hemisphere, the deflection is clockwise. It also affects wind. Ekman mass transport is a result of the Coriolis force. It is a depth integrated transport of water at an angle of 90° of the surface wind (Gill, 1982).

Pressure gradients force water to move. Both atmospheric pressure gradients and pressure gradients due to differences in water height should be taken into account. The inverse barometer effect is a result of pressure gradients.

Vertical shear transfers momentum to and from the water at the upper and lower boundaries of the sea.

Horizontal mixing of momentum transfers momentum horizontally in the domain.

Bottom stress is acting on the lowest layer of the water column. Its magnitude is a function of the near-bed velocity. The direction of the stress is against the near-bed flow. A surge will cause a return flow. This return flow results in a bottom stress in the direction of the storm surge, increasing the surge even more (Resio & Westerink, 2008).

2.2.3 Other processes

There are several other aspects which influence a storm surge: 1) tide-surge interactions, 2) sea level oscillations and 3) amplifying due to funnel shaped geometry. These aspects will be described here.

Tide-surge interactions make it difficult to model a storm surge and the tide independently of each other. For example, a high tide increases the propagation speed of the storm surge (Bode & Hardy, 1997).

Sea level oscillations can occur when multiple depressions pass by or when the propagation velocity of the storm matches the propagation velocity of the surge (Vilibić et al., 2005). The time between those forcing events can match with the natural resonance time of a local sea or bay.

Amplification due to local geometry is the rise of a storm surge when reaching shallow water (Madsen & Flemming, 2004) or entering a funnel-shaped bay, like the area near Bangladesh or the southern North Sea As-Salek (1998).

2.2.4 Selection of processes

Only the first two of the external influences described will be used in this study. Reduced atmospheric pressure and wind have the largest effect on the surge height and duration (Lowe et al., 2001). The other influences will therefore be neglected.

Two of the internal processes will not be incorporated. First, the Coriolis acceleration of the water mass will not be taken into account. For simplicity, only processes in one direction will be included. In such a one-dimensional model, Coriolis acceleration cannot be implemented because it requires two horizontal dimensions. The big advantage of a one-dimensional model is the short runtime. This allows to make a large amount of runs, which is necessary for Monte Carlo analysis. Note that details of the vertical velocity profile are not incorporated into a one-dimensional model. In such a model, bottom stress is related to the depth averaged flow velocity. Increasing of the surge due to bottom stress is thus excluded. The result of this choice is discussed in Chapter 6. Next, horizontal mixing of momentum is neglected in favor of vertical diffusion. This is allowed when the horizontal length scale of a disturbance is large relative to the vertical scale (Mellor & Blumberg, 1985), which is the case for large scale phenomena like storm surges (Gill, 1982). All other processes will be incorporated.

Of the other processes, only one effect (amplification due to local geometry) is partly incorporated. The non-linear effects of tides are neglected, because it is assumed that these effects have minimal effect on the surge height and duration. In some steps in this study, the tidal signal is simply summed with the surge level to compute the total water level. This assumption is discussed in Chapter 6. Sea level oscillations are not taken into account, since only one storm per event is taken into account. Amplification due to local geography is partly incorporated. The rise of a storm surge when reaching shallow water will be taken into account, but the horizontal effects on the other hand are not incorporated. This is because effects in the horizontal plane will be neglected for simplicity.

2.3 Conclusions

The meteorological processes which will be incorporated in this study are the following: one single depression per storm which causes an atmospheric pressure field, movement of the depression, gradient wind, the effect of friction on wind speed and direction and the influence of the depression movement on wind.

The incorporated hydrodynamical processes are the following: wind friction and forcing by reduced atmospheric pressure (forcing processes), acceleration, advection, pressure gradients, vertical shear and bottom stress (internal processes), amplification due to local geometry and sea level oscillations (other processes).

The implementation of these processes into the model is discussed in the next chapter.

Chapter 3

Model setup

The model used in this study consists of two parts: a meteorological model, which models the meteorological processes, and a hydrodynamical model, which models the hydrodynamical processes. The meteorological model generates input for the hydrodynamical model through wind stress and atmospheric pressure gradients.

Besides topographic data, the coupled meteorological-hydrodynamical model uses six input parameters (storm parameters). Those six parameters are the following:

- Storm track location ψ (°) latitude;
- Propagation speed C_{fm} (m/s);
- Direction of storm track ϕ (°) cardinal;
- Central pressure p_c (Pa);
- Radius to maximum winds (distance from storm center towards maximum wind speed) R_{max} (m);
- Holland-B parameter (-).

The incorporated processes, presented in the previous section, are implemented by using these storm parameters. This is presented in this chapter. First, a general model description of the model is discussed. Second, the meteorological model is discussed. The last section covers the hydrodynamical model. Testing of the hydrodynamical model is presented in Appendix C. This chapter answers the second research question, which is stated in section 1.4.

3.1 Model outline

The model domain of the coupled model is called a transect, which is a one dimensional line (it has no width). The model area is located in the North Sea. It is heading from a location at the Northern boundary of the North Sea towards Hoek van Holland at the Dutch coast. The transect makes an angle of 13° counter-clockwise from the North. It is 845 km long and can be seen in Figure 3.1. It is assumed that the largest surges will occur on this transect, because it is the longest track without disruptions between the boundaries of the North Sea which is on the continental shelf. This is the rationale for choosing this track location. The sensitivity of this model decision is discussed in section 4.4.

On the transect are 202 grid points, for which data is computed. The spatial step of the model is 4.2 km and the time step is 300 s (5 minutes). Reduction of the size of the spatial step and time step does not improve the model results significantly, but does increase computation time.

The meteorological model is a parametric model, which uses a few input parameters to determine a pressure field and a wind field. The model is process-based and approximates all incorporated atmospheric processes. Model output is atmospheric pressure and wind speed and wind direction.

The hydrodynamical model solves the shallow water equations, which include all incorporated hydrodynamical processes. These equations cannot be solved analytically, therefore a numerical finite differences approach is used. This model is one dimensional, so it models the depth averaged currents in one direction. The big advantage of a one dimensional model is the short computation time (only 0.6 s for this model). Output of the model is free surface elevation and depth averaged velocity.

Figure 3.1: The transect in the North Sea is denoted by the black line. Note that the projection used in this image results in a distorted view of the angle of the transect to the North.

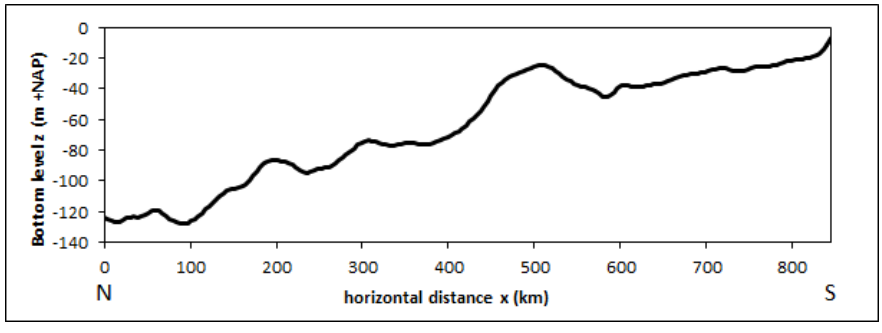

Figure 3.2: The bathymetry of the transect. The boundary located between Scotland and Norway is located at the left, the boundary at the Dutch coast is located on the right. Data is obtained from the British Oceanographic Data Centre of the North Sea (Van den Brink, 2013).

3.2 Meteorological model

The atmospheric pressure field of a storm and the movement of the storm is described by a parametric pressure model. The modeled pressure field is a simplification, and thus an approximation of the pressure field of a real storm. The wind is a result of pressure differences. Wind can therefore be determined by using equations, which approximate the real processes.

3.2.1 Pressure field

Different parametric pressure fields of tropical storms have been found in literature, such as the Rankine vortex model, the Fujita model, the Holland-B model and the model of DeMaria, all discussed by Leslie & Holland (1995). The model of Bijl (1997) describes the pressure field of extra-tropical storms. Of these models, the model of Holland (1980) is chosen as the one that will be used in this study because of its simplicity (it needs only 4 input parameters) and because it uses a shape factor to describe the pressure gradient, which is the driving force of wind. The model is widely used (Jakobsen & Madsen, 2004).

Holland-B model

The parametric pressure model by Holland (1980) is based on tropical storms. Unlike extra-tropical storms, tropical storms do not have fronts. Therefore, their pressure field has a circular shape. The model approximates the shape of the pressure field as a circle. It uses only 4 parameters to describe the pressure field and the pressure profile. These parameters are the central pressure p_c (Pa), the pressure difference between central pressure and ambient pressure Δp (Pa), the radius to maximum winds R_{max} (m) and a Holland-B parameter (-). Figure 3.3 displays cross sections of pressure fields with different values for B shown.

The atmospheric pressure p (Pa) at a distance r (m) from the storm center is given by:

$$p = p_c + \Delta p \cdot e^{\left[-\left(\frac{R_{max}}{r}\right)^B\right]} \tag{3.1}$$

The Holland-B parameter contributes to the shape of the pressure profile. Typical parameter values are between 1 and 2.5 (Holland, 1980). A higher value results in a steeper slope of the pressure profile, which in turn results in higher maximum winds.

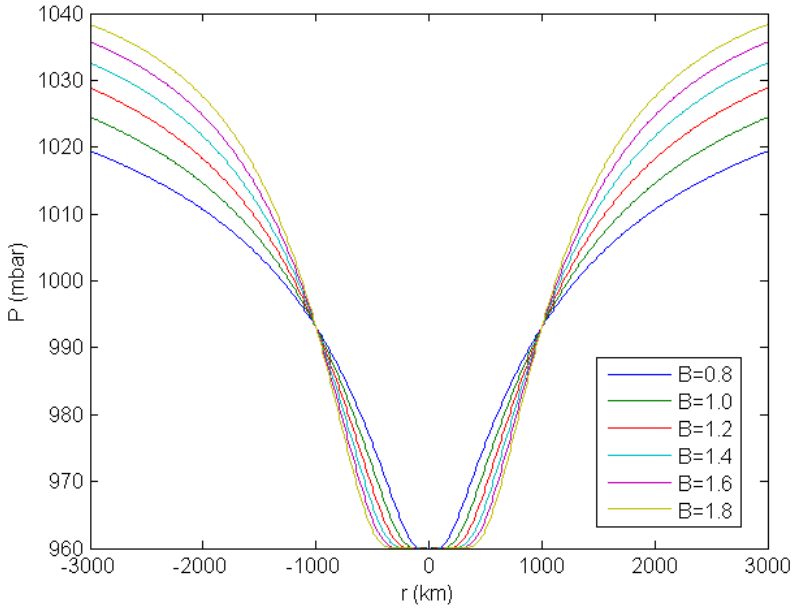

Figure 3.3: Cross sections of Holland-B pressure fields. Other parameter have averaged values: $R_{max} = 1000$ km, $p_c = 960$ mbar and $\Delta p = 90$ mbar.

Input for the model of Holland is reduced by assuming a constant ambient pressure of 1050 mbar (1050×10^3 Pa). The reason for this decision is that it is not always possible to obtain a parameter value from weather charts for validation data. Δp is now defined by the difference between p_c and the ambient pressure of 1050 mbar. According to the De Jong (2012) this assumption yields a good description of measured storms.

3.2.2 Storm track

The storm movement will be modeled as a forward movement on a straight line. Although in reality storms have complex movements, it is assumed that deviations from a straight line within the area in which the storms induces the surges are small enough to neglect. The implementation is shown in Figure 3.4. Three storm parameters define the movement of the storm: 1) location of a single point on the track, 2) the direction of the track and 3) the propagation speed:

Storm track location is given by one single coordinate. The wind moves counter-clockwise around a depression on the Northern hemisphere. Therefore, wind is blowing in a southerly direction when the storm has

passed the central part of North Sea. The surge is thus expected when the storm has passed the central North Sea. It is therefore important to approximate this location as accurately as possible. Therefore, the location of the track is defined at 5.5°E by ψ (°N). From this point, the track runs both in an easterly as in an westerly direction. The exact direction is given by the next discussed parameter.

Direction of the storm track from the direction of the storm towards its origin, is given by ϕ °).

Propagation speed C_{fm} (m s^{-1}) is assumed to be constant.

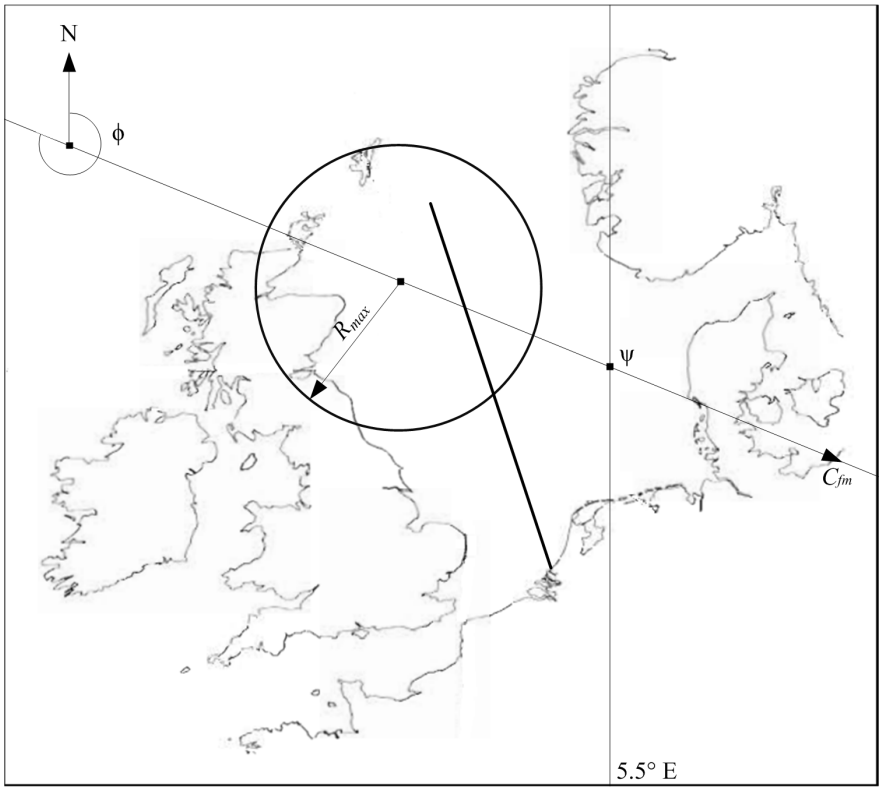

Figure 3.4: The storm track as implemented in the model.

3.2.3 Wind field

The wind field is modeled as a gradient wind. Forward movement of the storm and friction influence both wind speed and wind direction. These three aspects will be discussed here.

Gradient wind

Gradient wind is given by the following equation:

$$\frac{V_g^2}{r_t} + fV_g = -\frac{1}{\rho_a}\frac{\partial p}{\partial r} \tag{3.2}$$

in which V_g denotes gradient wind speed (m s^{-1}), r_t radius of curvature of the trajectory (m), f the Coriolis parameter (s^{-1}), ρ_a air density (kg m^{-3}) and p the atmospheric pressure (Pa). An air density of 1.27 kg m^{-3} is used, associated with an air temperature of 5°. The first term of the equation denotes centripetal acceleration, the second term Coriolis acceleration and the last term the pressure gradient. The Coriolis parameter represents the Coriolis force and is determined by:

$$f = 2\Omega \sin(\theta) \tag{3.3}$$

in which Ω being the angular velocity of the Earth (rad s^{-1}) and θ the latitude (°). The direction of the force is to the right in the Northern Hemisphere and to the left in the Southern Hemisphere, with respect to the direction of motion. For the Netherlands (latitude of 52°N), the Coriolis parameter equals $f = 1.15 \cdot 10^{-4}$ s^{-1}. This parameter is assumed to be constant in the whole area (f-plane approximation) (Gill, 1982).

The gradient wind circles in a counter-clockwise manner around the depression. The direction in which the wind is blowing is at an angle of 90° clock-wise with respect to the vector from the point of interest towards the storm center.

Forward movement of the storm

The movement of the storm influences the wind speed. For instance, when at a certain place the wind direction is equal to the direction of the storm track, the wind speed increases. To model this influence, Blaton's adjustment of the radius of curvature is implemented (Pita et al., 2012). In this method, the radius of curvature (r_t in equation (3.2)) is adjusted as a function of the angle between the direction of storm translation and the vector from the

storm center pointing towards the point of interest ξ (°). It is given by:

$$\frac{1}{r_t} = \frac{1}{r}\left(1 + \frac{C_{fm}}{V_g}\sin\xi\right). \tag{3.4}$$

Surface wind

Friction at the Earth surface influences wind speed and wind direction. This process is implemented by following Brunt (1934):

$$V_s = V_g(\sin\beta - \cos\beta) \approx \frac{2}{3}V_g \tag{3.5}$$

where V_s denotes surface wind at 10 m altitude and β the deflection of the surface wind direction towards the storm center. A value of β=17° is used, based on the work of De Jong (2012). This results in a ratio of 2/3.

3.2.4 Model implementation

The already discussed input parameters for the model, or storm parameters, are the following:

- Storm track location ψ (°);
- Propagation speed C_{fm} (m/s);
- Direction of storm track ϕ (°);
- Central pressure p_c (Pa);
- Radius to maximum winds R_{max} (m);
- Holland-B parameter (-).

The location of the storm center varies over time. Time is implemented in the model by using time steps (Δt = 300 s). The location per time step is determined with respect to the grid points on the transect. This is done on a rectangular grid with use of simple trigonometry. It is assumed that differences of the locations due to the curvature of the Earth are negligible. The location is determined per time step by using the track location, the direction of the storm track and the propagation speed. Thus, the time domain determines the range of the location of the storm center.

Per time step, the distance from the storm center towards each grid cell (r) is calculated by using trigonometry. With this distance known, the atmospheric pressure and the magnitude of the surface wind at each grid point can be calculated for all time steps. The wind direction of the surface

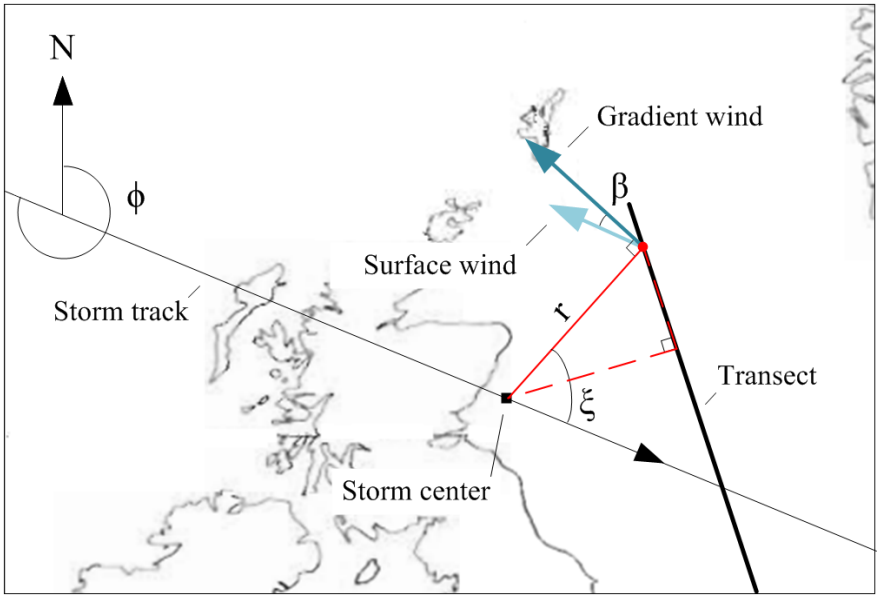

Figure 3.5: The location of the storm center, denoted by the black dot, with respect to an arbitrary point on the transect, denoted by the red dot, is calculated using trigonometry (the red triangle in the picture). The distance r and the angle ξ is shown. The gradient wind has an angle of 90° with line r. The angle between the surface wind and the gradient wind is denoted by β.

wind per grid cell does also follow from trigonometry, as illustrated in Figure 3.5.

The following output of the meteorological model serves as input for the hydrodynamical model: 1) atmospheric pressure, 2) wind speed, and 3) wind direction.

Atmospheric pressure at a distance r is determined by using equation (3.1). An example of a pressure field for various values of B is given in Figure 3.6.

Wind speed is following from the combination of equations (3.1), (3.2), (3.4) and (3.8). First, Blaton's adjustment of the radius of curvature (3.4) is substituted into the gradient wind equation (3.2):

$$V_g^2 + V_g \left(C_{fm} \sin \xi + rf\right) = \frac{r}{\rho_a} \frac{\partial p}{\partial r}. \tag{3.6}$$

The result can be solved for V_g:

$$V_g = W + \sqrt{W^2 + \frac{r}{\rho_a} \frac{\partial p}{\partial r}} \tag{3.7}$$

where

$$W = \frac{C_{fm} \sin \xi - rf}{2}. \tag{3.8}$$

The pressure gradient $\partial p / \partial r$ is obtained from the pressure field model (3.1):

$$V_g = W + \sqrt{W^2 + \frac{\Delta p B}{\rho_a} \left(\frac{R_{max}}{r} \right)^B e^{\left[-\left(\frac{R_{max}}{r} \right)^B \right]}} \tag{3.9}$$

The surface wind is given by (3.8). The final result is:

$$V_s = \frac{2}{3} \left(W + \sqrt{W^2 + \frac{\Delta p B}{\rho_a} \left(\frac{R_{max}}{r} \right)^B e^{\left[-\left(\frac{R}{r} \right)^B \right]}} \right) \tag{3.10}$$

A pressure field and an accompanying wind field is shown in Figure 3.7.

Wind direction defined as the direction in which the surface wind is blowing follows from trigonometry, as can be seen in Figure 3.5. With this information, the surface wind can be expressed in component $V_{s//}$ parallel to the transect and $V_{s\perp}$ perpendicular to the transect.

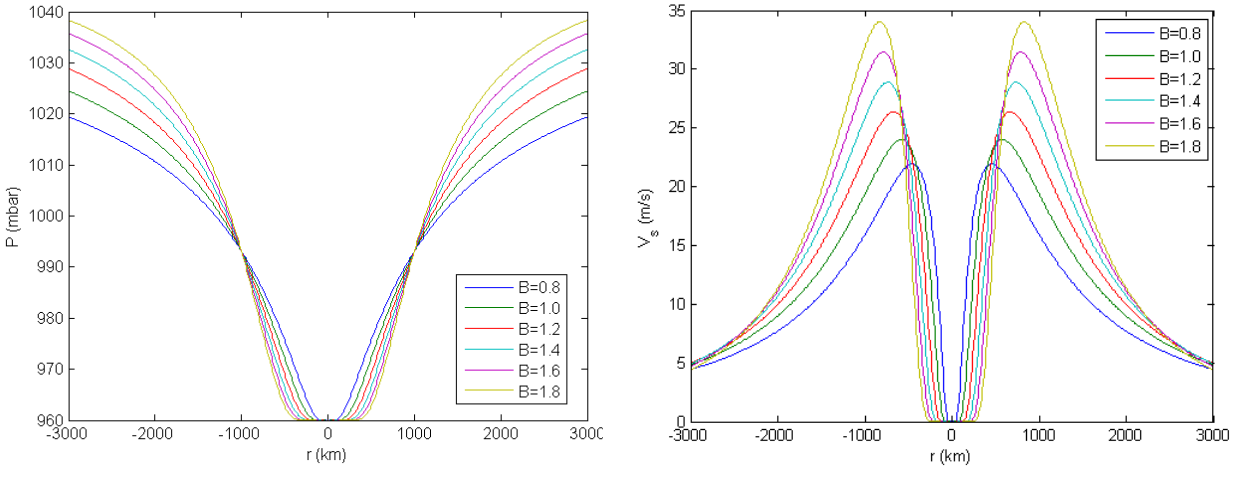

Figure 3.6: Left: Cross sections of Holland-B pressure fields, similar to Figure 3.3. **Right:** cross sections of the corresponding wind fields. $R_{max} = 1000$ km and $p_c = 960$ mbar. It is clear that a higher value for B corresponds to higher maximum winds.

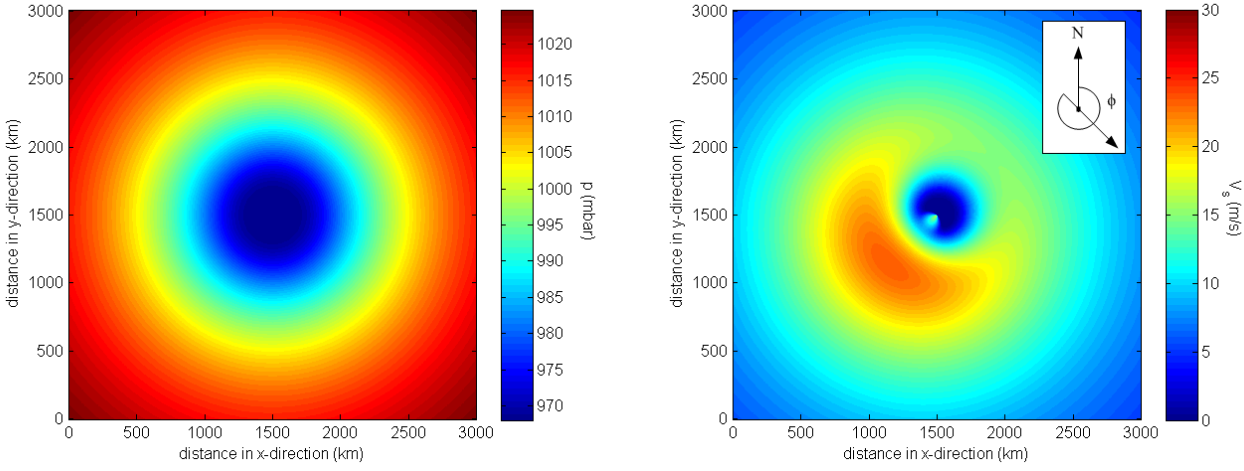

Figure 3.7: Left: the pressure field of a sample storm with averaged storm parameter values ($p_c = 960$ mbar, $B = 1.2$, $R_{max} = 1000$ km, $C_{fm} = 26.1$ m s^{-1} and $\phi = 315°$). **Right:** The associated wind field. Note that the pressure field corresponds to the pressure field plotted in red of Figure 3.6.

3.3 Hydrodynamical model

The hydrodynamical model solves the shallow-water equations in one dimension for the free surface elevation and the depth-averaged flow velocity. It models the transect shown in Figure 3.1 and uses input (atmospheric pressure and wind) of the meteorological model.

3.3.1 Shallow water equations

Derived from Navier-Stokes equations, the one-dimensional (depth-averaged) shallow-water equations are given by:

$$\frac{\partial U}{\partial t} + U\frac{\partial U}{\partial x} + g\frac{\partial \zeta}{\partial x} + \frac{1}{\rho_w}\frac{\partial p}{\partial x} + g\frac{U\,|U|}{C^2(H+\zeta)} = \frac{\tau_w}{\rho_w(H+\zeta)} \tag{3.11}$$

$$\frac{\partial \zeta}{\partial t} + \frac{\partial\left(U(H_0+\zeta)\right)}{\partial x} = 0 \tag{3.12}$$

with initial conditions:

$$\begin{cases} \zeta(x,0) = 0, & \text{for} \quad 0 < x < L, \\ U(x,0) = 0, & \text{for} \quad 0 < x < L, \end{cases} \tag{3.13}$$

and boundary conditions:

$$\begin{cases} \zeta(0,t) = \zeta_0, & \text{for} \quad t > 0, \\ U(L,t) = 0, & \text{for} \quad t > 0. \end{cases} \tag{3.14}$$

Here U denotes the depth-averaged flow velocity in the x-direction (m s^{-1}), t time (s), $0 < x < L$ the space domain (m) of length L (m), g gravitational acceleration (9.81 m s^{-2}), ζ free surface elevation (m), ρ_w water density (1000 kg m^{-3}), p atmospheric pressure (Pa), C Chézy coefficient (m$^{1/2}$ s^{-1}), H water depth (m) and τ_w wind friction (N m^{-2}). The length L is 845 km. Equation (3.11) is the momentum equation and equation (3.12) is the continuity equation. The coordinate system is shown in Figure 3.8. In equation (3.11), the first term denotes acceleration, the second term advection, the third term a hydrostatic pressure gradient due to free surface elevations, the fourth term a pressure gradient due to atmospheric pressure, the fifth term bottom friction and the last term wind stress.

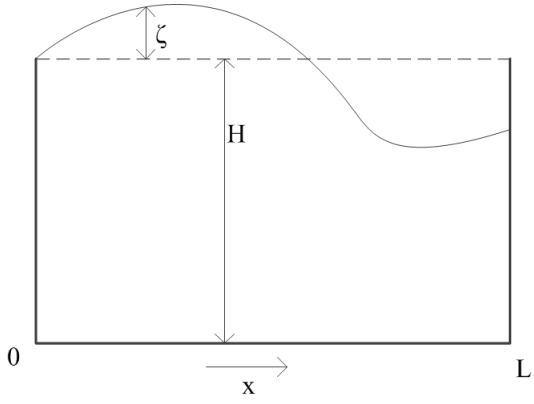

Figure 3.8: The coordinate system of shallow water equations. The total water depth is the sum of the water depth H and the free surface elevation ζ.

Bottom friction is implemented by using a non-linear friction term, where the Chézy coefficient is calculated by:

$$C = \frac{(H+\zeta)^{1/6}}{n} \tag{3.15}$$

where n is the Manning roughness coefficient (m$^{\frac{1}{3}}$ s^{-1}), with a typical value of 0.025 m$^{\frac{1}{3}}$ s^{-1} (Arcement Jr. & Schneider, 2000). This value is kept constant over the whole transect. The effect of using depth-averaged velocity instead of near-bottom velocity is discussed

in Chapter 6.

Wind friction τ_w is determined following Wu (1980):

$$\tau_w = \rho_a c_w \left|\mathbf{V_s}\right| \left(V_s\right)_{//} \tag{3.16}$$

where c_w denotes a dimensionless friction coefficient and where the vector $\mathbf{V_s}$ denotes the surface wind speed at 10 m altitude (m s^{-1}) with component ($V_{s//}$ parallel to the transect and $V_{s\perp}$ perpendicular to the transect. Wu (1980) found a linear relation for c_w as function of $|\mathbf{V_s}|$; Amorocho & DeVries (1980) found an upper limit for c_w due to a smooth layer of foam between the atmospheric layer and the sea, occurring for large wind speeds:

$$c_w = \begin{cases} \left(0.8 + 0.065\left|\mathbf{V_s}\right|\right) \times 10^{-3} & \text{for} \quad V_s < 26.8 \quad \text{m s}^{-1}, \\ 2.54 \times 10^{-3} & \text{for} \quad V_s \geq 26.8 \quad \text{m s}^{-1}. \end{cases} \tag{3.17}$$

Conditions at the open boundaries hold at the northern end of the transect. It is assumed that at this location, the piling up of water due to wind can be neglected compared to the inverse barometric effect. Equation (3.11) reduces locally to:

$$g\frac{\partial \zeta}{\partial x} + \frac{1}{\rho_w}\frac{\partial p}{\partial x} = 0, \tag{3.18}$$

which results in:

$$\zeta_0 = \frac{\Delta p}{g\rho_w}, \tag{3.19}$$

where $\Delta p = P_0 - P(0,t)$. Here is P_0 the average atmospheric pressure (1 bar, 101325 Pa) and $P(0,t)$ is local atmospheric pressure at the open boundary.

Conditions at the closed boundary which is located at the Southern end at the coast are as follows. At this location, it assumed that there is no flow through the coastal boundary, see (3.14).

Bathymetry of the transect is obtained from a data set of the British Oceanographic Data Centre of the North Sea. It has a spacial horizontal resolution of 0.0083° and a vertical resolution of 1 m. The bathymetry of the North Sea is shown in Figure 3.9. The bathymetry of the transect is shown in Figure 3.10 and given in bottom level z (m). The bathymetry is averaged in transverse direction by using 3 transects with an intermediate distance of 10 km. Next, the bathymetry

has been smoothed to erase local disturbances. Water depth H is defined by: $z = -H(x)$.

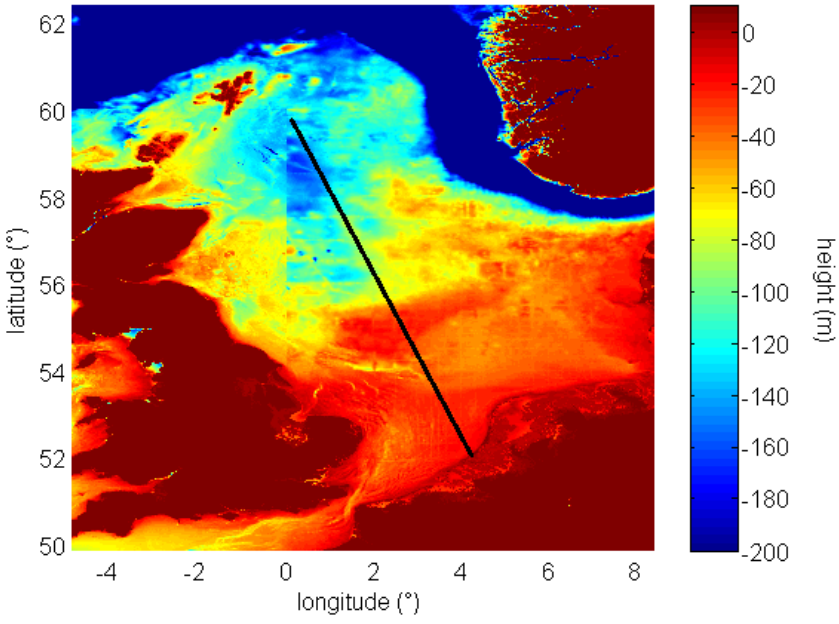

Figure 3.9: The bathymetry of (a part of) the North Sea. The transect is denoted by the black line. The Dogger bank is clearly visible in the southern North Sea. Data are obtained from the British Oceanographic Data Centre of the North Sea (Van den Brink, 2013).

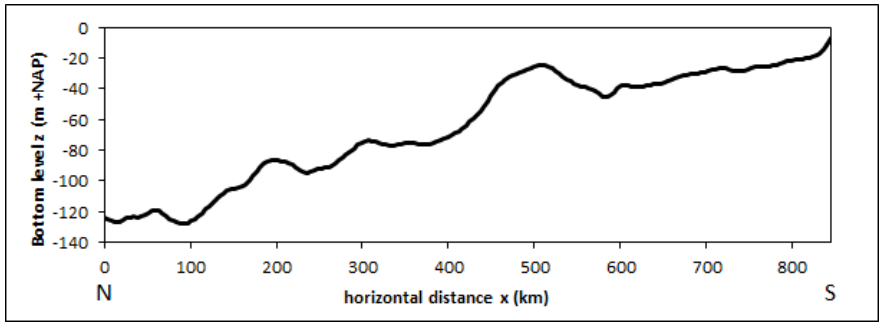

Figure 3.10: The bathymetry of the transect. The open boundary (adjacent to the Atlantic Ocean) is at the left, the closed boundary at Hoek van Holland is on the right. Water depth H equals the negative bottom level z. The Dogger bank is clearly visible at 500 km from the northern boundary. Data are obtained from the British Oceanographic Data Centre of the North Sea (Van den Brink, 2013).

3.3.2 Numerical discretization

The shallow-water equations are solved by use of numerical finite differences and a semi-implicit scheme. A staggered grid in space is used. The spatial grid consists of 202 grid points, so the spatial step is 4.2 km. The time step $\Delta t = 300$ s and the default total simulation time is 7 days. The terms of the momentum equation (3.11) are discretized in the following way: acceleration by using an Euler scheme on the current and next time step; advection velocity on the next time step, velocity differences using a central space scheme on the current time step; the hydrostatic pressure gradient due to surface gradients using a central space scheme on the next time step; pressure gradient due to atmospheric pressure using a central space term on the current time step; bottom friction using a central space scheme on the current time step; and wind stress using a central space term on the current time step. The first term of the continuity equation (3.12) is discretized using Euler on the current and next time step; the second term is discretized using a central difference scheme whereby averaged flow velocity is discretized on the next time step and the free surface elevation on the current time step. A complete overview of the numerical discretizations and model implementations can be found in Appendix B.1. Testing of the hydrodynamical model is discussed in Appendix C. Results are good and give confidence in the model.

3.4 Conclusions

The model is based on a single transect. This transect is located in the North Sea, from a point in the northern part halfway Scotland and Norway, towards the Dutch coast at Hoek van Holland. This transect is divided into 202 grid points of 4.2 km, on which computations are made.

The meteorological model computes wind speed and atmospheric pressure for each grid point. This is done in an analytical way.

The hydrodynamical model uses the atmospheric forcing to compute a storm surge. This is done using numerical approaches (Euler schemes and central space schemes).

Hydrodynamical model tests have been carried out. Both for equilibrium cases a for a non-equilibrium case, results are good. This gives faith in the hydrodynamical model and test results suggest that the model is numerical stable, since the model output does not diverges in time.

Calibration, validation and sensitivity of the model is discussed in the next chapter.

Chapter 4

Model validation, calibration & assessing model sensitivity

This chapter discusses validation, calibration, uncertainties in model input, and sensitivity of the model. First, data of historical storms are presented. These data are used for validation, calibration, and the assessment of the model sensitivity. Next, the validation of the meteorological model is presented. Then the coupled model is calibrated and results are shown for both maximum surge levels and surge courses. Last, uncertainties in model input are quantified and a sensitivity analysis is presented. In this chapter the third research question is answered, stated in section 1.4.

4.1 Historical data

Data used in this chapter consist of historical storms. The storm parameters of these storms are input for the model. A dataset of De Jong (2012) is used, which consists of 21 storms. This dataset will be discussed below. Data quality is discussed in Chapter 6.

Per year, many storms cross the North Sea and many storm surges occur. However, not all storms are included in the dataset. Storms are selected using the following criteria (De Jong, 2012):

- The storms are relevant in terms of extreme hydraulic loads;
- The storms are selected which result in the highest skewed set-up, it

is assumed that these storms also cause the highest straight set-up[1];

- Data necessary to determine storm characteristics value must be available;
- Validation data must be available for Hoek van Holland, in order to validate the model;
- The direction of the storm track (ϕ) must be between 270° and 360°;
- The observed skewed set-up of the storms is higher than 1.55 m.

De Jong used different sources for his dataset, like data written in reports and weather charts. The used data sources are the Delta report (Deltacommisie, 1961), storm surge reports and weather charts from the KNMI archive, the Wetterzentrale (Wetterzentrale, 2011), the storm catalogue (Groen & Caires, 2011) and the KNMI weather chart archive Europe (KNMI, 2013).

From these data sources, de Jong determined values for the six storm parameter for the selected storms. For a full overview of working assumptions, see De Jong (2012). De Jong uses two methods to determine R_{max} and B (Method 1 and Method 2), of which the later proves to be the best. The parameter values determined by this second method are therefore used in this study. The quality of these data is open for discussion and is discussed in Chapter 6.

The complete dataset of storms is as listed in Table 4.1:

[1]The skewed set-up is the difference in the maximum observed water level and the closest (in time) predicted high tide. The straight set-up is the difference in the maximum observed water level and the computed tide at that exact time.

Number	Date	ψ (°N)	C_{fm} (m/s)	ϕ (°)	p_c (Pa)	R_{max} (km)	B (-)
1	07-12-1895	62.4	12.1	327.8	96270	551	0.7
2	29-11-1897	55.7	13	276.2	95900	607	0.9
3	03-02-1898	57.3	18.2	311.2	97800	1158	2.3
4	30-12-1904	56.6	24.7	290.1	98270	669	1.0
5	7-1-1905	57.9	15.4	306.6	97700	578	1.4
6	21-2-1907	59.5	6.8	275.9	95600	954	1.2
7	23-11-1908	60.1	8.5	296.1	98470	883	1.3
8	13-1-1916	57.9	10.9	309.6	97800	577	1.0
9	19-12-1919	57.8	12.2	291.8	99000	664	1.1
10	26-11-1928	56.4	8.9	289.6	96930	1058	0.8
11	1-3-1949	56.3	16.2	295.8	98100	549	1.3
12	1-2-1953	55.8	10.1	312.3	96300	693	1.2
13	23-12-1954	57.9	14.1	297.8	97750	477	1.2
14	12-2-1962	61.7	22.5	286.5	95250	1055	1.9
15	17-2-1962	66.4	16.6	311.4	95250	861	2.2
16	3-1-1976	56.4	10.9	292.5	96750	341	0.9
17	14-2-1989	57.7	17.5	272.6	99000	463	1.4
18	12-12-1990	61.3	19	337.1	98200	523	0.9
19	21-12-2003	55.5	13.3	273.8	97000	363	0.7
20	9-11-2007	60.1	11	293.1	97900	569	1.3
21	1-3-2008	60.1	26.1	291.2	96800	854	1.1

Table 4.1: Complete overview of all storm parameters of all storms used in this research.

4.2 Validation of the meteorological model

The meteorological model provides wind speed and wind directions along the whole transect. Actual wind is observed at weather stations located at the mainland and at oil rigs at sea. Validation can be done for locations along the transect where actual wind data are available. The weather station nearest to the transect is that of Hoek van Holland. Wind speed and directions of the model will be compared with observations from this weather station. The calibration performed in the previous section has no influence on the meteorological model.

4.2.1 Validation data and model input

Observations are surface wind speed, with an accuracy of 0.1 m s^{-1}, and wind direction, given with an accuracy of 10°. Wind speed is measured at 16.6 m height and corrected to the wind speed at 10 m high (surface wind). Data are given per hour from 1962 until present and is provided by the KNMI (2011).

Historical storms described in section 4.1 are used as model input. Be-

cause validation data are available since 1962, the model can only be validated for storms 14 until 21.

4.2.2 Results

Validation is done for a time span of 24 hours (25 data points) around the storm maximum. Wind directions above 360° are not given in degrees with 0° as datum, but instead with 360° as datum. In this way, figures become more clear. Because computed storms are not absolute in time (the exact time for which the storm is located at ψ is not given), the computed wind fields are shifted in time until they match with the observed wind fields. Focus will be more on trends than on absolute values. Only one storm (storm 21) is presented in this section, see Figure 4.1. Results for storms 14 until 20 are discussed in Appendix D.

Storm 21

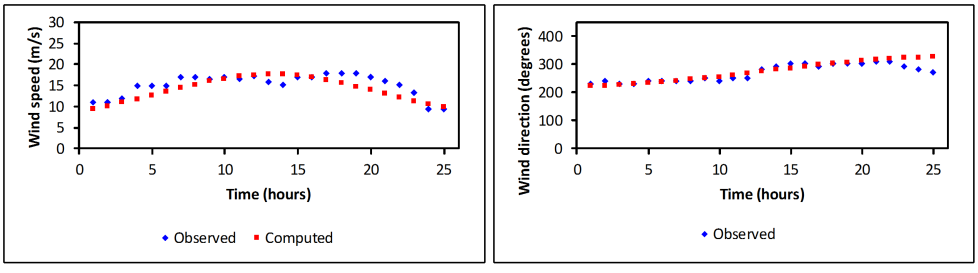

Figure 4.1: Wind speed and wind direction for the storm of 1 March 2008 (storm 21).

The computed wind speed matches the course of the observed wind speed. The storm peak is a bit underestimated, wind speed before and after the peak are underestimated. This can be explained by the fact that during this storm, multiple depressions succeeded one another. However, observed wind direction is described fairly well by the model.

4.2.3 Summary of the validation of the meteorological model

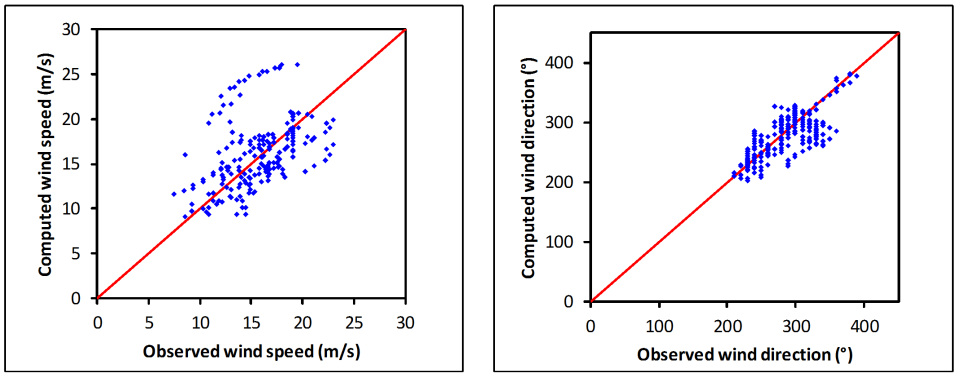

Figure 4.2: Scatter plots of computed data with respect to observed data.

Figure 4.2 shows all data (25 data points per storm) of the eight storms in two plots. The red line ($y = x$) presents the line of equality. The scatter for both plots shows that the agreement is far from perfect. Especially the two storms of 1962 contribute to this deviation. It should be noted that the current validation is only valid for one single point at the far end of the transect (near Hoek van Holland). It therefore not known how the model performs for other places at the transect. However, for many storms, the results are very good for such a simple model of the complex meteorological processes.

4.3 Calibration of the coupled model

For all storms of the dataset, the computed surge levels will be compared with observed surge levels. A calibration factor will be determined to minimize the deviation between computed and observed surges. In this way, the whole model is calibrated in one step, instead of calibrating the meteorological model and the hydrodynamical model separately.

4.3.1 Calibration data

Calibration is done by comparing observed and computed free surface elevations. However, the tidal signal is also included in observed water elevations but is excluded in the computed data. This tidal signal can be computed

for many places around the world for all periods in time, using harmonic analysis. This computed tidal signal is subtracted from the observed data. The computed tidal signal does not include relative sea level rise. Therefore the tidal signal for events in the past is adjusted. By simply subtracting the computed tidal signal, tide-surge interactions as described are neglected. It is assumed that these interactions can be neglected so no adjustment is made. In this section 1) observed data, 2) tidal data and 3) relative sea level rise will be discussed.

Observed water elevations are provided by storm reports (De Jong, 2012) and given in m +NAP. The data are given for Hoek van Holland. Data resolution is in cm. The time of the peak of the surge is also given in the storm reports.

Tidal signal for the moment of the peak of the surge is calculated by using Delft Dashboard software (Deltares, 2013). This software includes the XTide database (Flater, 2013). With the XTide database, the tidal signal has been computed for Hoek van Holland. Different bathymetrys are available, of which 'RWS vaklodingen', with NAP as datum, is used. Data resolution is in cm.

Relative sea level rise (y_{slr}) is calculated by following equation (4.1), as a single number per year (T). This number represents the rise of the sea level in m, compared to 2009 with NAP as datum. This relation is used by Rijkswaterstaat (unpublished) and is a modified version of a relation described by Dillingh et al. (1993). For surge number 1, this the relative sea level rise is 0.028 m.

$$y_{slr}(\mathrm{m}) = \begin{cases} -\left(0.12 \cdot (2009 - T) + 16.8\right)/100 & \text{for} \quad T < 1965, \\ -16.8/100 & \text{for} \quad T = 1965, \\ -\left(0.33 \cdot (2009 - T)\right)/100 & \text{for} \quad T > 1965. \end{cases} \tag{4.1}$$

4.3.2 Method

The model is calibrated by using a dimensionless calibration factor $C(-)$. This factor is defined as the ratio between observed water levels and computed water levels:

$$\zeta_{calibrated} = C \cdot \zeta_{raw}. \tag{4.2}$$

The calibration factor is a function of the six storm parameters. This function uses seven calibration constants and is defined as follows:

$$C = \alpha_0 + \alpha_1 \frac{\psi}{\psi_0} + \alpha_2 \frac{C_{fm}}{C_{fm_0}} + \alpha_3 \frac{\phi - \phi_{01}}{\phi_{02}} + \alpha_4 \frac{p_c}{p_{c0}} + \alpha_5 \frac{R_{max}}{R_{max0}} + \alpha_6 \frac{B}{B_0} \quad (4.3)$$

The zero-subscript parameters are used for a scaling procedure. They are based on the maximum values of the storm parameters of the database. In this way, the calibration constants have all the same order of magnitude. By varying the calibration constants, a value for the calibration factor is calculated for each storm. This factor is compared to the ratio between the observed and the computed surge (the so called preferred factor). Values for the calibration constants α_i are found by minimizing the sum of deviations between the preferred calibration factors and the calculated calibration factors. This is done with Generalized Reduced Gradient non-linear optimization techniques in the Excel software package. Other functions to determine the calibration factor, like non-linear functions, did not lead to better results.

The regression yields the following values for the calibration constants, shown in Table 4.2.

Storm parameter	**Calibration constant**	**Value**	**Normalizing constant**	**Value**
	α_0	-20.0944	-	-
ψ	α_1	1.0939	ψ_0	66.4°
C_{fm}	α_2	-0.4838	C_{fm_0}	26.1 m s^{-1}
ϕ	α_3	0.0108	ϕ_{01}	347°
			ϕ_{02}	-9.9°
p_c	α_4	20.4751	p_{c0}	99000 Pa
R_{max}	α_5	1.2854	R_{max0}	$1158 \cdot 10^3$ m
B	α_6	-0.8769	B_0	2.3

Table 4.2: Complete overview of all storm parameters of all storms used in this research.

4.3.3 Results for maximum surge heights

The maximum surge heights for the 21 storms before and after calibration are presented in Figure 4.3.

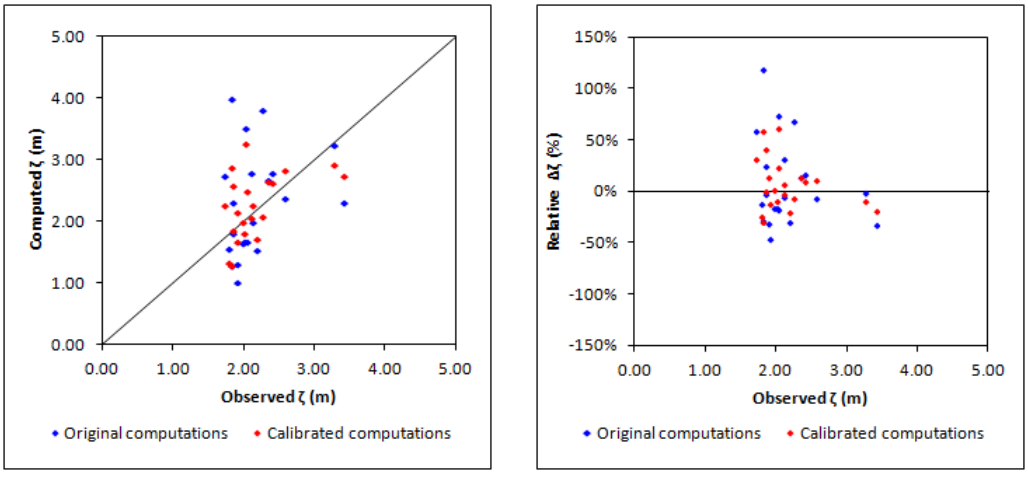

Figure 4.3: Left: Scatter plot with computed surge heights as function of observed surge heights. **Right**: Relative deviation of surge heights as function of observed surge heights.

The figures show that most of the computed peaks, without calibration, approximate the observed peaks. The scatter plot is distributed around line $y = x$, which represents a perfect computed surge. This means that on average, the model does not overestimate or underestimate the surges. However, a few outliers are clearly distinguished. It can be seen that due to calibration the absolute and relative deviations are reduced.

Table 4.3 shows that the largest relative deviation (of all surges) is decreased to 61%, compared to an overall largest deviation of 119% before calibration. On the other hand, for some surges the relative deviation is increased after calibration.

A quantity to measure the deviation between the model output and observations is defined as the averaged absolute relative deviation:

$$\mathrm{MD} = \frac{1}{n} \sum_{\mathrm{i}}^{n} |\mathrm{RD_i}| \tag{4.4}$$

where MD denotes the model deviation, RD the relative deviation, i the storm number and n the total number of storms. This model deviation only gives the averaged relative absolute deviation between the model output and observations, so it does not indicate model underestimation or overestimation. For the uncalibrated model, the model deviation is 31.3%, whereas for the calibrated model the model deviation is 19.2%. All in all, the results of this model are pretty good.

Although the effect of this calibration step is limited for these 21 storms,

Storm #	Observed ζ (m)	Original computations ζ (m)	Original computations Relative deviation	Calibrated computations ζ (m)	Calibrated computations Relative deviation
1	1.83	1.29	-29%	1.27	-31%
2	1.73	2.73	58%	2.25	30%
3	3.42	2.29	-33%	2.72	-21%
4	2.19	1.52	-31%	1.71	-22%
5	2.03	3.50	73%	3.27	61%
6	1.98	1.64	-17%	1.99	1%
7	1.91	1.01	-47%	1.66	-13%
8	2.58	2.38	-8%	2.82	9%
9	2.04	1.67	-18%	2.49	22%
10	1.90	1.30	-32%	2.14	12%
11	2.35	2.66	14%	2.64	13%
12	3.27	3.22	-2%	2.92	-11%
13	2.41	2.78	15%	2.61	8%
14	1.83	4.00	119%	2.87	57%
15	2.26	3.80	68%	2.08	-8%
16	2.11	2.77	31%	2.04	-3%
17	2.01	1.68	-17%	1.79	-11%
18	1.86	2.30	24%	2.58	39%
19	1.80	1.56	-13%	1.33	-26%
20	2.12	1.98	-6%	2.25	6%
21	1.86	1.81	-3%	1.84	-1%

Table 4.3: Computed surge heights before and after calibration, compared to observed surge heights.

the effect is larger when one calculates surges of extreme storms (see section 5.1.3): the surge level of a $1 \cdot 10^{-4}$ year^{-1} surge reduces, due to this calibration step, from 13 m to a more realistic 6 m.

4.3.4 Results for surge courses

For recent surges, water-level measurement data are available. With these data, it is possible to look at the development and course of the surge (the hydrographs).

Observational data

Observed water elevations are provided by Rijkswaterstaat (2013) and given in m +NAP. The data are given for Hoek van Holland. Data resolution is in cm, observation frequency is once per 10 minutes for data after 1980, once per hour for data between 1971 and 1980 and once per 3 hours for data before 1971. The observations are adjusted for the tidal signal and relative sea level rise by using the XTide database and equation (4.1).

Only for storms after 1980 the resolution of the observation data is high

enough to determine the development of a surge. Therefore, only storms 17 until 21 are used for validation of the model. The model input is described in section 4.1. The bathymetry used in the model is adjusted to relative sea level rise using equation (4.1).

Method

Observed and computed surge hydrographs are compared in a qualitative way. Next, the time for which the water levels are above a certain threshold is compared. This threshold is set to 75% of the observed peak water level.

Results

As stated before, the modeled surge is not computed to absolute time. There is a degree of freedom in shifting the storm surge in time. Therefore, the modeled surge is moved in time until the modeled and observed surges coincide. Results are presented with a time span of 24 hours around the peak of the surge. Only the results for storm 21 are presented here (Figure 4.4). The results of storms 17 until 20 are discussed in Appendix E.

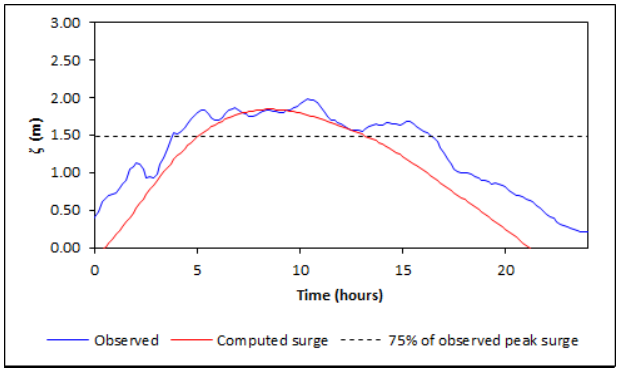

Figure 4.4: The observed and computed surge for the storm of 1 March 2008 (storm 21).

On average the observed surge is a bit higher than the computed surge, the rise and fall of the surges show good agreement with the observations. The observed surge level is 12.67 hours above the threshold of 1.49 m, compared to 8.17 hours for the computed surge.

The time for surges to exceed a threshold of 75% of the observed peak surge height is presented in Table 4.4. It is clear that surge duration is underestimated by the model.

Storm	Observed duration (hours)	Computed duration (hours)	Deviations
17	8.67	4.67	-46%
18	9.67	8.50	-13%
19	9.83	0.00	-100%
20	11.67	10.33	-11%
21	12.67	8.17	-36%
Total	**52.50**	**31.67**	**-40%**

Table 4.4: The time for surges to exceed a threshold of 75% of the maximum observed surge height.

4.3.5 Summary of the calibration of the coupled model

The coupled model is calibrated using seven calibration constants.

The effect of the calibration step on computed peak surge heights is positive: the largest relative deviation is reduced to 61%, compared to an overall largest deviation of 119% before calibration. For the uncalibrated model, the model deviation is 31.3%, whereas for the calibrated model the model deviation is 19.2%. On average, the model does not underestimate or overestimate peak surge levels.

Although peak surge levels are computed well, computed water levels before and after the peak are underestimated compared to observations. This is most likely due to the forcing of other storms and pressure fields, which are not included into the model. The result is that duration of the surges is underestimated by the model. The averaged underestimation of 5 surges is as much as 40%.

A reason for deviations between model output and observations could be the quality of the input data, obtained by De Jong (2012), and the exact time of the peak of the surges, also given by de Jong. The points in time are used to calculate the tidal signal. An error of 2 hours can already make a huge difference for the free surface elevation used as validation data. It is impossible to verify these data, since they are not available. The uncertainty of model input is high for certain storm parameters, which is presented in section 4.4.1. Chapter 6 (Discussion) elucidates quality of the input data. Of course, the other reason for the deviations in validation is the quality and simplicity of the model. Finally, tide-surge interactions are not taken into account during the calculation of observed water levels. The real storm surge set-up is therefore unknown and could differ from the observations used in this section. This is also discussed in Chapter 6.

4.4 Assessing model sensitivity

The sensitivity of the calibrated model is analyzed following Janssen & Rotmans (2004). First, the uncertainty of the input parameters and the uncertainty in bottom friction and bathymetry are determined. Second, the sensitivity of the model results to the input data is assessed. The parameters for which the input are qualified as highly uncertain and for which the model is most sensitive, have the largest contribution to the uncertainty of the model results. The sensitivity of the model to the track location is determined as well. Uncertainty in model input (concerning transect location) is not determined, since there is no uncertainty in the track location (it is a model choice).

4.4.1 Quantification of uncertainty in model input

Uncertainty in model input will be discussed here. It is impossible to describe uncertainty in quantitative way, caused by the way input data are obtained. Therefore, uncertainty is qualified by using three levels: high, medium and low.

Storm parameters

The storm parameter values are obtained by De Jong (2012).

Storm track location ψ at 5.5° eastern longitude is determined using weather charts. The latitude at that exact longitude is often not shown in the charts (that would be a coincidence), but is obtained from linear integration of the two closed given locations. Because the storm tracks are mostly linear, the uncertainty in the storm track location is qualified as **low**.

Propagation speed C_{fm} is determined by the time it took for a storm to travel between two boundaries. Those boundaries are located at 5.5° and 12.5° eastern longitude. Elapsed time and locations are taken from the weather charts. Because forward speed is more or less constant, the uncertainty in the forward movements of storms is qualified as **low**.

Direction of storm track ϕ is taken from the weather charts, as the averaged direction between the two boundaries. Because variation in direction is small, the uncertainty in the storm direction is qualified as **low**.

Central pressure p_c is not given by the weather charts. De Jong (2012) estimates the central pressure by assuming a linear slope of the pressure field near the storm center. The slope of the pressure field is extrapolated to obtain a value for the cental pressure. Due to this approximation, the uncertainty in the storm central pressure is qualified as **medium**.

Radius to maximum winds R_{max} is obtained from weather charts. However, the exact distance is not given in weather charts. Next, this value can vary per direction. Therefore, the given values are a rough estimate and thus the uncertainty of the radius to maximum winds is qualified as **high**.

Holland-B parameter values are determined by using the radius to maximum winds, because a weak correlation between Holland-B and the radius to maximum winds is found. De Jong (2012) found a linear relation with a Coefficient of determination (R^2) of 0.51. Because there is a high level of uncertainty in the radius to maximum winds and due to this weak correlation, the uncertainty in the Holland-B parameter is qualified as **high**.

Bottom friction

Bottom friction is implemented by using a constant Manning roughness coefficient n (see equation (3.15)). This coefficient is mainly used for modeling water flow in open channels. However, it also used in models of the North Sea (Prandle, 1978). The value used in this study is based on expert knowledge and the study of Prandle. However, the exact values for the locations used in this present study are not known. Therefore, the uncertainty in bottom friction is qualified as **medium**.

Bathymetry

Bathymetry is obtained from a dataset of the British Oceanographic Data Centre with quite a high resolution, see section 3.3 (Van den Brink, 2013). However, it not known how these data are obtained. Therefore, the uncertainty in bathymetry is qualified as **medium**.

4.4.2 Sensitivity analysis

The effect of variations in model input on the model outcome is investigated. When assessing sensitivity of the model to changes in bottom friction and

bathymetry, the model is not calibrated again. This means, that the sensitivity of the model as used in this specific research, is assessed.

Input data

A default value for the input parameters is determined. Input will be slightly changed around this default value. This is based on the historical dataset for the storm parameters and default model input for bottom friction and bathymetry. An extensive description of the input data is described in Appendix F.

Storm parameter input data are taken from probability functions, given by De Jong (2012). These functions are based on the historical dataset, see Table 4.1. The default values for the storm parameters are the mean values. Next, input is varied independently by taking parameter values according to probabilities of occurrence of -20%, -10%, +10% and +20% from the mean values.

Bottom friction is determined by equation (3.15), using Manning's n roughness coefficient. The default value for this coefficient is 1/40 $\mathrm{m}^{\frac{1}{3}}\mathrm{s}^{-1}$. For the sensitivity analysis, input is determined by using expert knowledge. Input is as follows: 1/30 $\mathrm{m}^{\frac{1}{3}}\mathrm{s}^{-1}$, 1/35 $\mathrm{m}^{\frac{1}{3}}\mathrm{s}^{-1}$, 1/45 $\mathrm{m}^{\frac{1}{3}}\mathrm{s}^{-1}$ and 1/50 $\mathrm{m}^{\frac{1}{3}}\mathrm{s}^{-1}$.

Bathymetry is given in Figure 3.10. The sensitivity of the model to changes in bathymetry is determined by using linear approximations of this bathymetry. A linear profile is found using a simple regression technique. Next, this linear slope is increased and decreased by 5%. Finally, the height of the whole (linear) slope is increased and decreased by 5% of the height at the coast.

The transect The sensitivity of the model to the location of the transect is determined by adjusting the length of the transect by -10% and +10%, and by varying the angle of the transect with -10° and +10°.

Results

The surge at Hoek van Holland for the default parameter values is computed. For all other input sets, surge heights are compared to this default surge. It should be noted, that the outcome of this analysis, depends on the storm parameter values used as default values. For example, when more extreme parameters values are chosen as input for the sensitivity analysis

instead of the current averaged values, results will be different. However by using averaged input values, results do have certain meaning. Sensitivity is qualified in a qualitative way using the plots of the results, by using three levels: high, medium and low. Reference values to qualify model sensitivity are used and shown in Table F.3. Extensively discussed results and figures are presented in Appendix F.

Storm parameter's effect on model sensitivity is shown in Figure F.3. For the parameter central pressure p_c, the sensitivity is qualified as **low**. Sensitivity is qualified **medium** for the the propagation speed C_{fm}, the direction of storm track ϕ, and the radius to maximum winds R_{max}. The model is sensitive for the latitude ψ and Holland-B parameter, so the sensitivity is qualified as **high**.

Bottom friction's effect on the sensitivity of the model is shown in Figure F.4. It is qualified as **medium**.

Bathymetry's effect on model sensitivity (Figure F.5) is qualified as **medium**. Model outcome with the five linear slopes is compared to the original model outcome.

The transect location's effect on the location of the transect on the model results are shown in Figure F.6. The angle of the transect has a **small** influence on the surge height. The influence of 10% increase and the decrease of the length of the transect on the computed surge height is qualified as **medium**. Apparently, a longer fetch results in higher surges.

It should be noted that for a new track location, the model must be calibrated again. Thus, the calibration factor depends on the transect location. When the model with a different transect location is calibrated, the effect on the model outcome is minimal and qualified as **low**. Calibration results for the four different transects are found in Appendix F.3.

4.4.3 Summary of assessing model sensitivity

The model is most sensitive for storm track location and the Holland-B parameter. These parameters are, most likely, the most determinative for the calibration constant as presented in section 4.3.2. It could be investigated to bring down the number of calibration constants by excluding the storm

parameter for which the model is least sensitive (which is central pressure). This is however not researched in this study.

The results of the sensitivity analysis are shown in Figure 4.5. The Holland-B parameter and, to a lesser extent the radius to maximum winds has the largest contribution to the uncertainty of results obtained by the model. Improving the model results should start with a better understanding of these parameters. The transect location is not included in this matrix, because there is no associated uncertainty in input.

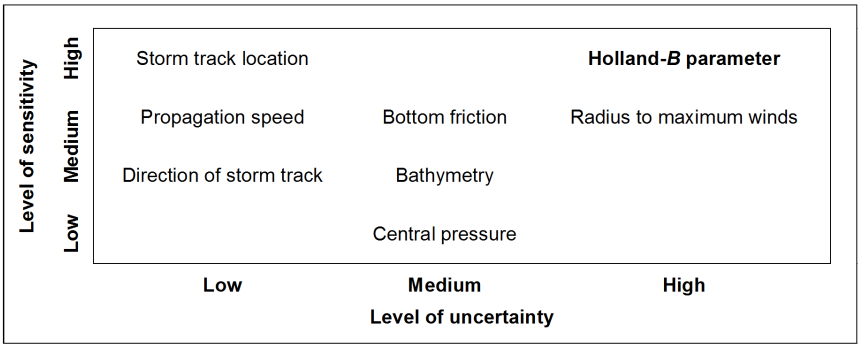

Figure 4.5: Matrix of the uncertainty and sensitivity of the input parameters, following Janssen & Rotmans (2004).

4.5 Conclusions

Model calibration, model validation, and model sensitivity are discussed in this chapter.

The meteorological model is validated for the course of wind speed and wind direction on one measurement location using eight storms. Focus is on the trend in results and to a lesser extent on absolute values and results are good for such a simple model. Deviations before and after the peak are a result of the influence of other storms and depressions, which are not incorporated in the model.

The coupled model is calibrated using 21 historical surges. The most extreme deviation in computed surge height reduces from 119% to 61%. For the calibrated model the model deviation is 19.2%. For 15 of the 21 surges, only two surges differ more than more than 10% after calibration. On average, the model does not underestimate or overestimate peak surge levels. Surge duration is overestimated by the calibrated model. This overestimation is on average 40% for the last five surges.

Sensitivity in model input is qualified in three levels. The highest uncertainty is in the Holland-B parameter and in the radius to maximum winds. A sensitivity analysis on the calibrated model shows that the model is most sensitive for the storm track location and the Holland-B parameter. Improving the model should start with better understanding of these parameters. The sensitivity of the calibrated model to the location of the transect is medium for the length of the transect and low for the angle of the transect.

The model with different transects is calibrated again. Differences in model outcome, compared to the original model, are minimal. This is an important conclusion, since this means that the transect location does not have a large effect on model results, due to the calibration step.

Now the model is validated, calibrated and the model sensitivity is known, Monte Carlo calculations will be done to analyze extreme surges. This is presented in the next chapter.

Chapter 5

Monte Carlo analysis

The model, discussed in the previous two chapters, is used for a Monte Carlo analysis. A Monte Carlo analysis consists of many runs of the same model. Model input is chosen using probability distributions. For this study, 1,000,000 surges are computed. For each surge, the associated return period is determined. This is discussed in the first section. The second section covers the differences in storm parameters values of surges with different return periods. The last section discusses the duration of $1 \cdot 10^{-4}$ year surges. Surges with this return period are of interests, because coastal protection at Hoek van Holland is designed to withstand such a surges. This chapter answers the last research question, stated in section 1.4.

5.1 Computation of extreme surges

Using Monte Carlo techniques, 1,000,000 surges will be computed. The associated return periods will be computed. The reason for this large amount is that it results in a large number of surges with extreme return periods, which will be analyzed in this section. Accuracy of the surge height associated with extreme return periods is not the reason for this large number. The surge height associated to a $1 \cdot 10^{-4}$ year^{-1} event does not differ significantly from the result of calculations of 50,000 surges. This calculation of return periods is presented here.

5.1.1 Model input

Probability distributions are given for the storm parameters by De Jong (2012), based on the dataset of 21 historical storms which will be used in

the present work. Of these storms, only the 18 storms after 1900 are used, due to availability of data. These distributions are already used for the sensitivity analysis, see section 4.4.2. The way probability distributions are derived is discussed in Chapter 6. Dependency exists between R_{max} and the Holland-B parameter. The following relation is given:

$$B = \left(R_{max} \cdot 1.4 \cdot 10^{-6} + 0.33\right) \cdot \epsilon \tag{5.1}$$

where ϵ represents the 95% confidence interval for values for B. The quantity ϵ has a normal distribution with $\mu = 1$ (-) and $\sigma = 0.175$ (-). Storm track direction ϕ is given in cardinal degrees with 270° (West) as reference. A complete overview of the probability distributions is given in Table 5.1.

Storm parameter	**Probability distribution**	**Mean**	**Standard deviation**
ψ (°)	Lognormal	58.61	2.6
C_{fm} (m/s)	Lognormal	14.67	5.25
ϕ (°)	Rayleigh	22.46	-
p_c (mbar)	Normal	975	15.05
R_{max} (km)	Lognormal	668	236
B, given by ϵ (-)	Normal	1	0.175

Table 5.1: Input for the Monte Carlo analysis

These probability distributions are used to set up an input database of 1,000,000 storms. Per storm, the storm parameter values are all independently chosen, except for the values of B. Surges according to the storm parameter values are computed and are adjusted for 1) the tidal signal and 2) the averaged water level:

Tidal signal is assumed to be a constant value for all storms. This assumption follows the method used in the hydraulic boundary conditions (Ministerie van Verkeer en Waterstaat, 2007). In this directive, the averaged tidal signal is added to the surge set-up, such that the maximum surge coincides with maximum tidal high water. Thus, the maximum total water level equals the averaged tidal amplitude plus the maximum surge level. The averaged tidal amplitude at Hoek van Holland is given by the *'slotgemiddelden'* (Rijkswaterstaat, 2011) and is 0.87 m.

Averaged water level at Hoek van Holland is 0.07 m +NAP. This value is used as reference level for the calculations.

5.1.2 Method

The model has run 1,000,000 times using the input dataset. For each peak surge level, an accompanying return period is determined using the methodology of Gringorten (Shaw, 1994). Shaw prefers to use this methodology over the methodology of Weibull. The methodology of Gringorten is very similar to the often used methodology of Weibull (Shaw, 1994), except for the second step, listed below. Differences in results are discussed in Chapter 6. The methodology of Gringorten consists of the following steps:

1. The computed surges are ranked descending;
2. A threshold is applied. A threshold value equal to the lowest observed surge is used, which is 2.28 m. Surges lower than this threshold are excluded;
3. $P(X)$, the probability of a surge equaling or exceeding X in any given year, is calculated by (Gringorten, 1963):

$$P(X) = \frac{r - 0.44}{N + 0.12} \tag{5.2}$$

   where r is the rank number of the surge, X a surge level (m) and N the total number of surges;
4. The probability of underestimation $F(X)$ is calculated by:

$$F(x < X) = 1 - P(X); \tag{5.3}$$

5. The return period T is than computed by:

$$T(X) = \frac{F(X) - 1}{F(X)}; \tag{5.4}$$

6. The return period T is adjusted by a factor (108/18) for the fact that the input database consists of 18 storms, which occurred in a period of 108 years:

$$T_{Adjusted}(X) = T(X) \cdot \frac{108}{18}; \tag{5.5}$$

7. The adjusted probability of underestimation is defined by:

$$F_{Adjusted}(X) = \frac{T(X)_{Adjusted} - 1}{T_{Adjusted}(X)}. \tag{5.6}$$

5.1.3 Results

The surges and associated return periods are presented in a Gumbel plot. In this plot, surges are set out to adjusted probabilities of underestimation on the x-axis to cover extreme events in one clear figure. The probabilities are adjusted in the following way:

$$F_{Gumbel}(X) = -\ln\left(-\ln(F_{Adjusted}(X))\right). \tag{5.7}$$

Results are shown in Figure 5.1. A return period of 10,000 years equals an adjusted probability of 9.2. To associated surge height is around 6 m. Note that without calibration, discussed in section 4.3, the $1 \cdot 10^{-4}$ year surge would be 13 m.

Return periods for the 18 observed surges (including the tidal set-up), are calculated using the same procedure. With extreme value theory (Shaw, 1994), surge heights and associated return periods can be estimated for extreme situations. For this purpose, a Gumbel distribution is fitted to the 18 surges. The results and the 95% confidence limits are shown in Figure 5.1.

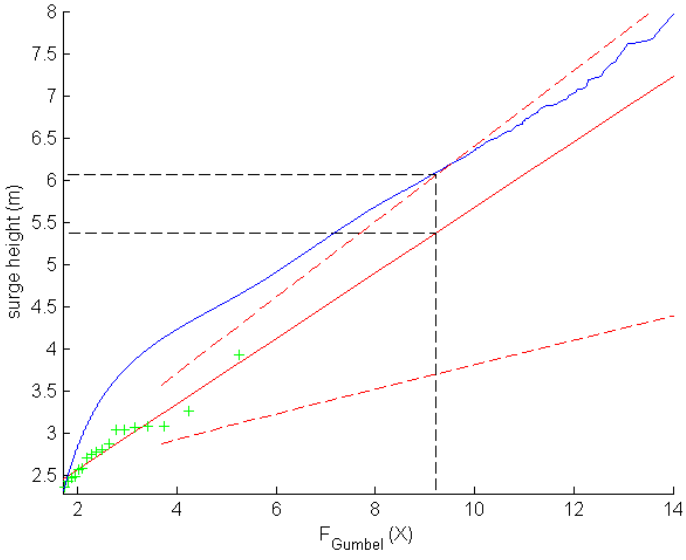

Figure 5.1: Modeled surges are denoted by the blue line and observed surges are denoted by the green crosses. The fitted Gumbel distribution is shown by the red line. The dashed red lines denote the 95% confidence limits of the extrapolation based on the observed surges. The dashed black lines represent the surges with a return period of 10,000 years.

Analyzing this figure, a few things stand out.

1. For surges with a relatively low return period, computed surge heights do not match with the observed surges. This cannot be explained easily, since the input data for the model are based on these observed surges. A possible explanation is given in Chapter 6.
2. The surge height including tide with a return period of 10,000 years is roughly 6 m according to the model results and 5.4 m with 95% confidence limits of 3.7 m and 6.1 m according to the extreme value theory applied to 18 observations. According to the hydraulic boundary conditions (Ministerie van Verkeer en Waterstaat, 2007), the surge height including tide is 5.10 m. Concluding, the surge height with a 10,000 year return period is most likely a bit overestimated by the model, since it falls outside the 95% confidence limits and is more or less 1 m higher than the currently used value.
3. When data are distributed by a Gumbel distribution, data in a Gumbel plot with adjusted x-axis would show a linear trend. This is the case with the observed surges, but is not the case with the modeled surges. The model results are thus not distributed by a Gumbel distribution. This has, however, no effects for this study.

5.2 Analysis of surges with different return periods

Due to the large number of computed surges, there are many surges with more or less the same height as the surge for a given return period. Storm parameter values of 100 of these surges will be compared to the distribution of the input database of 1,000,000 storms. This will be done for 5 different return periods: 10,000 years (Figure 5.2), 5,000 years (Figure G.1), 1,000 years (Figure G.2), 100 years (Figure G.3) and 10 years (Figure G.4). Results will be presented in histograms. Note that the distribution of the input database is shown on the left y-axis, the distribution of 100 storms is shown on the right y-axis.

5.2.1 Return period of 10,000 years

Following the model results, the surge height which occurs statistically once per 10,000 years is 6 m. Exact model outcome is 6.06 m, the range of 100

surges is between 6.04 m and 6.10 m. Figure 5.2 shows the histograms of storm parameter values.

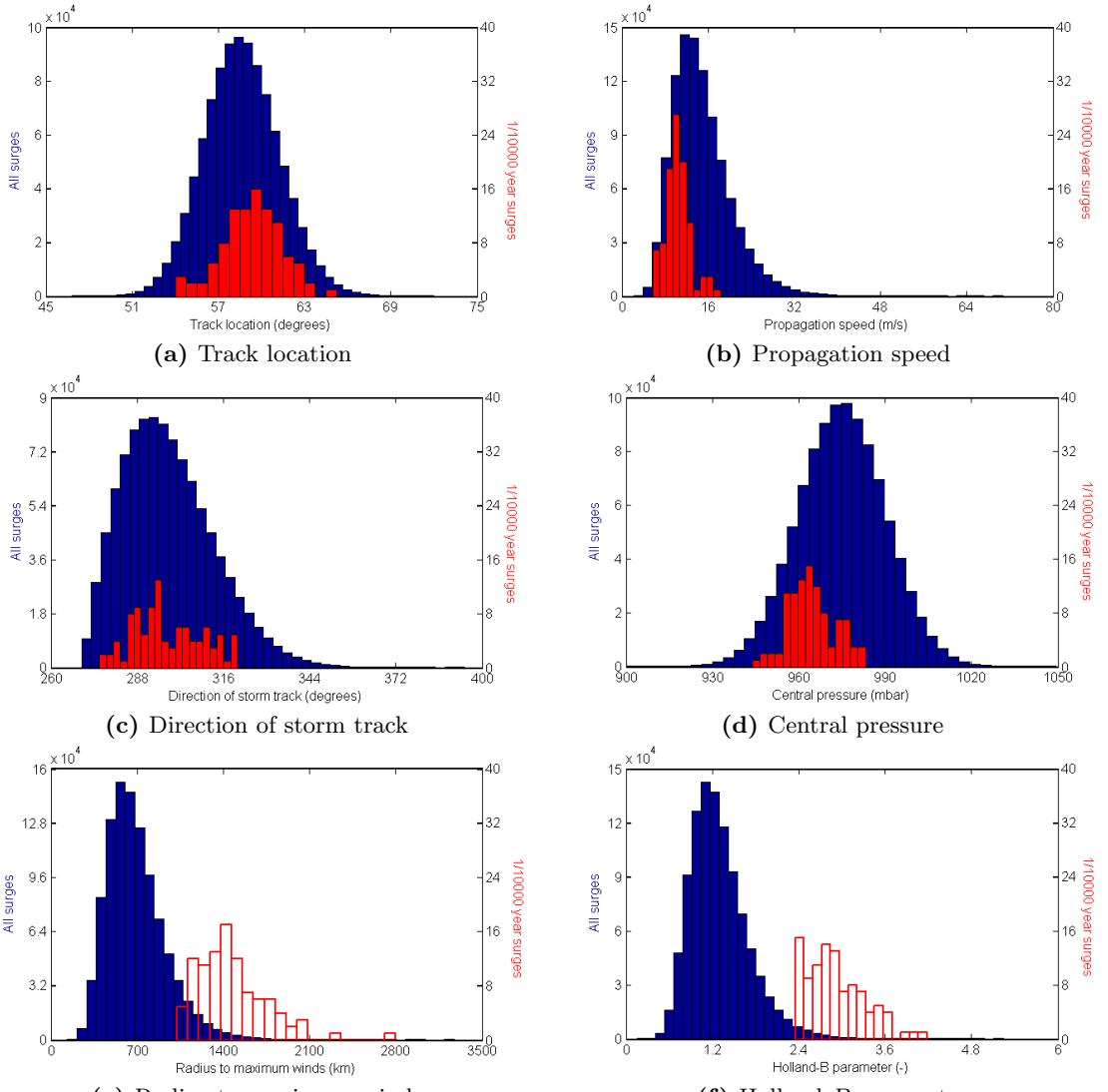

(a) Track location **(b)** Propagation speed

(c) Direction of storm track **(d)** Central pressure

(e) Radius to maximum winds **(f)** Holland-B parameter

Figure 5.2: Distributions of storm parameter values of all surges (in blue) and surges with a return period of ±10,000 year (in red).

The track location histogram of the set of 100 surges (Figure 5.2a) is a bit shifted towards higher values compared to the overall input. This means that storms causing these extreme surges, tend to occur a bit more towards to north.

Propagation speed distributions of the set of 100 storms (Figure 5.2b) are shifted towards lower values. The dataset of 100 storms does not contain high propagation speeds.

For storm track location a clear trend is absent (Figure 5.2c), although it looks like the direction of the set of 100 storms tends to be a bit more north-south oriented compared to the overall dataset.

Central pressure distributions of the storms causing the $1 \cdot 10^{-4}$ year^{-1} surges is shifted towards lower values (Figure 5.2d).

The radius to maximum wind speed histogram shows the most clear shift compared to the histogram of the input dataset (Figure 5.2e). The radius to maximum winds is (on average) larger than the input dataset.

Holland-B parameter distributions show another clear difference compared to the averaged input histogram. Values are larger than that of averaged storms.

5.2.2 Other return periods

Plots for surges with return periods of 5,000 year, 1,000 year, 100 year and 10 year are presented in Appendix G. The associated computed surge levels and the range of sets of 100 surges are presented in Table 5.2. Accuracy is given in m, because a higher level of accuracy cannot be given due to the many model assumptions.

Return period (years)	Surge height (m)	Exact model outcome (m)	Range of 100 surges (m)
10,000	**6**	6.06	6.04 - 6.10
5,000	**6**	5.82	5.81 - 5.84
1,000	**5**	5.26	5.25 - 5.26
100	**4**	4.44	4.44
10	**4**	3.61	3.61

Table 5.2: Return periods and associated surge levels, with the range of 100 storms close to those surges.

From Figures G.1 - G.4, it can be seen that the distributions of storm parameter values are between those of the $1 \cdot 10^{-4}$ year surge and the overall input dataset. The histograms of the $5 \cdot 10^{-3}$ year^{-1} surge are more like those of the $1 \cdot 10^{-4}$ year^{-1} surge, the histograms of the $1 \cdot 10^{-1}$ year^{-1} surge are almost the same as the histograms of the input dataset and the distributions of the $1 \cdot 10^{-2}$ year^{-1} surge are in between.

5.2.3 Summary of the analysis of surges with different return periods

The storms causing surges that occur more or less $1 \cdot 10^{-4}$ year^{-1} have large Holland-B parameter values and lower central pressures. This means, that these storms have stronger winds than average storms. This is as expected: strong winds and low atmospheric pressures result in large atmospheric forcing, which causes large surges. The radius of maximum winds of these storms is (very) large (an averaged value of 1,400 km). This is probably an effect of the model, since the Holland-B parameter and the radius to maximum winds are positively correlated. Too little is known about extreme storms on the North Sea, to say whether or not these values are realistic. The large radius to maximum winds is probably the reason that the track location of these storms is relatively far to the north (the averaged track location is close to Oslo, Norway). In this way, the maximum winds occur closer to the North Sea. The trend that the track direction of the extreme storms is slightly more north than averaged, results in a longer lasting atmospheric forcing on the North Sea than storms which head more in an easterly direction. The relatively low propagation speed can be explained by the fact that the forcing of these storms acts longer on the North Sea, which causes higher surges.

As mentioned in section 5.2.2, the storm parameter values of the storms which cause less extreme surges (i.e. surges with a lower return period) are in essence not different than the storms causing the $1 \cdot 10^{-4}$ year^{-1} surge. Those storm parameter values are only less extreme; the parameter values are closer to the averaged values of the input database.

5.3 Duration of $1 \cdot 10^{-4}$ year^{-1} surges

The 100 modeled storm surges with statistical return periods of closest to 10,000 years will be discussed in more detail. The development of these surges (the surge course) is determined by the model. Outcome is compared

to the surge course according to the hydraulic boundary conditions (Ministerie van Verkeer en Waterstaat, 2007). The tidal signal is excluded from this analysis.

5.3.1 Surge course according to the hydraulic boundary conditions

The surge course for a $1 \cdot 10^{-4}$ year storm surge is included in the hydraulic boundary conditions to design dikes. According to the hydraulic boundary conditions (Ministerie van Verkeer en Waterstaat, 2007), the course of the surge is symmetrical in time (the rise in surge level has the same shape as the fall in surge level). It is shown in Figure 5.3. The total time is 35 hours. For four hours around the maximum surge level, the course is a bit flat (only 0.10 m increase and decrease in 2 hours). For Hoek van Holland, the maximum surge level (level B in Figure 5.3) equals an 'assessment level' of 5.10 m (Ministerie van Verkeer en Waterstaat, 2007) minus an averaged tidal amplitude of 0.87 m (Rijkswaterstaat, 2011). The minimum surge level (level A in Figure 5.3) equals the averaged water level of 0.07 m (Rijkswaterstaat, 2011). This means that increase of the water level due to the surge is 4.16 m. When tide is included, the averaged tidal signal is imposed on the surge level, such that the maximum tidal level coincides with the maximum surge level.

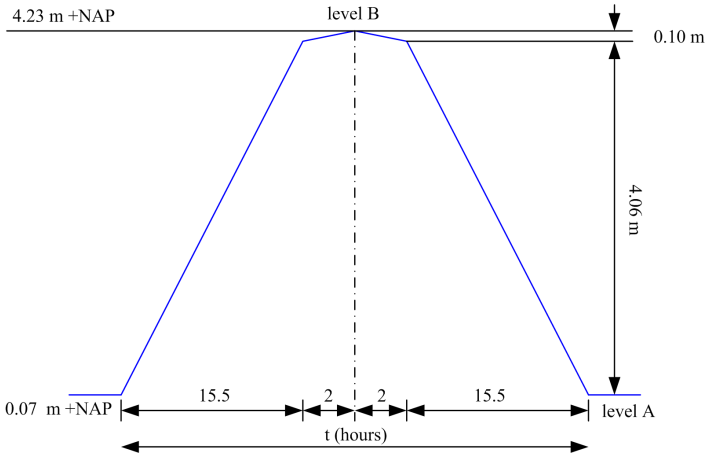

Figure 5.3: The course of a storm surge for Hoek van Holland, according to the hydraulic boundary conditions.

5.3.2 Hydrographs of $1 \cdot 10^{-4}$ year^{-1} surges

Surge levels will be presented without the tidal signal. The total surge height according to the hydraulic boundary conditions is 4.16 m, whereas the computed surges are about 5 m. Because the focus is on surge course and surge duration, rather than absolute surge heights, all surges are normalized. This done by dividing the surge courses by the surge's maximum. It follows from section 4.3 that surge duration is underestimated by 40%. Since this amount is based upon only 5 surges, there will be no correction for the surge duration. However, it should be kept in mind.

The normalized courses of the 100 surges and the surge course according to the hydraulic boundary conditions are presented in Figure 5.4. Note that only normalized water levels above 0.5 are shown, because lower water levels are of less interest. The surge courses are presented in such a way that all the peaks of the surges occur at $t = 0$ hours.

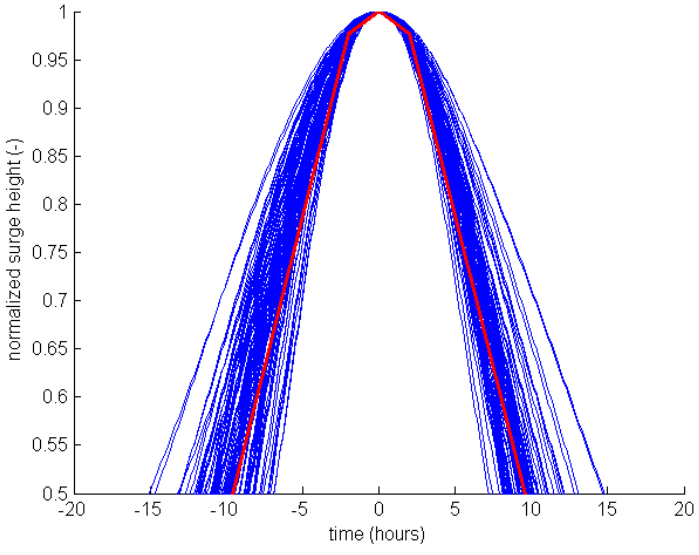

Figure 5.4: The courses of the 100 normalized modeled surges are presented in blue. The surge course according to the hydraulic boundary conditions is shown in red. Only water levels above 0.5 are shown.

In Figure 5.4 can be seen that, according to the model results, the duration of the surge given by the hydraulic boundary conditions is too short in time. When looking at high water levels, it can be seen that the time that water heights are above a certain threshold is longer (more or less two hours) for modeled surges than for the surge given by the hydraulic bound-

ary conditions. The lower part of the surges is of less interest, those water levels occur more often and are less important when considering extreme events.

5.3.3 Time to rise from and fall to 75% of the peak surge height

The time it takes for surges to rise from a certain water height to the peak water height (at $t = 0$ hours) and back to that certain water level can be presented in histograms. Figure 5.5 shows histograms for a relative water height of 75%. The x-axis denotes time, relative to the peak of the surges ($t = 0$ hours).

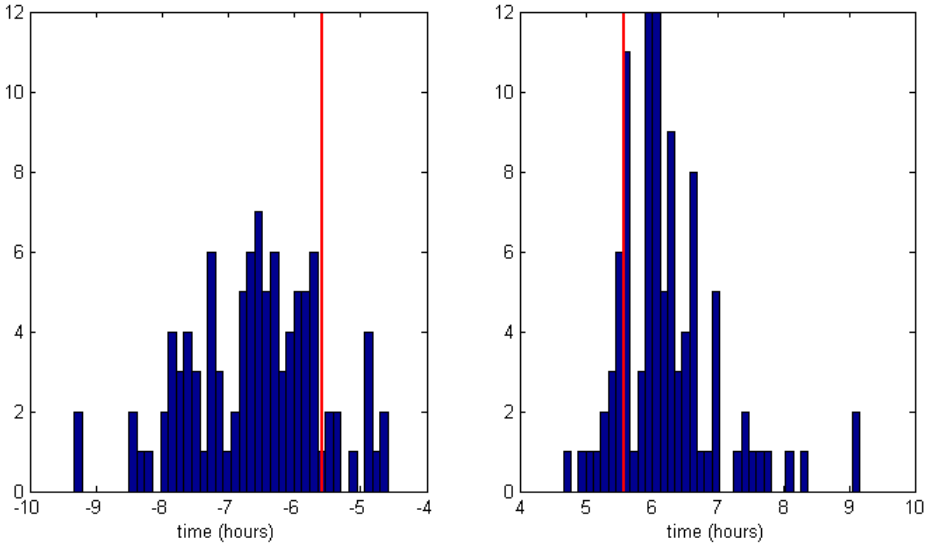

Figure 5.5: Histograms of the distributions of the time it takes for the water to rise (**left**) and fall (**right**) between 75% of the maximum surge height and the maximum surge height. This time span, according to the hydraulic boundary conditions, is shown in red.

It can be seen in Figure 5.5 that the distribution of the left plot is wider than that of the right plot. This means that, according to the model results, the time it takes for the water to rise has a larger spread than the time it takes for the water to fall. The time span of the surge according to the hydraulic boundary conditions is relatively short compared to the model results. The difference is more or less an hour, both for the rise of surge as for the fall of the surge.

These plots, however, do not give information about the total duration of the surges. Therefore, a histogram of the total time it takes to rise from 75% of the maximum surge height, to the maximum surge height and fall back to the 75% of the maximum surge height, is presented in Figure 5.6. It can be seen that the duration of the surge course, according to hydraulic boundary conditions, is too short. The difference is more or less two hours.

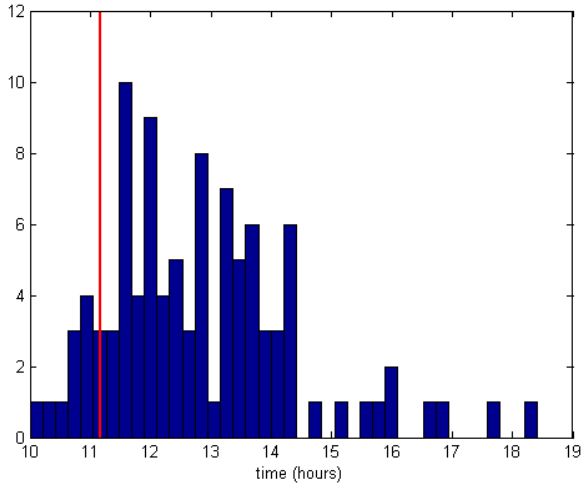

Figure 5.6: Histogram of the distribution of the total time it takes for the water to rise from and fall to 75% of the maximum surge height. This time span, according to the hydraulic boundary conditions, is shown in red.

5.3.4 Storm parameters values of short and long surges

The differences in storm parameter values of the 25 shortest and 25 longest surges of the set of 100 surges with a return period of 10,000 years (measured at a relative water height of 75%), are presented in Figure 5.7.

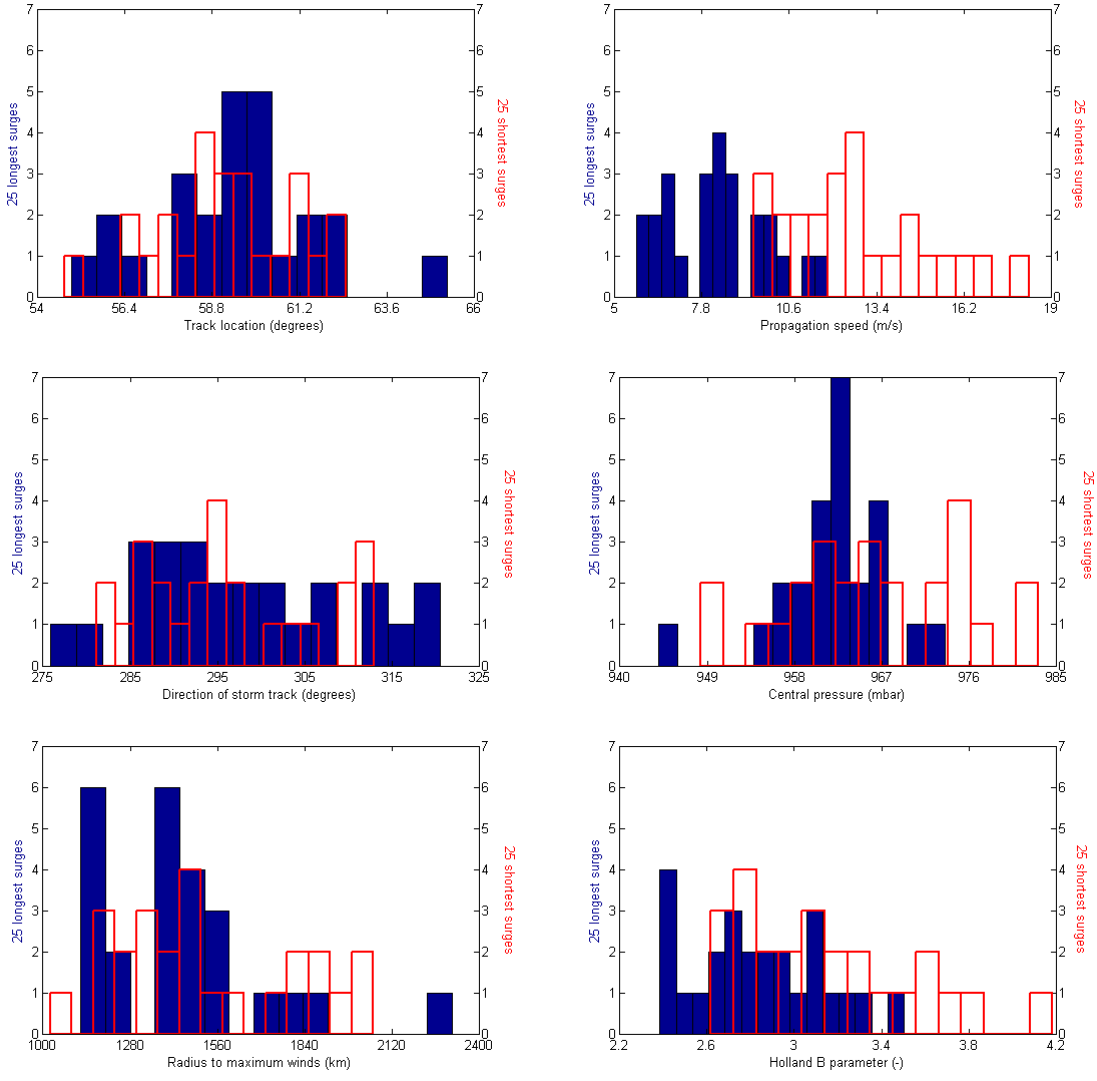

Figure 5.7: Distributions of storm parameter values of the 25 shortest and longest surges with a return period of ±10,000 years.

Differences in distributions of the storm parameter values can be seen for the propagation speed, the central pressure and the Holland-B parameter. For the other storm parameters, no clear differences can be seen. Differences,

for shorter surges, are a faster moving storm, a slightly less low central pressure and a higher Holland-B value. The faster movement of the storm is easily explained: the atmospheric forcing is acting for a shorter time on the North Sea, which results in a shorter surge duration. For the other two differences in the histograms there is no clear explanation.

5.4 Conclusions

With Monte Carlo analysis, 1,000,000 surges are computed. The surge level (including tide) with a statistical return period of 10,000 years is around 6 m (exact model outcome is 6.06 m), compared to 5.10 m according to the hydraulic boundary conditions used by Dutch government (Ministerie van Verkeer en Waterstaat, 2007). Extrapolation of the observed surges (21 in total) results in a surge level of 5.4 m, with a broad confidence interval (between 3.7 m and 6.1 m for 95% confidence).

The distribution of storm parameters values of $1 \cdot 10^{-4}$ year^{-1} surges are compared to the distributions of model input. The largest differences are found for the radius to maximum winds and the Holland-B parameter. Distributions of these two parameters are shifted towards larger values. Other, less clear differences, are that these extreme surges are caused by storms which are located a bit more to the north, travel slower and have a lower central pressure. Storm track direction tends to be, on average, a bit more north-south orientated. For storms with less high return periods, the trends in shifts of distributions of parameter values is the same, only less extreme.

The duration of computed surges with a return period of 10,000 years is, on average, more or less two hours larger than the design value of the hydraulic boundary conditions, especially for high water levels. This could be even more, since the model underestimates surge duration. Differences in storm parameter values for short and long $1 \cdot 10^{-4}$ year^{-1} surges are found in the propagation speed, the central pressure and the Holland-B parameter. Longer surges tend to have lower propagation speed, a slightly less central pressure and a lower value for the Holland-B parameter.

Chapter 6

Discussion

In the previous chapters the set-up of an idealized process-based storm surge model is presented. Next, model performance is analyzed using historical data. Finally, the model is used to determine surge heights of extreme surges. These surges have been analyzed. In this chapter, some important assumptions and model choices will be discussed. Model input based on previous research is discussed as well.

6.1 One dimensional hydrodynamical model

In order to perform a Monte Carlo analysis, model runtime needs to be low. Therefore it has been decided to model the hydrodynamical processes in a one dimensional (depth averaged) way. By doing so, several processes are ignored in the model. The effects of this decision are discussed in two sections: effects in the horizontal dimension and effects in the vertical dimension.

6.1.1 Effects in the horizontal plane

Problems

Three problems will be discussed here: 1) the forcing of surges to move along a single transect, 2) neglecting Coriolis acceleration and 3) amplification due to local geometry.

1. Only one transect is implemented into the model. The result is that all surges are forced to travel along this single transect. An assumption, based on the work of Voortman (2002), is that a surge will travel in the direction of dominant wind speed. This is not possible in this

model, due to the predefined transect. Thus, surges which are forced by a dominant wind direction at an angle with respect to the transect, cannot reach the coast at a point in accordance to this assumption. Instead, they are forced to the travel along the transect to reach Hoek van Holland which results in a different fetch length. For example, during westerly wind, the surge heading to Hoek van Holland start west of Hoek van Holland at the English coast. The associated fetch is much shorter than the transect in the model, which may result in a lower surge. This may explain why surges with relatively low return periods are much higher than the observed surges used as model input (see Figure 5.1). The calibration step performed in section 4.3 has partly taken care of this effect.

2. A second effect of neglecting the horizontal dimension is the absence of the Coriolis acceleration. The Coriolis acceleration is acting perpendicular (90° to the right) to the direction of the surge. This implies that surges moving along the transect should be deflected towards the west in the direction of the English coast.

3. Amplification due to local geometry is neglected in the horizontal dimension. Since the North Sea has more or less a shape of a triangle, the width of the surge front is decreased when moving south. However, the total energy is conserved (neglecting friction and forcing). The result is a higher total energy per unit width which results in higher surges. Surges could therefore be underestimated by the model.

Solutions

Besides the calibration step, in which the storm parameters (responsible for the direction of dominant winds) are used to determine the calibration factor, two other solution methods, not reported here in detail, have been investigated.

A solution for the first problem (the forcing of surges to move along a single transect) is the adjustment of the model. The model has been modified by implementing 6 different transects, with intermediate angles of 15°. The transects are shown in Figure 6.1.

When running the model the direction of the dominant wind speed is determined first. Next, the transect closest to this direction is used for the hydrodynamical model. For four transects the boundary condition at the open boundary should be adjusted, since it becomes a closed boundary. This is however not yet incorporated in the hydrodynamical model.

Figure 6.1: Six transects with an intermediate angle of 15°.

Calibration results indicate that this method needs to be improved. In Figure 6.2 the results for the 21 storms before and after calibration are shown. The model deviation before calibration is 41.8% and is 39.6% after calibration. The current calibration method does almost not improve results. It can be seen that both the results (before and after calibration) overestimate the surge levels. The calibrated model overestimates surges more than the uncalibrated model.

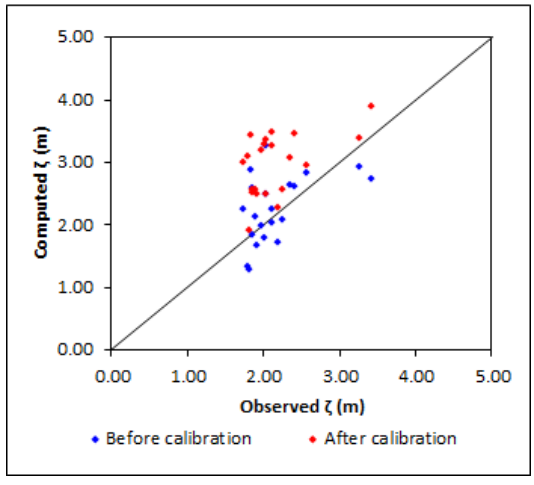

Figure 6.2: Calibration results of the model with six different transects.

A Monte Carlo analysis of 10,000 surges, shown in Figure 6.3, shows

that surges with relatively low return periods are still too high compared to the observations. The surge with a return period of 10,000 years is almost 8 m. However, this method should be investigated further before definite conclusions can be drawn.

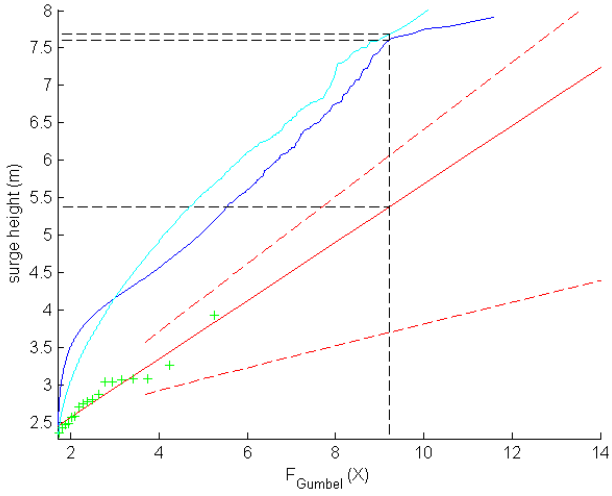

Figure 6.3: Gumbel plot of a Monte Carlo analysis for the model with multiple fetches. Results with the calibrated model are shown in blue, results without model calibration are shown in cyan.

To cover all three problems, a coarse 2DH-hydrodynamical model of the North Sea is set up in the Delft3D software package. This model covers all the processes which occur in the horizontal dimension. A disadvantage of 2DH-modeling is the long runtime. The meteorological model discussed in this research forces the 2DH-hydrodynamical model. The 21 storms, used for calibration and validation, were used as model input. Results are different compared to the 1D-model, but validation shows the same range in deviations. However, this solution should be deepened more before conclusions can be drawn. Results will therefore not be presented here.

6.1.2 Effects in the vertical dimension

Because the hydrodynamic processes are modeled in a depth-averaged way, bottom friction in the model is based on the depth-averaged flow. In reality, however, bottom friction depends on near-bottom flow. During a surge, a near-bottom return flow will occur (Gill, 1982). This return flow results in a bottom stress in the direction of the storm surge, increasing the surge even more (Resio & Westerink, 2008). By excluding this effect, surge heights could be underestimated. This effect could be included by using a 2DV-model or a 3D-model. A drawback of such models is (often) the long computation time.

6.2 Storm parameter values

The validation, calibration, and Monte Carlo analysis in this study are based on the storm parameters values of 21 historical storms (21 for calibration and validation, 18 for sensitivity analysis and Monte Carlo analysis), obtained from the work of De Jong (2012). Storm parameter values and the probability distributions will be discussed here.

6.2.1 Historical data

Even though storm parameter values have not been checked thoroughly, some results indicate that there might be some errors in this dataset. For example, the computed surge of 12 February 1962 (storm 14) is 4.00 m before calibration and 2.87 m after calibration, compared to an observed surge of 1.83 m (see Table 4.3). The associated radius to maximum winds is 1055 km (Table 4.1). This extreme large radius is checked on weather charts, where a smaller radius is found. This suggests that some research in obtaining storm parameter values needs to be redone. Focus should be on the Holland-B parameter and the radius to maximum winds, according to the sensitivity analysis. A first step is already made: p_c, Holland-B and R_{max} are redetermined by the method described in Appendix H.

Detailed results are presented in Appendix H. Two methods have been used to fit the Holland-B model to observations of weather maps: minimizing differences in atmospheric pressure and in atmospheric pressure gradients. The second method performs better on calibration (model deviation of 15.2%). There is no clear under- or overestimation of surge levels. A quick Monte Carlo analysis have been executed with newly determined probability distributions, without and with dependency between R_{max} and p_c. Espe-

cially for low return periods, water levels are closer to observations. It is suggested to extend this analysis, since results are promising.

6.2.2 Determination of probability distributions

The method to determine the probability distributions from the historical dataset is open for discussion. De Jong (2012) based the probability distributions of the storm parameters on 18 storms. These storms force the most extreme surges at the Dutch coast, so one can assume that these storms are extreme events. It is questionable whether it is statistically correct to predicate probability distributions, used to determine extreme conditions, upon these extreme events. Figure 6.4 illustrates an example for the central pressure distribution. For other storm parameters, like the forward movement, parameter values of extreme storms are not necessarily distributed in the tail of the distribution.

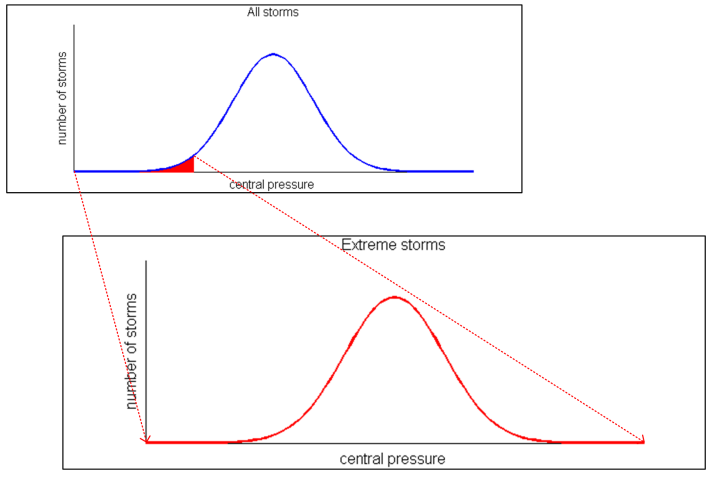

Figure 6.4: This figure shows the currently used method. The upper part of this figure represents the distribution of central pressure of all depressions (blue). A new probability distribution, used to predict *extreme* conditions, is based on the tail of the distribution of *all* depressions (red).

A different approach would be to determine the probability distributions for the storm parameters on all types of storms (mild storms, intermediate storms and severe storms) and to use these distributions to determine extreme conditions. This is illustrated in Figure 6.5.

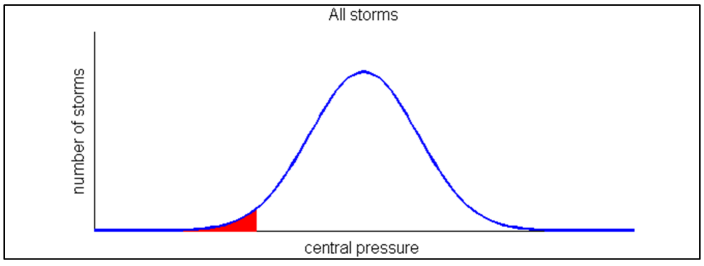

Figure 6.5: This figure shows the proposed method. The distribution of central pressure of *all* depressions (blue) is used to predict *extreme* conditions (red).

6.3 Methodology of Gringorten

The methodology of Gringorten (1963), used in section 5.1, is recommended by Shaw (1994) over the methodology of Weibull. Both methods are used for flood analysis Hirsch (1987). The difference between these two methods is the way the exceedance frequency $P(X)$ is calculated:

$$P(X) = \begin{cases} \dfrac{r}{N+1} & \text{Weibull,} \\ \dfrac{r-0.44}{N+0.12} & \text{Gringorten.} \end{cases} \tag{6.1}$$

where r is the rank number of the surge, X a surge level (m) and N the total number of surges (Gringorten, 1963; Hirsch, 1987).

The differences in results using both methods are shown in Figure 6.6. For the computed surges, differences are negligible and indistinguishable in the figure since the number N is large (1,000,000). For the observations, differences are more clear since the value of N is only 21. The extrapolated surge height based on observations is 5.8 m using Weibull and 5.4 m using Gringorten. This difference has no large consequence for this study.

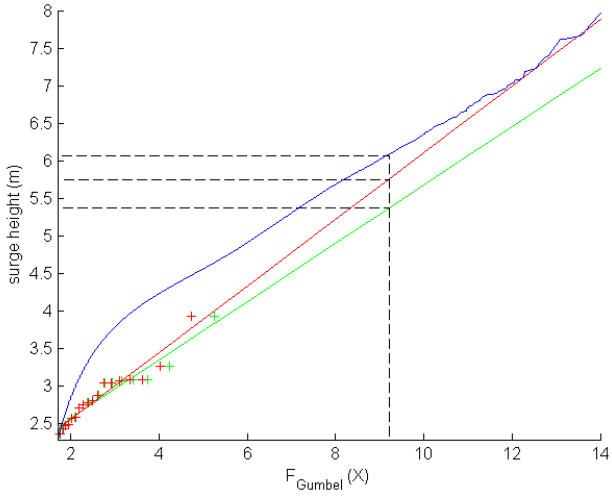

Figure 6.6: The computed surges are shown in blue. Differences in results are not visible. Results for observations using Weibull are denoted in red and using Gringorten in green.

6.4 Excluding tide

Storm surges are the non-tidal residual of excess sea levels. The combination of tide and surge level result in the observed water level, which is determined for coastal protection. In this research, tide is often excluded or simply superimposed on the surge level. However, by doing this, nonlinear tide-surge interactions are neglected. The tidal level which is superimposed is based on guidelines, which is another drawback of this method. Heaps (1983) found a deviation of approximately 0.1 m for tides in the North Sea, which is less than the accuracy of the model predictions presented in this thesis.

Tides and tide-surge interactions could be included by imposing the tidal signal (which can be calculated using tidal database as XTide) on the open boundaries in a 2DH-model. This also improves the computation of extreme surge levels, see section 5.1.

6.5 Simplicity of the storm field

The model used in this study computes surges with one single depression per storm as input. The depression has a circular atmospheric pressure field. This Holland-B model is suitable for modeling hurricanes. The rationale for choosing this model is that it uses only a few input parameters. In reality however surges on the North Sea are forced by extra-tropical storms, some-

times consisting of multiple consecutive depressions, with warm and cold fronts. These fronts affect the pressure and wind fields. The simplification of these storms in the model is a reason for deviations between computations and observations in model validation and calibration presented in this study. When more complicated pressure fields are implemented in the model, for example using the model of Bijl (1997), results of the Monte Carlo analysis would be different as well. However it will be hard to formulate probability distributions for all input parameters of these models. It is unknown whether surges are under- or overestimated by the currently used model.

6.6 Conclusions

The one-dimensional approach of the hydrodynamical model results in several drawbacks: the forcing of surges to move along a single transect, excluding Coriolis acceleration and partly excluding the amplification due to local geometry. Solutions for these drawbacks are the implementation of multiple transects and the use of a two-dimensional hydrodynamical model. The first solution is quickly analyzed and does not lead to better results, but more research is needed before clear conclusions can be drawn.

Research indicates that there is some error in the storm parameters values of the historical database. Three storm parameters have been redetermined for the historical storms. These new data improve both calibration and Monte Carlo results.

Differences in output of Monte Carlo analysis, using methodologies of Weibull and Gringorten, are discussed. Differences in model results are negligible, but results of extrapolation of water-level measurements show some differences.

Last, the exclusion of the tidal signal is discussed. Effects are most likely small compared to uncertainty in model outcome.

The next chapter presents final conclusions of this research and some recommendations.

Chapter 7

Conclusions and recommendations

This research focuses on extreme surges and the influence of storm parameters on extreme surges at the Dutch coast, through idealized process-based modeling. This final chapter presents concluding remarks by answering the research questions, posed in the first chapter. Recommendations will be given based on the answers to the research questions and the discussion, presented in Chapter 6.

7.1 Conclusions

1. What are relevant physical processes that need to be included in a model to predict storm surge events at the Dutch coast?

This question has been answered in Chapter 2. Storm surges are driven by the meteorological processes of a depression or multiple depressions. The complexity of multiple depressions per storm is circumvented by taking only one depression per storm into account. The depression has a life course which will not be incorporated in the model, because it is assumed that the storms are fully developed and do not change while passing the North Sea. On the other hand, the pressure field of the depression and the movement of the depression are implemented. Also the following processes are incorporated: gradient wind, the effect of friction on wind speed and direction and the influence of the depression movement on wind.

A storm surge is mainly driven by reduced atmospheric pressure and wind. Other factors also contribute to the forcing of a storm surge, like

buoyancy differences, storm-driven rainfall and waves. Only the first and second forcing processes are implemented. Internal processes of hydrodynamics are acceleration, advection, pressure gradients, vertical shear and stresses. Of these terms, only Coriolis acceleration and horizontal mixing of momentum are excluded. There are several other aspects which influence a storm surge: tide-surge interactions, sea level oscillations and amplifying due to funnel shaped geometry. Only amplification due to local geography is (partly) incorporated. The rise of a storm surge when reaching shallow water will be taken into account, but the horizontal effects on the other hand are not incorporated.

2. How can we formulate a coupled idealized process-based meteorological-hydrodynamical model suitable for the prediction of storm surge events at the Dutch coast?

This question has been answered in Chapter 3. The model uses six storm parameters to describe a storm. Those six parameters are storm track location, propagation speed, direction of storm track, central pressure, radius to maximum winds and the Holland-B parameter.

The one-dimensional hydrodynamical model is based on a single transect. This results in a relatively simple implementation of bottom stress and forces all surges to travel along the transect. This transect is located on the North Sea, from a point in the northern part halfway Scotland and Norway, towards the Dutch coast at Hoek van Holland. The transect is divided in 202 grid points, on which computations are made.

The meteorological model computes wind speed and atmospheric pressure for each grid point in an analytical way. The hydrodynamical model uses the atmospheric forcing to compute a storm surge. This is done using numerical approaches (Euler schemes and central space schemes).

3. How accurate does the model describe the storm surge characteristics (surge height and surge duration) of surges in the North Sea and which parameters of the model have a strong influence on these characteristics?

This question has been answered in Chapter 4, where model validation, model calibration and a sensitivity analysis are presented.

The meteorological model is validated for the course of wind speed and wind direction on one measurement location using eight storms. Results are

rather good for such a simple model. Focus is more on the trend in the results than on absolute values. Deviations between observations and model predictions before and after the peak might be a result of the influence of other storms and depressions, which are not incorporated into the model.

The coupled model is calibrated based on 21 historical surges using a calibration factor. This factor depends on the storm parameter values. The most extreme deviation in computed surge height reduces from 119% to 61%. For 15 of the 21 surges, only 2 surges differ more than more than 10% after calibration. The averaged absolute deviation of the calibrated model is 19.2%. On average, the model does not underestimate or overestimate peak. Surge duration is underestimated, on average 40% for 5 surges. surge levels. All in all, results are good.

Uncertainty in model input is qualified in three levels. The highest uncertainty is in the Holland-B parameter and radius to maximum winds.

A sensitivity analysis on the calibrated model shows that the model is most sensitive for the storm track location and the Holland-B parameter. Improving the model should start with better understanding of these parameters.

The sensitivity of the calibrated model to the location of the transect is medium for the length of the transect and low for the angle of the transect. When the model is calibrated again, sensitivity of the calibrated model with respect to the location of the transect is low. This means that the transect location does not have a large effect on model results, due to the calibration step.

4. What are the governing storm parameters affecting the storm surge characteristics for extreme conditions?

This question has been answered in Chapter 5. With Monte Carlo analysis, 1,000,000 surges are computed. The computed surge level (including tide) with a statistical return period of 10,000 years is 6 m, compared to 5.10 m according to the hydraulic boundary conditions used by Dutch government. Extrapolation of the observed surges (21 in total) results in a surge level of 5.4 m, with a broad confidence interval (between 3.7 m and 6.1 m for 95% confidence).

The distribution of storm parameters values of $1 \cdot 10^{-4}$ year^{-1} surges are compared to the distributions of model input. The largest differences are found for radius to maximum winds and Holland-B parameter. Distributions of these two parameters are shifted towards larger values. This means that

these storms are (very) large with strong atmospheric pressure gradients. Other, less clear differences, are that these extreme surges are caused by storms which are located a bit more to the north, travel slower and have a lower central pressure. Storm track direction tends to be, on average, a bit more north-south orientated. For storms with less high return periods, the trend in shifts of distributions of parameter values is the same, only less extreme.

The duration of computed surges with a return period of 10,000 years is, on average, more or less two hours larger than the design value of the hydraulic boundary conditions, especially for high water levels. This could be more since the model underestimates surge duration. Differences in storm parameter values for short and long $1 \cdot 10^{-4}$ year^{-1} surges are found in the propagation speed, the central pressure and the Holland-B parameter. Longer surges tend to have lower propagation speed, a slightly less central pressure and a lower value for the Holland-B parameter.

7.2 Recommendations

Further research, based on this study, should start by improving the input dataset. The storm of 12 February 1962 suggests that not all storm parameter values are correct. This affects model calibration, validation, and the probability distributions used for Monte Carlo analysis. A first start on this topic has already been made. Next, it should be checked whether probability distributions used to model extreme conditions can be based on extreme storms.

Next, the model can be extended to two dimensions (a 2DH-model), to incorporate the hypothesis stated in the previous chapter that surges will travel in the direction of dominant wind speeds. This may improve results for relatively low return periods. A drawback of this approach is increasing computation time.

Third, tide-surge interactions could be implemented by imposing the tidal signal on the model domain boundaries. This way results will include the tidal signal. This gives a better estimation of the surge heights according to the norms then the method used in this study. The course of the combined tide-surge levels can be researched to gain better insight in the duration of surges.

Fourth, the importance of the increasing effect of surges due to bottom friction can be studied by comparing the results of this study with 2DV-model results. When this effect turns out to be significant, it should be

incorporated in further research in line with this study.

Last, it is not the purpose of this research to predict extreme water levels with high accuracy. It is not recommended to use this method to predict water levels for extreme conditions, since the methods currently used to determine the hydraulic boundary conditions exceed this method in accuracy. However, more information on surge duration can improve the design of coastal defenses and this type of research can provide this. Maybe, one time, we can predict surge duration of extreme surges with the same accuracy as the height of those surges.

Bibliography

Amorocho, J. & DeVries, J. J. (1980). A new evaluation of the wind stress coefficient over water surfaces. *Journal of geophysical research*, *85*(C1).

Arcement Jr., G. & Schneider, V. (2000). Guide for selecting manning's roughness coefficients for natural channels and flood plains. Technical report, USGS.

As-Salek, J. (1998). Coastal trapping and funneling effects on storm surges in the Meghna estuary in relation to cyclones hitting Noakhali-Cox's Bazar coast of Bangladesh. *Journal of Physical Oceanography*, *28*(2), 227–249.

Bijl, W. (1997). Impact of a wind climate change on the surge in the southern part of the north sea. *Climate Research*, *8*.

Bode, L. & Hardy, T. (1997). Progess and recent developments in storm surge modeling. *Journal of Hydraulic Engineering*, *123*.

Brown, E., Colling, A., Park, D., Philips, J., Rothery, D., & Wright, J. (1999). *Waves, tides and shallow-water processes*. The Open University.

Brunt, D. (1934). *Physical and dynamical meteorology*. Cambridge University Press.

De Jong, M. (2012). Developing a parametric model for storms to determine the extreme surge level at the Dutch coast. Master's thesis, Delft University of Technology.

Deltacommisie (1960). Eindrapport en interim adviezen van de deltacommissie. Technical report, Rijkswaterstaat.

Deltacommisie (1961). Rapport deltacommissie. deel 4. bijdragen 3: Beschouwingen over stormvloeden en getijbewegingen. Technical report, Rijkswaterstaat.

Deltares (2013). Delft dashboard. `https://publicwiki.deltares.nl/display/OET/DelftDashboard`.

Deltares & Witteveen+Bos (2010). Criteria voor toepassing bekleding waterkeringen. hulpmiddel voor ontwikkeling van innovatieve dijkbekledingen. Technical report, Deltares, Witteveen+Bos.

Deutschen Wetterdienstes (1984). Weather chart. `http://www.knmi.nl/samenw/hydra/extremes/d19840114/dwd1984011412.gif`.

Dillingh, D., de Haan, L., Helmers, R., Können, G., & van Malde, J. (1993). De basispeilen langs de nederlandse kust. statistisch onderzoek. Technical report, Rijksinstituut voor Kust en Zee.

Flater, D. (2013). XTide. `http://www.flaterco.com/xtide/`.

Gautier, C. & Groeneweg, J. (2012). Achtergrondrapportage hydraulische belasting voor zee en estuaria. Technical report, Deltares.

Gerritsen, H. (2005). What happened in 1953? The big flood in the Netherlands in retrospect. *Philosophical Transactions of the Royal Society*, *363*.

Gerritsen, H., de Vries, J., & Philippart, M. (2005). The dutch continental shelf model. In *Quantitative Skill Assessment for Coastal Ocean*. American Geophysical Union.

Gill, A. (1982). *Atmosphere-Ocean Dynamics*. Academic Press, Inc.

Gringorten, I. (1963). A plotting rule for extreme probability paper. *Journal of Geophysical Research*, *68*(3), 813–814.

Groen, G. & Caires, S. (2011). Storm catalogue the netherlands. `http://www.knmi.nl/samenw/hydra/stormcatalogus/`.

Heaps, N. (1983). Storm surges, 1967–1982. *Geophysical Journal International*, *74*(1), 331–376.

Hinton, C., Townend, I., & Nicholls, R. (2007). Coastal processes. In *Future flooding and coastal erosion risks*. Thomas Telford Publishing.

Hirsch, R. M. (1987). Probability plotting position formulas for flood records with historical information. *Journal of Hydrology*, *96*.

Holland, G. (1980). An analytical model of the wind and pressure profiles in hurricanes. *Monthly weather review*, *108*.

Jakobsen, F. & Madsen, H. (2004). Comparison and further development of parametric tropical cyclone models for storm surge modelling. *Journal of Wind Engineering and Industrial Aerodynamics*, *92*.

Janssen, P. & Rotmans, J. (2004). *Gevoeligheidsanalyse en Onzekerheidsanalyse; een Inventarisatie van Ideeën, Methoden en Technieken*. Rijksinstituut voor volksgezondheid en milieuhygiene.

KNMI (2011). KNMI-HYDRA MetaDataConnection. `http://www.knmi.nl/samenw/hydra/cgi-bin/meta_data.cgi`.

KNMI (2013). Weerkaarten archief europa. analyses vanaf 1 januari 2003 t/m gisteren. `http://www.knmi.nl/klimatologie/daggegevens/weerkaarten/`.

Leslie, L. & Holland, G. (1995). On the bogussing of tropical cyclones in numerical models: A comparison of vortex profiles. *Meteorology and Atmospheric Physics*, *56*(1-2).

Lowe, J., Gregory, J., & Flather, R. (2001). Changes in the occurrence of storm surges around the United Kingdom under a future climate scenario using a dynamic storm surge model driven by the Hadley Centre climate models. *Climate Dynamics*, *18*, 179–188.

Madsen, H. & Flemming, J. (2004). Cyclone induced storm surge and flood forecasting in the northern Bay of Bengal. *Coastal Engineering*, *51*(4), 277 – 296.

Mellor, G. & Blumberg, A. (1985). Modeling vertical and horizontal diffusivities with the sigma coordinate system. *Monthly Weather Review*, *113*(8), 1379–1383.

Ministerie van Verkeer en Waterstaat (2007). Hydraulische randvoorwaarden primaire waterkeringen voor de derde toetsronde 2006-2011.

National Oceanic and Atmospheric Administration (2012). Norwegion cyclone model. `http://www.srh.weather.gov/srh/jetstream/synoptic/cyclone.htm`.

Orton, P., Georgas, N., Blumberg, A., & Pullen, J. (2012). Detailed modeling of recent severe storm tides in estuaries of the New York City region. *Journal of Geophysical Research*, *117*.

Pita, G., Pinelli, J., Cocke, S., Gurley, K., Mitrani-Reiser, J., Weekes, J., & Hamid, S. (2012). Assessment of hurricane-induced internal damage to low-rise buildings in the florida public hurricane loss model. *Journal of Wind Engineering and Industrial Aerodynamics*, *104106*, 76 – 87.

Prandle, D. (1978). Residual flows and elevations in the Southern North Sea. *Proceedings of the Royal Society of London, Series A, Mathematical and Physical Sciences*, *359*, 1697.

Proudman, J. (1953). *Dynamical Oceanography*. Methuen & Co. LTD.

Pugh, D. (1987). *Tides, Surges and Mean Sea-Level*. John Wiley & Sons.

Resio, D. & Westerink, J. (2008). Modeling of the physics of storm surges. *Physics Today*, *33*.

Rijkswaterstaat (2011). Referentiewaarden waterstanden.

Rijkswaterstaat (2013). Waterhoogte in cm t.o.v. normaal amsterdams peil in oppervlaktewater. `http://live.waterbase.nl/`.

Robusto, C. (1957). The cosine-haversine formula. *The American Mathematical Monthly*, *64*.

Shaw, E. (1994). *Hydrology in practice* (third ed.). Routledge.

Slobbe, D., Verlaan, M., Klees, R., & Gerritsen, H. (2012). Obtaining instantaneous water levels relative to a geoid with a 2d storm surge level. *Continental Shelf Research*, *52*.

Steetzel, H., Diermanse, F., van Gent, M., Coeveld, E., & van de Graaff, J. (2007). Dune erosion. product 3: Probabilistic dune erosion prediction method. Technical report, WL Delft Hydraulics.

Van den Brink, H. (2013). Private communication.

Vilibić, I., Domijan, N., & Čupić, S. (2005). Wind versus air pressure seiche triggering in the Middle Adriatic coastal waters. *Journal of Marine Systems*, *57*(1), 189–200.

Voortman, H. (2002). *Risk-based design of large-scale flood defence systems*. PhD thesis, Delft University of Technology.

Wetterzentrale (2011). Ncep reanalysis: Informationen. `www.wetterzentrale.de`.

Wieringa, J. & Rijkoort, P. (1983). *Windklimaat van Nederland*. Staatsuitgeverij.

Wu, J. (1980). Wind stress coefficients over sea surface near neutral conditions - a revisit. *Journal of Physical Oceanography*, *10*.

Appendix A

List of frequently used symbols

Roman

B	-	Holland-B parameter
C	$\mathrm{m}^{0.5}\ \mathrm{s}^{-1}$	Chézy coefficient
C_{fm}	$\mathrm{m\ s}^{-1}$	propagation speed of a storm
H	m	water depth
$P0$	Pa	average atmospheric pressure (101325 Pa)
R_{max}	m	distance from storm center towards radius of maximum winds
T	years	year of occurrence of a storm surge
U	$\mathrm{m\ s}^{-1}$	depth averaged flow velocity in x-direction
V_g	$\mathrm{m\ s}^{-1}$	gradient wind speed
V_s	$\mathrm{m\ s}^{-1}$	surface wind speed
$V_{s\perp}$	$\mathrm{m\ s}^{-1}$	surface wind speed perpendicular to the transect
$V_{s//}$	$\mathrm{m\ s}^{-1}$	surface wind speed parallel to the transect
c_w	-	friction coefficient
f	s^{-1}	Coriolis parameter ($1.15 \cdot 10^{-4}\ \mathrm{s}^{-1}$)
g	$\mathrm{m\ s}^{-1}$	gravitational acceleration ($9.81\ \mathrm{m\ s}^{-1}$)
n	$\mathrm{m}^{\frac{1}{3}}\ \mathrm{s}^{-1}$	Manning roughness coefficient
p	Pa	atmospheric pressure at sea level
r	m	distance from storm center to point of interest
r_t	m	radius of curvature of isobars of a depression
t	s	time
y_{slr}	m	relative sea level rise
z	m	bottom level

Greek

Δp	Pa	difference in central pressure and ambient pressure
Ω	rad s^{-1}	angular frequency of the Earth's rotation
β	$^\circ$	deflection of the surface wind direction towards the storm center
ϵ	-	parameter to determine 95% confidence interval of B
ζ	m	free surface elevation
θ	^{o}	latitude
ρ_a	kg m^{-3}	density of air (1.27 kg m^{-3})
ρ_w	kg m^{-3}	density of water (1000 kg m^{-3})
ϕ	$^\circ$	direction of storm track
ξ	$^\circ$	angle between direction of storm translation and the vector from the storm center towards the point of interests
ψ	$^\circ$	Northern latitude at 5.5 Eastern longitude

Appendix B

Solution method of the hydrodynamical model

In this appendix, the solution method of the hydrodynamical model as presented in section 3.3 is discussed. First, the numerical discretizations are assessed; next, the numerical solutions are presented.

B.1 Numerical discretizations

The shallow water equations are solved by use of numerical finite differences and a semi-implicit scheme. A staggered grid in space is used. The spatial grid consists of 202 grid point, so the spatial step 4.2 km. Time step $\Delta t =$ 300 s and the default total simulation time is 7 days. Spacial steps are defined by $x_i = i\Delta x$, with $i = 0, 1, 2, \ldots, N_x + 1$, with $N_x = 202$ and time steps are defined by $t_n = n\Delta t$, with $n = 0, 1, 2, \ldots, N_t$ with $N_t = 2026$. The continuity equation is solved for ζ on the even grid points, the momentum equation is solved for U on the odd grid points. The grid is shown in Figure

B.1. The following numerical arrays are defined:

$$\begin{cases} \zeta_i^n = \zeta(x_i, t_n) & \text{for} \quad i = 0, 2, 4, \ldots, N_x, \\ U_i^n = U(x_i, t_n) & \text{for} \quad i = 1, 3, 5, \ldots, N_x + 1, \\ p_i^n = p(x_i, t_n) & \text{for} \quad i = 0, 2, 4, \ldots, N_x, \\ (V_{s//})_i^n = V_{s//}(x_i, t_n) & \text{for} \quad i = 1, 3, 5, \ldots, N_x - 1, \\ (V_s\perp)_i^n = V_s\perp(x_i, t_n) & \text{for} \quad i = 1, 3, 5, \ldots, N_x - 1, \\ C_i^n = C(x_i, t_n) & \text{for} \quad i = 1, 3, 5, \ldots, N_x - 1, \\ {c_w}_i^n = c_w(x_i, t_n) & \text{for} \quad i = 1, 3, 5, \ldots, N_x - 1, \\ {\tau_w}_i^n = \tau_w(x_i, t_n) & \text{for} \quad i = 1, 3, 5, \ldots, N_x - 1. \end{cases} \tag{B.1}$$

with $n = 0, 1, 2, \ldots, N_t$. The quantities $p(x_i, t_n), V_{s//}(x_i, t_n)$ and $V_s\perp(x_i, t_n)$ are calculated by the meteorological model. The water depth H follows from bathymetry and is constant over time. For each grid point the water depth is determined. It is implemented as the following numerical array:

$$H_i = H(x_i) \qquad \text{for } i = 1, 2, 3, \ldots, N_x. \tag{B.2}$$

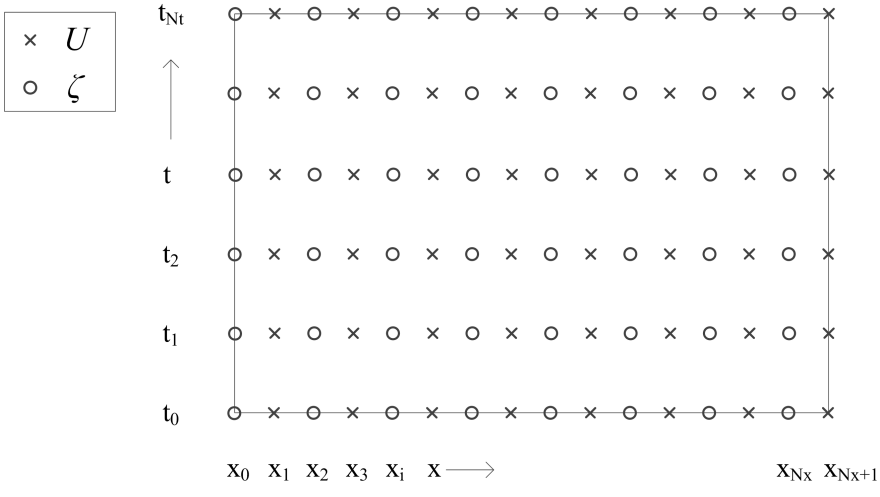

Figure B.1: The even grid points are denoted by a circle. On these points the continuity equations are solved for ζ. On the odd grid points the momentum equations are solved for U.

The momentum equation (3.11) is discretized by:

$$\frac{U_i^{n+1}-U_i^n}{\Delta t}+U_i^{n+1}\frac{\frac{U_{i+2}^n+U_i^n}{2}-\frac{U_i^n+U_{i-2}^n}{2}}{2\Delta x}+g\frac{\zeta_{i+1}^{n+1}-\zeta_{i-1}^{n+1}}{2\Delta x}+ \frac{1}{\rho_w}\frac{p_{i+1}^{n+1}-p_{i-1}^{n+1}}{2\Delta x}+\frac{g}{(C_i^n)^2\left[H_i+\frac{\zeta_{i+1}^n+\zeta_{i-1}^n}{2}\right]}\left|U_i^n\right|U_i^n=\frac{{\tau_w}_i^{n+1}}{\rho\left[H_i+\frac{\zeta_{i+1}^n+\zeta_{i-1}^n}{2}\right]}, \tag{B.3}$$

with:

$$C_i^n=\frac{(H_i+\zeta_i^n)^{1/6}}{n}, \tag{B.4}$$

$${c_w}_i^n=\begin{cases}\left(0.8+0.065\sqrt{\left((V_{s//})_i^n\right)^2+\left((V_{s\perp})_i^n\right)^2}\right)\times 10^{-3}\ldots \\ \qquad\qquad \text{for}\quad \sqrt{\left((V_{s//})_i^n\right)^2+\left((V_{s\perp})_i^n\right)^2}<26.8\quad \text{m s}^{-1}, \\ 2.54\times 10^{-3}\quad \text{for}\quad \sqrt{\left((V_{s//})_i^n\right)^2+\left((V_{s\perp})_i^n\right)^2}\geq 26.8\quad \text{m s}^{-1}.\end{cases} \tag{B.5}$$

$${\tau_w}_i^n=\rho_a{c_w}_i^n\sqrt{\left((V_{s//})_i^n\right)^2+\left((V_{s\perp})_i^n\right)^2}(V_{s//})_i^n. \tag{B.6}$$

for $i=1,3,5,\ldots,N_x-1$ and $n=0,1,2,\ldots,N_t$. All discretizations are of first order in Δt and of second order in Δx. The continuity equation (3.12) is discretized by:

$$\frac{\zeta_i^{n+1}-\zeta_i^n}{\Delta t}+\frac{U_{i+1}^{n+1}\left[H_{i+1}+\frac{\zeta_{i+2}^n+\zeta_i^n}{2}\right]-U_{i-1}^{n+1}\left[H_{i-1}+\frac{\zeta_i^n+\zeta_{i-2}^n}{2}\right]}{2\Delta X}=0 \tag{B.7}$$

for $i=2,4,6,\ldots,N_x$, and $n=1,1,2,\ldots,N_t$. All discretizations are of first order in Δt and of second order in Δx. The initial conditions (3.13) at $n=0$ are implemented as:

$$\begin{cases}\zeta_i^0=0 & \text{for}\quad i=0,2,4,\ldots,N_x, \\ U_{N_{x+1}}^0=0 & \text{for}\quad i=1,3,5,\ldots,N_{x+1},\end{cases} \tag{B.8}$$

and the boundary conditions (3.14) at $i=0$ and $i=N_{x+1}$ are implemented as:

$$\begin{cases}\zeta_0^n=-\dfrac{P_0-p_0^n}{g\rho_w}, & \text{for}\quad n=0,1,2,\ldots,N_t, \\ U_{N_{x+1}}^n=0 & \text{for}\quad n=0,1,2,\ldots,N_t.\end{cases} \tag{B.9}$$

B.2 Numerical solution

The set of equations can be solved for each time step by setting up a linear system of equations in matrix form. Therefore, the equations (B.3) and (B.7) are written in a different way. The equations can be written in terms of U and ζ:

$$\mathcal{A}\zeta_{i-1}^{n+1} + \mathcal{B}_i U_i^{n+1} + \mathcal{C}\zeta_{i+1}^{n+1} = \mathcal{G}_i, \tag{B.10}$$

$$\mathcal{D}_i U_{i-1}^{n+1} + \mathcal{E}\zeta_i^{n+1} + \mathcal{F}_i U_{i+1}^{n+1} = \mathcal{H}_i, \tag{B.11}$$

with:

$$\mathcal{A} = -g\frac{\Delta t}{2\Delta x}, \tag{B.12}$$

$$\mathcal{B}_i = 1 + \frac{\Delta t}{2\Delta x}\left[\frac{U_{i+2}^n + U_i^n}{2} - \frac{U_i^n + U_{i-2}^n}{2}\right], \tag{B.13}$$

$$\mathcal{C} = g\frac{\Delta t}{2\Delta x}, \tag{B.14}$$

$$\mathcal{G}_i = U_i^n - \frac{1}{\rho_w}\frac{p_{i+1}^{n+1} - p_{i-1}^{n+1}}{2\Delta x} \tag{B.15}$$

$$- \frac{g}{(C_i^n)^2\left[H_i + \frac{\zeta_{i+1}^n + \zeta_{i-1}^n}{2}\right]}\left|U_i^n\right| U_i^n + \frac{{\tau_w}_i^{n+1}}{\rho_w\left[H_i + \frac{\zeta_{i+1}^n + \zeta_{i-1}^n}{2}\right]}, \tag{B.16}$$

$$\mathcal{D}_i = -\frac{\Delta t}{2\Delta x}\left[H_{i-1} + \frac{\zeta_i^n + \zeta_{i-2}^n}{2}\right], \tag{B.17}$$

$$\mathcal{E} = 1, \tag{B.18}$$

$$\mathcal{F}_i = \frac{\Delta t}{2\Delta x}\left[H_{i+1} + \frac{\zeta_{i+2}^n + \zeta_i^n}{2}\right], \tag{B.19}$$

$$\mathcal{H}_i = \zeta_i^n. \tag{B.20}$$

This gives, per time step, the following set of equations, for $1 \leq n \leq N_x$. At $n = 1$ and $n = N_x$, the equations are a bit different to incorporate the boundaries.

$$\begin{bmatrix} \mathcal{B}_1 & \mathcal{C} & 0 & 0 & 0 & 0 & \dots & 0 \\ \mathcal{D}_2 & \mathcal{E} & \mathcal{F}_2 & 0 & 0 & 0 & \dots & 0 \\ 0 & \mathcal{A} & \mathcal{B}_3 & \mathcal{C} & 0 & 0 & \dots & 0 \\ 0 & 0 & \mathcal{D}_4 & \mathcal{E} & \mathcal{F}_4 & 0 & \dots & 0 \\ 0 & 0 & 0 & \mathcal{A} & \mathcal{B}_5 & \mathcal{C} & \dots & 0 \\ 0 & 0 & 0 & 0 & \mathcal{D}_6 & \mathcal{E} & \dots & 0 \\ \vdots & \vdots & \vdots & \vdots & \vdots & \vdots & \ddots & \vdots \\ 0 & 0 & 0 & 0 & 0 & 0 & \dots & \mathcal{E} \end{bmatrix} \begin{bmatrix} U_1^{n+1} \\ \zeta_2^{n+1} \\ U_3^{n+1} \\ \zeta_4^{n+1} \\ U_5^{n+1} \\ \zeta_6^{n+1} \\ \vdots \\ \zeta_{N_x}^{n+1} \end{bmatrix} = \begin{bmatrix} \mathcal{G}_1 + \mathcal{A} \\ \mathcal{H}_2 \\ \mathcal{G}_3 \\ \mathcal{H}_4 \\ \mathcal{G}_5 \\ \mathcal{H}_6 \\ \vdots \\ \mathcal{H}_{N_x} - \mathcal{F}_{N_x} \end{bmatrix}$$

At time step n, all values of ζ_i^n and U_i^n are known. Together with the boundary conditions (B.9), the linear set of equations can be solved for ζ_i^{n+1} and U_i^{n+1}. This gives numerical values for the next time step $n+1$:

$$\zeta_i^n = \zeta_i^{n+1}, \tag{B.21}$$

$$U_i^n = U_i^{n+1}. \tag{B.22}$$

Appendix C

Testing of the hydrodynamical model

The numerical hydrodynamical model, presented in section 3.3, is tested to gain insight into the numerical stability and reliability of the model. Arbitrarily chosen input is used to compute output in an analytical way and by the software package SOBEK. This output is used as data to compare with the model results. First, the model will be tested for an equilibrium situation with constant wind forcing. Second, an equilibrium situation is obtained with a constant pressure field as forcing. Last, a non-equilibrium case is computed with SOBEK and compared with model output.

C.1 Equilibrium situation 1: constant wind

When a constant wind is blowing above the transect, an equilibrium situation will occur. Depth-averaged flow will reduce to zero and wind friction is in balance with the surface water elevation. In this situation, the atmospheric pressure gradient is set to zero. The shallow water equations are reduced to a set of equations which can be solved analytically. The result is compared to the model output.

C.1.1 Analytical solution

In an equilibrium situation it follows that $U = 0$. The shallow water equations (3.11)-(3.14) reduce to:

$$g\frac{\partial \zeta}{\partial x} = \frac{\tau_w}{\rho_w(H+\zeta)} \tag{C.1}$$

with a boundary condition:

$$\zeta(0) = 0. \tag{C.2}$$

This differential equation can be solved for ζ:

$$\zeta(x) = \sqrt{2\left(\frac{\tau_w}{g\rho_w}x\right) + H^2} - H. \tag{C.3}$$

C.1.2 Model input

Model input for the hydrodynamical model and equation (C.3) is as follows: $L = 1 \times 10^6$ m, $H = 25$ m and spatially uniform, wind speed perpendicular to the transect $V_{s//} = 25$ m s^{-1} , $g = 9.81$ m s^{-2}, $\rho_w = 1000$ kg m^{-3} and $\rho_a = 1$ kg m^{-3}. Wind friction is determined by (3.16) and (3.17).

C.1.3 Results

The runtime of the model is set to 200 days. After 200 days, the flow at the open boundary is reduced to only $8 \cdot 10^{-4}$ m s^{-1} so it is assumed that equilibrium has been reached. In Figure C.1 (left) the analytically calculated free surface elevation along the transect is shown. Figure C.1 (right) shows the difference between the numerically computed and analytically computed free surface elevation. Differences are very small, which gives confidence in the model.

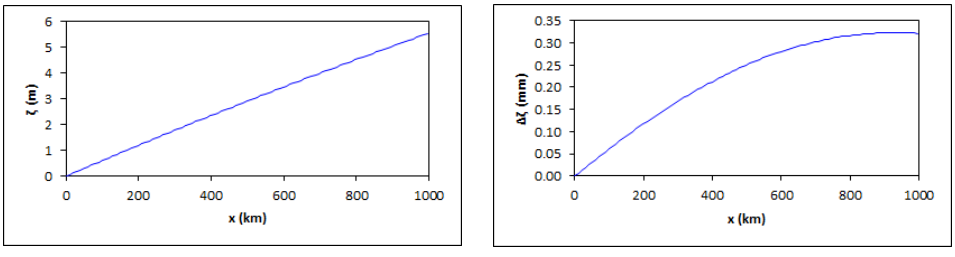

Figure C.1: Left: Analytically calculated free surface elevation. **Right**: Differences between the analytically and numerically calculated values.

C.2 Equilibrium situation 2: constant atmospheric pressure

An equilibrium will also occur when the atmospheric pressure is constant over time. Wind is not included in this case. In this way, the contribution of atmospheric pressure to the surge is tested. The inverse barometric effect

should occur. Again, the shallow water equations reduce to a set which can be solved analytically.

C.2.1 Analytical solution

The shallow water equations (3.11)-(3.14) with $U = 0$ and $\tau_w = 0$ reduce to:

$$g\frac{\partial \zeta}{\partial x} + \frac{1}{\rho_w}\frac{\partial p}{\partial x} = 0, \tag{C.4}$$

with a boundary conditions:

$$\zeta(0) = 0 \text{ m}, \tag{C.5}$$

$$p(0) = p_0. \tag{C.6}$$

This differential equation can be solved for ζ:

$$\zeta(x) = -\frac{1}{g\rho_w}p(x) + \frac{p_0}{g\rho_w}. \tag{C.7}$$

C.2.2 Model input

Input parameter values for the model and equation (C.7) are the following: a length $L = 1,000,000$ m, a water depth $H = 25$ m and spatially uniform, $g = 9.81$ m s^{-2} and $\rho_w = 1000$kg m^{-3}. The atmospheric pressure profile is arbitrary chosen as:

$$p(x) = p_0 - \Delta p \sin\left(\frac{\pi}{L}x\right), \tag{C.8}$$

where $\Delta p = 500$ Pa and $p_0 = 101325$ Pa. The profile is shown in Figure C.2.

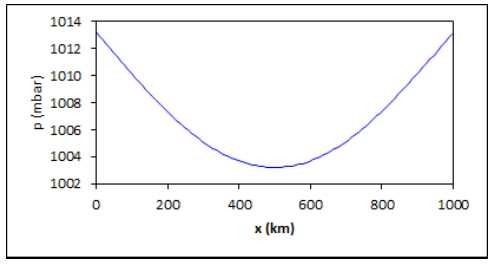

Figure C.2: Arbitrary chosen pressure field.

C.2.3 Results

Again, the runtime of the model is set to 200 days. Depth-averaged flow at the open boundary has been reduced to $7 \cdot 10^{-4}$ m s^{-1} so equilibrium has approximately been reached. Figure C.3 (left) shows the analytically calculated free surface elevation. When comparing this figure with Figure C.2, it is clear that the inverse barometric effect is correctly reproduced by the model. Figure C.3 (right) shows the difference between the numerically computed and analytically computed free surface elevation. Differences are again very small, which demonstrates that also the atmospheric pressure forcing is well implemented in the model.

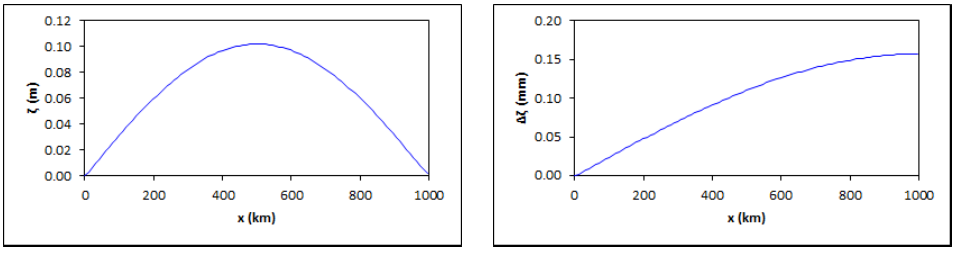

Figure C.3: Left: Analytically calculated free surface elevation. **Right**: Differences between the analytically and numerically calculated values.

C.3 Non-equilibrium case

The equilibrium situations will not occur in reality, because a steady forcing for 200 days will never occur during real storms. The non-equilibrium situations cannot easily be solved analytically. Therefore, use is made of the SOBEK software package. Unfortunately, atmospheric pressure gradients are not implemented in SOBEK. Therefore, atmospheric pressure is not taken into account.

C.3.1 Testing data

Testing data are computed with SOBEK. Data consist of free surface elevation with an accuracy of 0.01 m. The used time step is 5 minutes, the total runtime is 10 days. The SOBEK model consists of 100 grid points. It is not possible to increase the resolution, since the amount of grind points is limited in the used SOBEK version. The data for which the model will be validated are free surface elevation at the closed boundary. Some parameter values in SOBEK can not be adjusted. Therefore, the input for the hydro-

dynamical model is adjusted to be in accordance with the values used in SOBEK.

C.3.2 Model input

Input parameter values for SOBEK and hydrodynamical model are the following: $L = 1,000,000$ m, $H = 25$ m and spatially uniform, $g = 9.81$ m s^{-2}, $\rho_w = 1000$ kg m^{-3} and a steady wind speed perpendicular to the transect $V_{s//} = 25$ m s^{-1}. Bottom friction is determined by equation (3.15) with $C = 68.4$ m$^{0.5}$ s^{-1} and wind friction is determined by equation (3.16) with $c_w = 0.002$. The time step Δt for the hydrodynamical model is also 5 minutes. Boundary conditions for both models are arbitrary chosen as:

$$\zeta(0) = 0 \text{ m}, \tag{C.9}$$

$$U(L) = 0 \text{ m s}^{-1}. \tag{C.10}$$

C.3.3 Results

Figure C.4 (left) shows the calculated free surface elevation by SOBEK and Figure C.4 (right) shows the difference between the model data and the SOBEK data. The results show that the model outcome is a bit higher than the SOBEK data, differences are up to 35 mm near the end of the model time. Differences in free surface elevation are smaller at relative high water heights than at relatively low water heights. The deviations seem to be increasing with increasing time but is still relatively small at the end of the model run. Because it assumed that storms will pass within the model time of 10 days, this deviation is not seen as a problem.

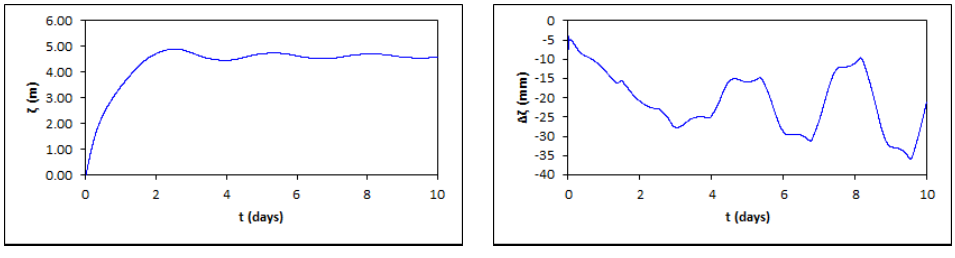

Figure C.4: Left: Analytically calculated free surface elevation. **Right**: Differences between the analytically and numerically calculated values.

Appendix D

Validation of the meteorological model

This appendix presents and discusses validation of the meteorological model as presented in section 4.2. Validation is done for a time span of 24 hours (25 data points) around the storm maximum. Wind directions above 360° are not given in degrees with 0° as datum, but instead with 360° as datum. In this way, figures become more clear. Because computed storms are not absolute in time (the exact time for which the storm location ψ is valid is not given), the computed wind fields are shifted in time until they match with the observed wind fields. Focus will be more on trends than on absolute values. Storms 14 until 20 are discussed here, storm 21 is presented in section 4.2.

Storm 14

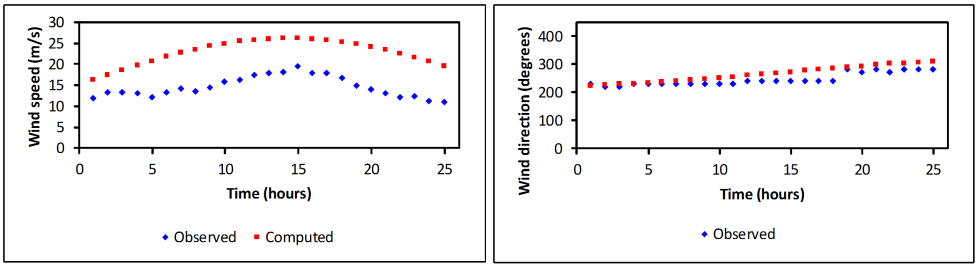

Figure D.1: Wind speed and wind direction for the storm of 12 December 1962 (storm 14).

Wind speed is overestimated. The course of the wind speed matches well with the observations. The wind direction is a bit overestimated, but the increasing trend is reproduced well.

Storm 15

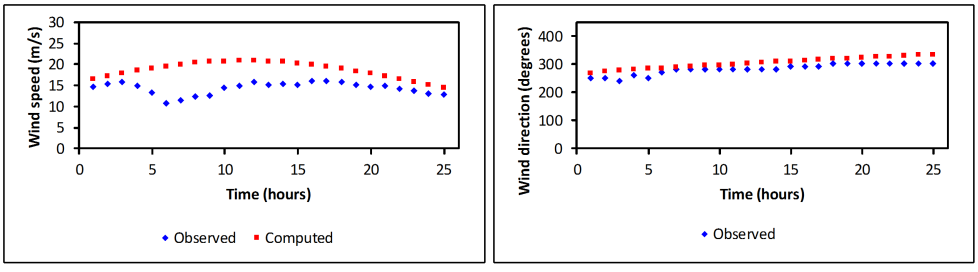

Figure D.2: Wind speed and wind direction for the storm of 17 December 1962 (storm 15).

Wind speed is overestimated, especially near the storm peak. Weather charts are not available to check meteorological conditions. The course of the wind speed at the beginning and end of the plot show good agreement, the dip in the middle of the observations however cannot be seen in the computations. Wind direction is a bit overestimated but makes a good fit.

Storm 16

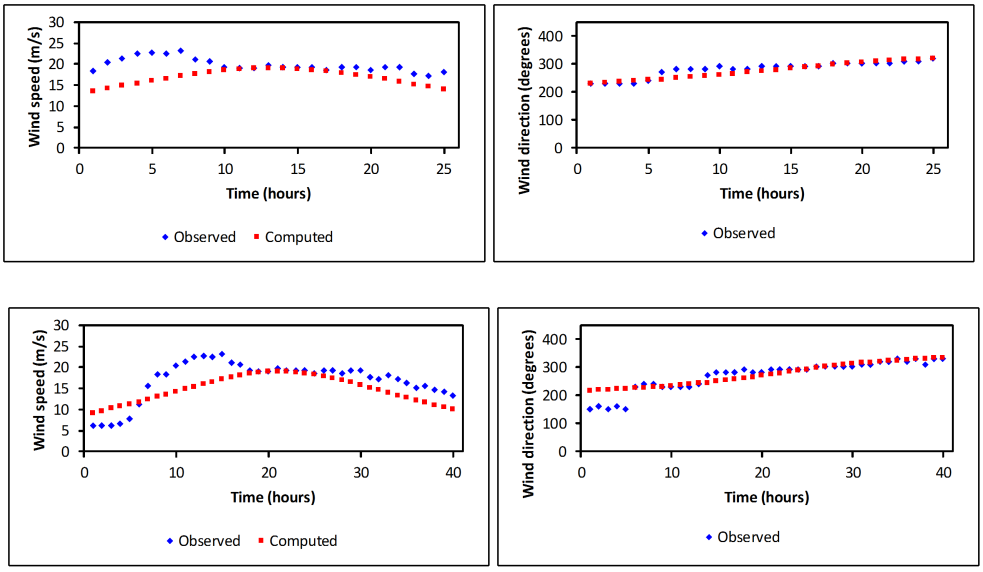

Figure D.3: Wind speed and wind direction for the storm of 3 January 1976 (storm 16). The upper two figures show data for 24 hours, the lower two figures show data for a time span of 40 hours.

Validation is done for a time span of 24 hours and 40 hours, because the storms passes relative slowly at a large distance (about 1500 km). The storm consisted of two atmospheric depressions of which only the largest is modeled. Therefore, the computed wind field does not correspond well with the observed wind field. Wind speed is on average underestimated, wind direction a bit as well. The period with maximum winds is missed completely in the calculations. When looking at the plots with the 25 hour time span, it appears that the course of the computed wind speed does not correspond with the observations. The plots with the 40 hours time spans however, show that the courses of the observed and computed storms make a better match.

Storm 17

The wind near Hoek van Holland is during this storm influenced by two atmospheric depressions, of which the most influential is used as input for the model. The storm peak is a bit overestimated, the wind direction is underestimated (especially during the peak of the storm). This can be explained by the fact that the wind direction is affected by two depressions.

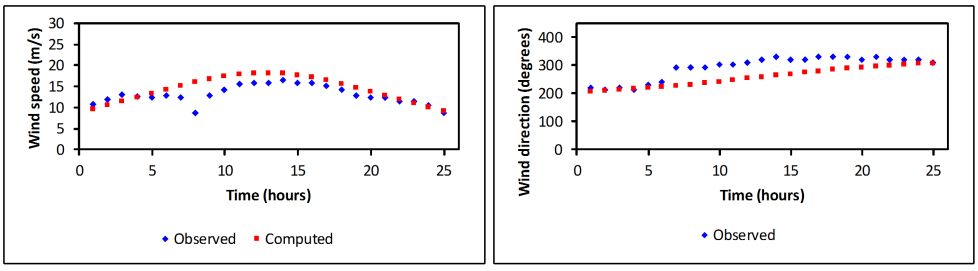

Figure D.4: Wind speed and wind direction for the storm of 14 February 1989 (storm 17).

The course of the wind speed at the beginning and end of the plot show good agreement with the observations.

Storm 18

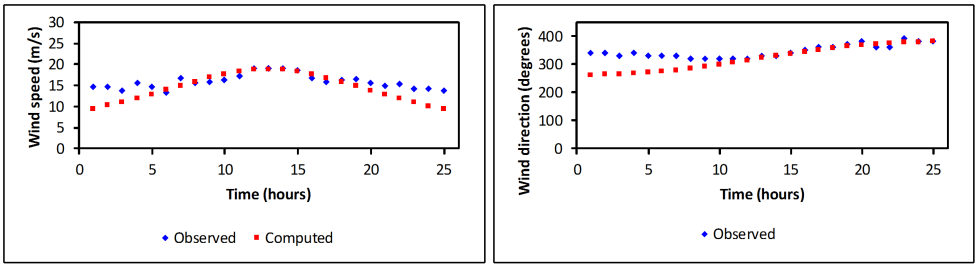

Figure D.5: Wind speed and wind direction for the storm of 12 December 1990 (storm 18).

Wind speed shows a good fit for the storm peak. Before and after the peak, wind speed is underestimated. In total, the observations show less decrease in wind speed before and after the peak than the model results. Wind direction is underestimated before the storm peak, this can be explained by the passing of a cold front and occlusion front. These fronts influence the wind direction, but are not included in the model.

Storm 19

This storm develops in the North Sea area. However, computed wind speed shows good agreement with the observations. Wind direction is somewhat underestimated but shows a good fit.

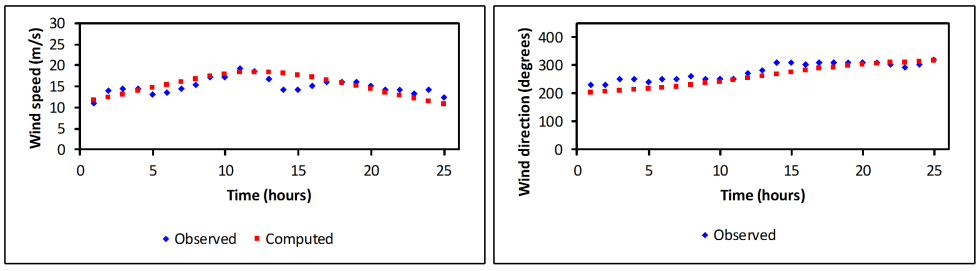

Figure D.6: Wind speed and wind direction for the storm of 21 December 2003 (storm 19).

Storm 20

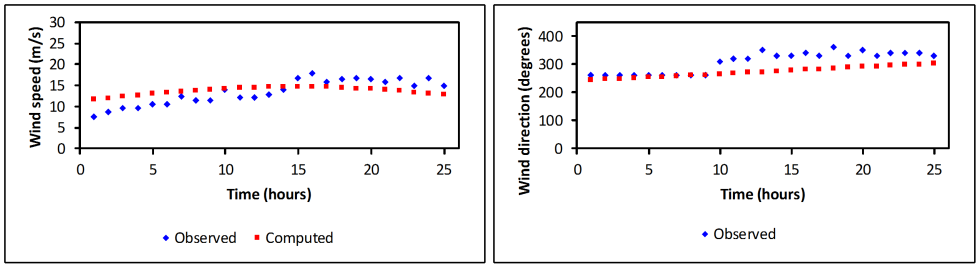

Figure D.7: Wind speed and wind direction for the storm of 12 December 2007 (storm 20).

During passing the North Sea, a second depression occurred west of the storm depression. Only the first and largest depression is used as input for the model. Therefore, only the first part of the storm is relevant to investigate. Here, the wind speed is overestimated but the courses show good agreement. The first part of computed wind direction matches the observed wind direction well.

Appendix E

Calibration results for surge courses

This appendix presents and discusses calibration results for the coupled model as presented in section 4.3.4, focusing on surge duration. The time for which the water levels are above a certain threshold is compared. This threshold is set to 75% of the observed peak water level. The results of storms 17 until 20 are discussed here. Storm 21 is presented in section 4.3.4.

Storm 17

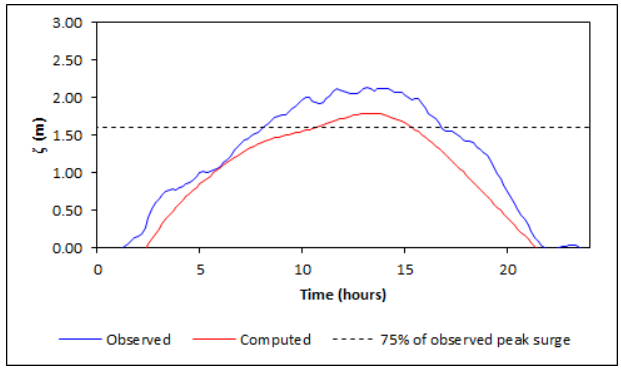

Figure E.1: The observed and computed surge for the storm of 14 February 1989 (storm 17).

The course of the modeled surge shows good agreement with the observed surge. It is clear that rise of the surge is less steep than the falling, which coincides with the observations. The surge height however is underestimated

by half a meter. A reason for this underestimation could be the deviation in computed wind direction, see Figure D.4. The observed surge level is 8.67 hours above the threshold of 1.60 m, compared to 4.67 hours for the computed surge.

Storm 18

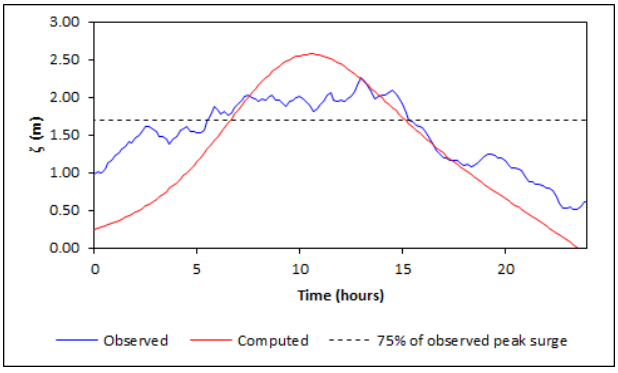

Figure E.2: The observed and computed surge for the storm of 12 December 1990 (storm 18).

The rise of the computed surge is too steep compared to the observations, the fall of the surge shows better agreement. Wind fields by other depressions are most likely responsible for this. Observations show a flat surge peak, whereas the model computes a clearly distinguishable peak. Surge heights are on average underestimated. The observed surge level is 9.67 hours above the threshold of 1.70 m, compared to 8.50 hours for the computed surge.

Storm 19

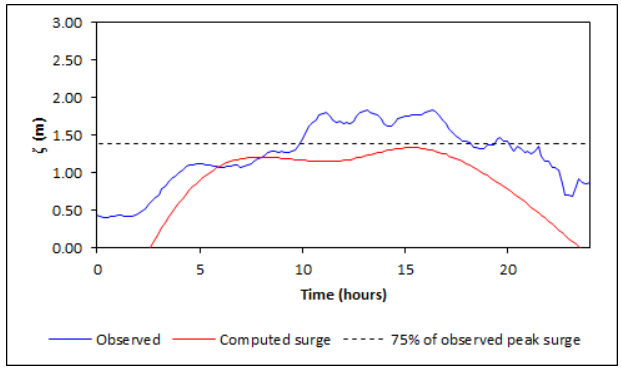

Figure E.3: The observed and computed surge for the storm of 21 December 2003 (storm 19).

The small dip during the rise of the observed surge is also modeled, although the height of this dip is to high compared to the surge peak. The computed peak lasts longer than the observed peak, due to forcing of other storms. The observed surge level is 9.83 hours above the threshold of 1.38 m. The computed surge does not exceed the threshold at all.

Storm 20

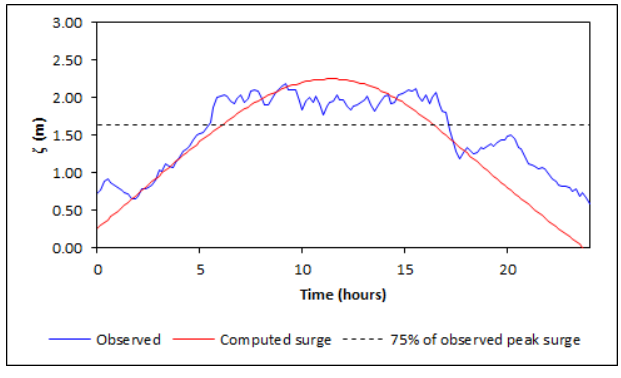

Figure E.4: The observed and computed surge for the storm of 9 November 2007 (storm 20)

The rise of the modeled surge is a bit too flat compared to the observations. On the other hand, the fall of the surge show good agreement. The duration of the surge peak is underestimated. This can be explained by the influence of a second depression which influences the wind and pressure field, see Figure D.7. Due to the flat peak of the observed surge show the

maximum water levels good agreement, but on average, the computed surge is a bit too low. The observed surge level is 11.67 hours above the threshold of 1.64 m, compared to 10.33 hours for the computed surge.

Appendix F

Sensitivity analysis

This appendix presents an extensive description of the input data and results of the sensitivity analysis, presented in section 4.4.2.

F.1 Input data

Storm parameter input data are obtained from the dataset described in Table 4.1. From this dataset, De Jong (2012) derived probability distributions for five of the six storm parameters, using all storms which occurred after 1900 due to data availability (18 in total). The last parameter (Holland-B) is determined using an empirical relation. The Holland-B parameter is calculated width a function of the radius to maximum winds, given in meters:

$$B = R_{max} \cdot 1.4 \cdot 10^{-6} + 0.33. \tag{F.1}$$

The probability distributions of the storm parameters are shown in Table F.1. Storm track direction ϕ is given in cardinal degrees with 270° (West) as reference.

Storm parameter	**Probability distribution**	**Mean**	**Standard deviation**
ψ (°)	Lognormal	58.61	2.6
C_{fm} (m/s)	Lognormal	14.67	5.25
ϕ (°)	Rayleigh	22.46	-
p_c (mbar)	Normal	975	15.05
R_{max} (km)	Lognormal	668	236

Table F.1: Probability distributions for storm parameters.

The default values for the storm parameters are the mean values. Next, input is varied independently by taking parameter values according to probabilities of occurrence of -20%, -10%, +10% and +20% from the mean values. Values for Holland-B are determined using equation (F.1). This results in the following input data (Table F.2).

Storm parameter	**-20%**	**-10%**	**+10%**	**+20%**
ψ (°)	57.1	57.9	59.2	59.9
C_{fm} (m/s)	11.6	12.7	15.6	11.7
ϕ (°)	289.0	292.7	300.4	304.9
p_c (mbar)	967	971	978	983
R_{max} (km)	548	600	708	755
B (-)	1.10	1.17	1.32	1.39

Table F.2: Storm parameter values used as input for the sensitivity analysis.

Bottom friction is determined by equation (3.15), using Manning's n roughness coefficient. The default value for this coefficient is 1/40 $\mathrm{m}^{\frac{1}{3}}\mathrm{s}^{-1}$. For the sensitivity analysis, input is determined by using expert knowledge. Input is as follows: 1/30 $\mathrm{m}^{\frac{1}{3}}\mathrm{s}^{-1}$, 1/35 $\mathrm{m}^{\frac{1}{3}}\mathrm{s}^{-1}$, 1/45 $\mathrm{m}^{\frac{1}{3}}\mathrm{s}^{-1}$ and 1/50 $\mathrm{m}^{\frac{1}{3}}\mathrm{s}^{-1}$.

Bathymetry is given in Figure 3.10. The sensitivity of the model to changes in bathymetry is determined by using linear approximations of this bathymetry. Using a simple regression technique, a linear profile is found. Because the water depth at Hoek van Holland has large influence on the surge, this value is kept constant. Next, this linear slope is increased and decreased by 5%. Finally, the height of the whole (linear) slope is increased and decreased by 5% of the height at the coast. The linear slope is shown in Figure F.1. The other four profiles are not shown in this figure, since deviations of this linear slope are too small to distinguish on this large scale.

The transect The sensitivity of the model to the location of the transect is determined by adjusting the length of the transect by -10% and +10%, and by varying the angle of the transect with -10° and +10°. This shown in Figure F.2.

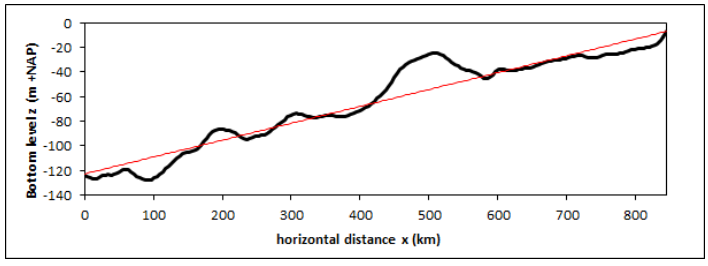

Figure F.1: The bathymetry and the linear slope. The other four profiles are not shown in this figure, since deviations of this linear slope are too small to distinguish on this large scale.

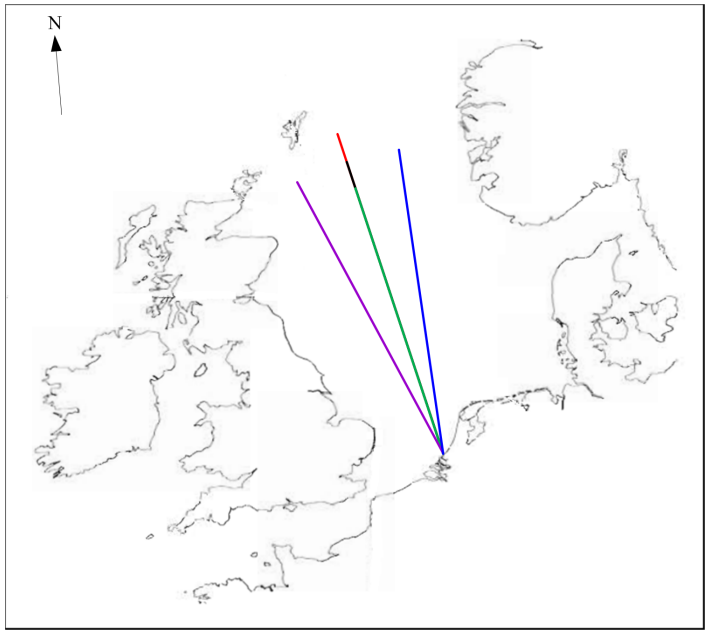

Figure F.2: The transects used to determine model sensitivity to the transect locations. The black transect is the default transect. The length is adjusted with an increase of 10% (red) and a decrease of 10% (green). The angle is adjusted with an increase of 10° (purple) and a decrease of 10° (blue).

F.2 Results

The surge at Hoek van Holland for the mean parameter values is computed. This surge is 2.99 m high. For all other input sets, surge heights are given in relative increases or decreases. Sensitivity is qualified in a qualitative way using the plots of the results, by using three levels: high, medium and low. Qualification is done by using Table F.3. For the storm parameters and bathymetry and transect location, results are summed per category (e.g. latitude input with variations of -10% and +10% have a total effect of 10%, which result in a medium qualification).

		low	**medium**	**high**
Storm parameters	-10% & +10%	$< 5\%$	5% - 10%	$> 10\%$
	-20% & +20%	$< 5\%$	5% - 15%	$> 15\%$
Bottom friction	1/30 $m^{1/3}$ s^{-1}	$< 5\%$	5% - 15%	$> 15\%$
	1/35 $m^{1/3}$ s^{-1}	$< 5\%$	5% - 10%	$> 10\%$
	1/45 $m^{1/3}$ s^{-1}	$< 5\%$	5% - 10%	$> 10\%$
	1/50 $m^{1/3}$ s^{-1}	$< 5\%$	5% - 15%	$> 15\%$
Bathymetry	Constant slope	$< 5\%$	5% - 10%	$> 10\%$
	Slope increase	$< 5\%$	5% - 10%	$> 10\%$
	Level increase	$< 5\%$	5% - 10%	$> 10\%$
Transect location	Angle	$< 5\%$	5% - 10%	$> 10\%$
	Length	$< 5\%$	5% - 10%	$> 10\%$

Table F.3: Reference values to qualify model sensitivity.

Storm parameter's effect on model sensitivity is shown in Figure F.3. For the parameter central pressure p_c, the sensitivity is qualified as **low**. Sensitivity is qualified **medium** for the the propagation speed C_{fm}, direction of storm track ϕ and the radius to maximum winds R_{max}. The model is sensitive for the latitude ψ and Holland-B parameter, so the sensitivity is qualified as **high**.

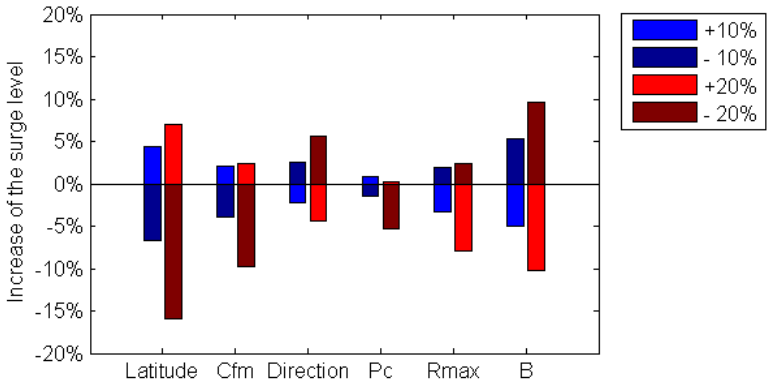

Figure F.3: Sensitivity of the model with respect to the storm parameters.

Bottom friction's effect on the sensitivity of the model is shown in Figure F.4. It is qualified as **medium**.

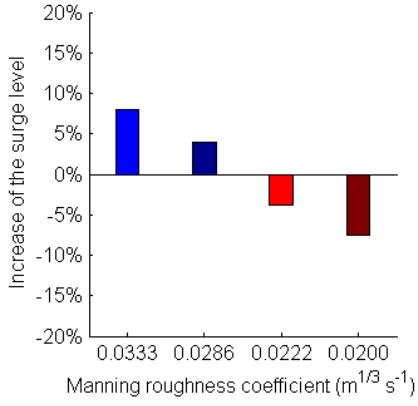

Figure F.4: Sensitivity of the model with respect to bottom friction.

Bathymetry's effect on model sensitivity (Figure F.5) is qualified as **medium**. Model outcome with the five linear slopes is compared to the original model outcome. A linear slope increases the surge height with 5%. The effects of relative large adjustments to this linear approximation are only between values of 1% and 10%.

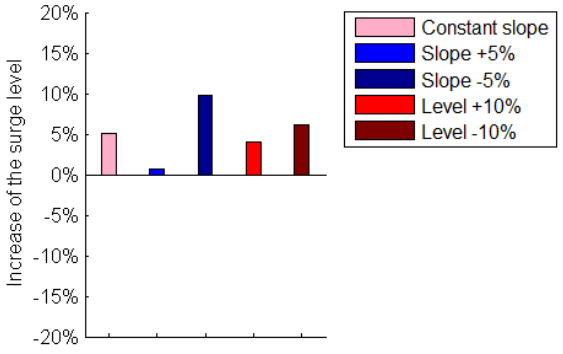

Figure F.5: Sensitivity of the model with respect to the bathymetry.

The transect location's effect on the location of the transect on the model results are shown in Figure F.6. The angle of the transect has a **small** influence on the surge height (only 2% to 3%). The influence of 10% increase and decrease of the length of the transect on the computed surge height is more or less 5% and is qualified as **medium**.

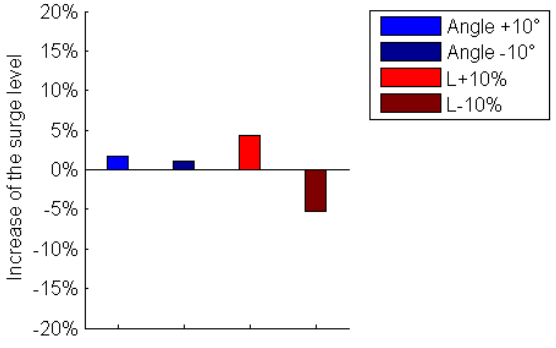

Figure F.6: Effect of the transect used in the model on the sensitivity.

F.3 Calibration for adjusted transects

The model is calibrated for each adjusted transect, see Figure F.2. Calibration results are presented in Figures F.7 and F.8. In these figures the results are compared with the original calibrated model, as used in this study. The model deviations, according to equation 4.4, are shown in Table F.4. Results do not differ significantly from the original calibrated model.

	ME
Original calibration	19.2%
Angle +10°	18.1%
Angle -10°	20.1%
Length +10%	19.9%
Length -10%	18.8%

Table F.4: Results of the model deviations according to equation 4.4 for models with adjusted transect locations.

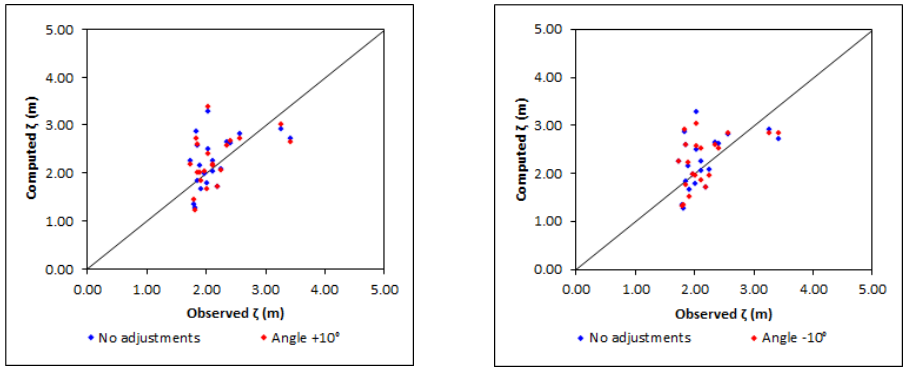

(a) Angle +10° **(b)** Angle -10°

Figure F.7: Calibration results for transect locations with an adjusted angle.

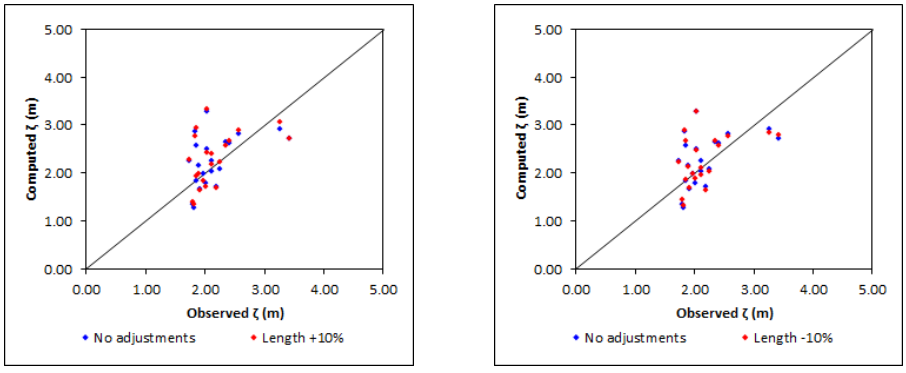

(a) Length +10% **(b)** Length -10%

Figure F.8: Calibration results for transect locations with an adjusted length.

In Figure F.9 the sensitivity of the model is shown respect to the transect location. The model is calibrated for each new transect and model sensitivity is **low**. Comparing this figure to Figure F.6, it can be seen that differences with the reference surge are much smaller for the newly calibrated models than for the models without the extra calibration step.

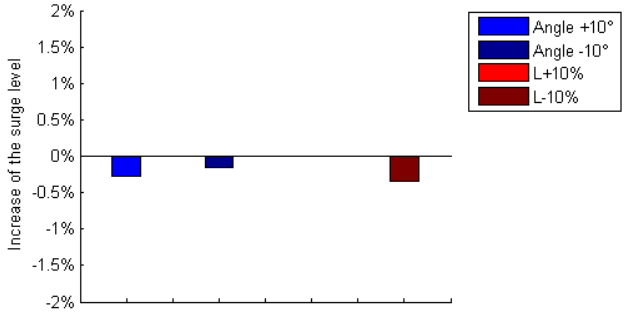

Figure F.9: Sensitivity of the model with respect to the transect location. The model is calibrated for each different transect. Note that the scale on the y-axis is much smaller compared to the previous figures in this appendix. The increase of surge level of the model with an increased transect length is too small (rounded to 0.0 %) to show on this figure.

Appendix G

Storm parameter distributions of different types of surges

This appendix shows histograms of the storm parameter values for different surge levels, as presented in section 5.2. Note that the distribution of the input database is shown on the left y-axis, the distribution of 100 storms is shown on the right y-axis.

Return period of 5,000 years

Following the model results, the surge height which occurs statistically once per 5,000 years is 6 m. Exact model outcome is 5.82 m, the range of 100 surges is between 5.81 m and 5.84 m. Results are shown in Figure G.1.

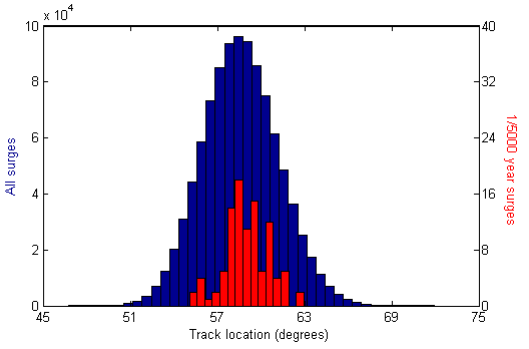

(a) Track location

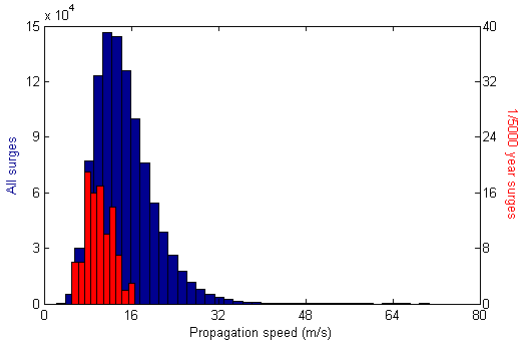

(b) Propagation speed

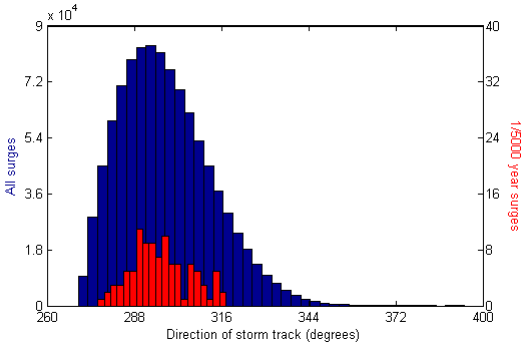

(c) Direction of storm track

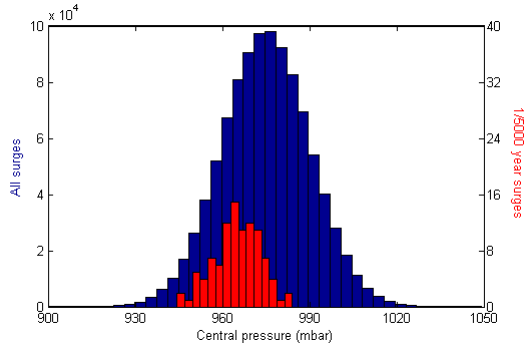

(d) Central pressure

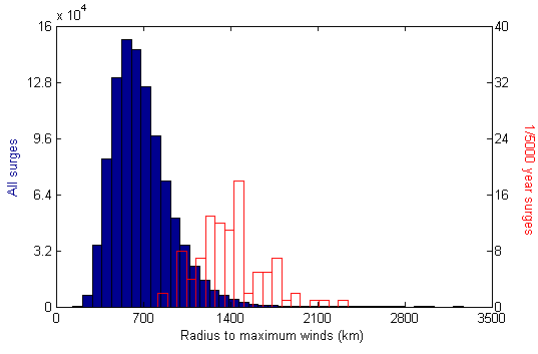

(e) Radius to maximum winds

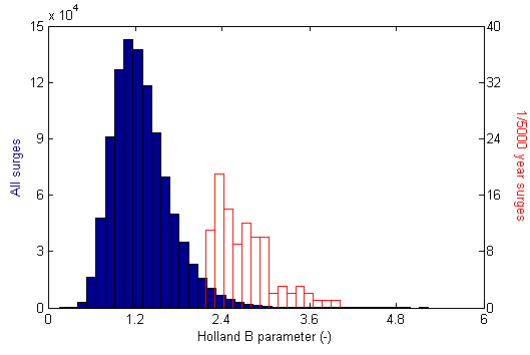

(f) Holland-B parameter

Figure G.1: Distributions of storm parameter values of all surges (in blue) and surges with a return period of ±5,000 years (in red).

Return period of 1,000 years

Following the model results, the surge height which occurs statistically once per 1,000 years is 5 m. Exact model outcome is 5.26 m, the range of 100 surges is between 5.25 m and 5.26 m. Results are shown in Figure G.2.

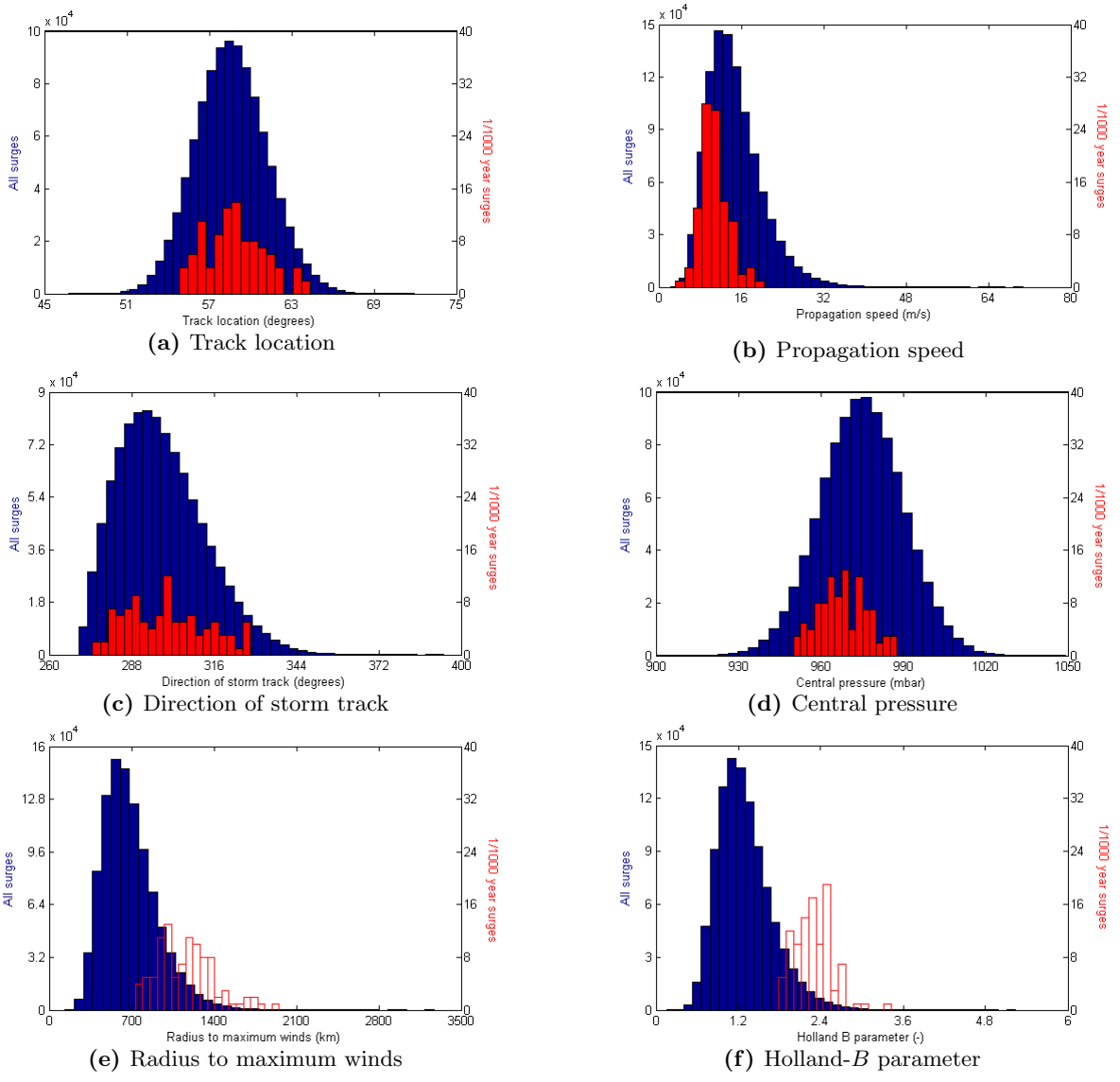

(a) Track location

(b) Propagation speed

(c) Direction of storm track

(d) Central pressure

(e) Radius to maximum winds

(f) Holland-B parameter

Figure G.2: Distributions of storm parameter values of all surges (in blue) and surges with a return period of ±1,000 years (in red).

Return period of 100 years

Following the model results, the surge height which occurs statistically once per 100 years is 4 m. Exact model outcome is 4.44 m, the 100 surges have all the same height. Results are shown in Figure G.3.

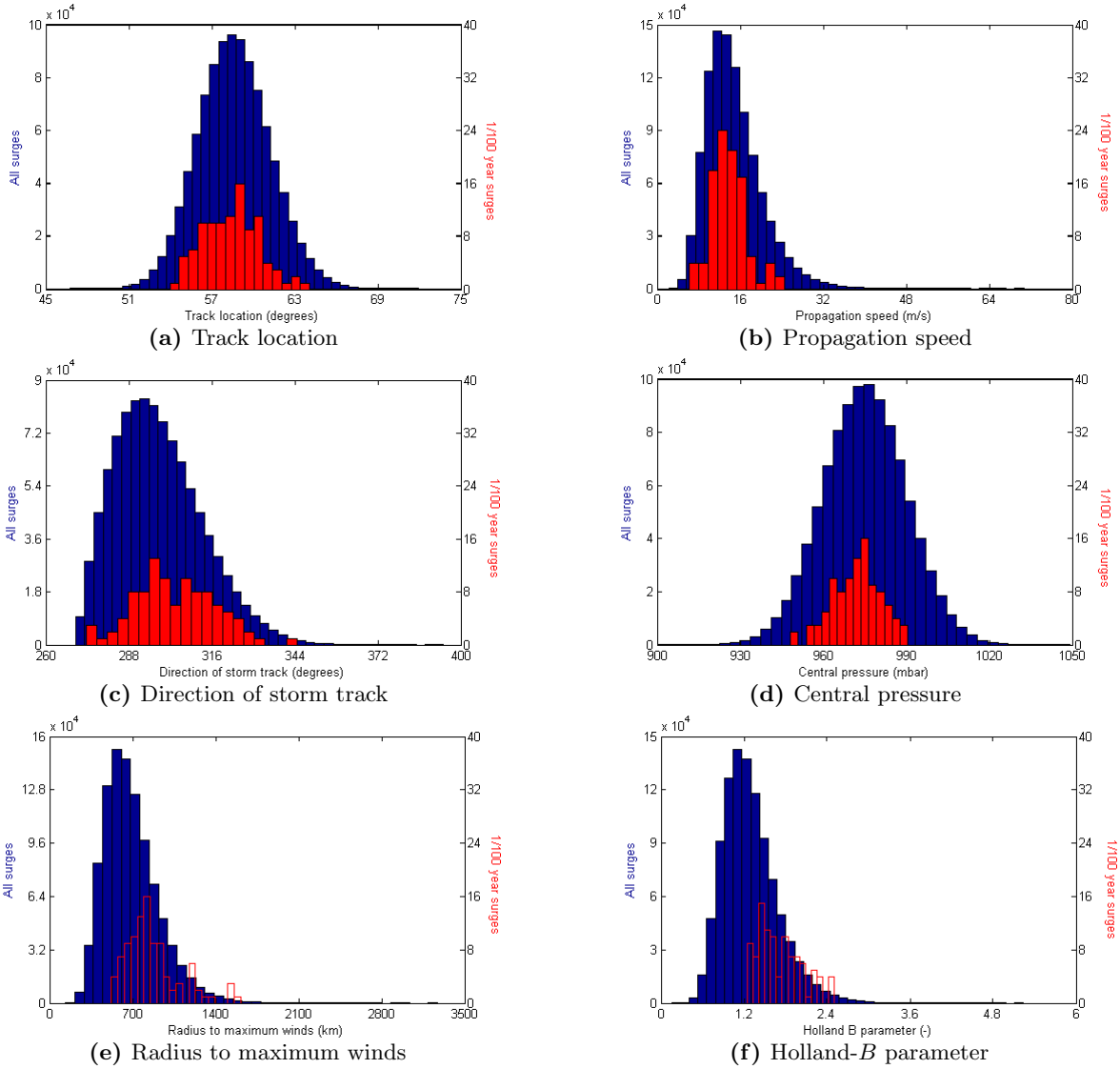

(a) Track location **(b)** Propagation speed

(c) Direction of storm track **(d)** Central pressure

(e) Radius to maximum winds **(f)** Holland-B parameter

Figure G.3: Distributions of storm parameter values of all surges (in blue) and surges with a return period of ± 100 years (in red).

Return period of 10 years

Following the model results, the surge height which occurs statistically once per 10 years is 4 m. Exact model outcome is 3.61 m, the 100 surges have all the same height. Results are shown in Figure G.4.

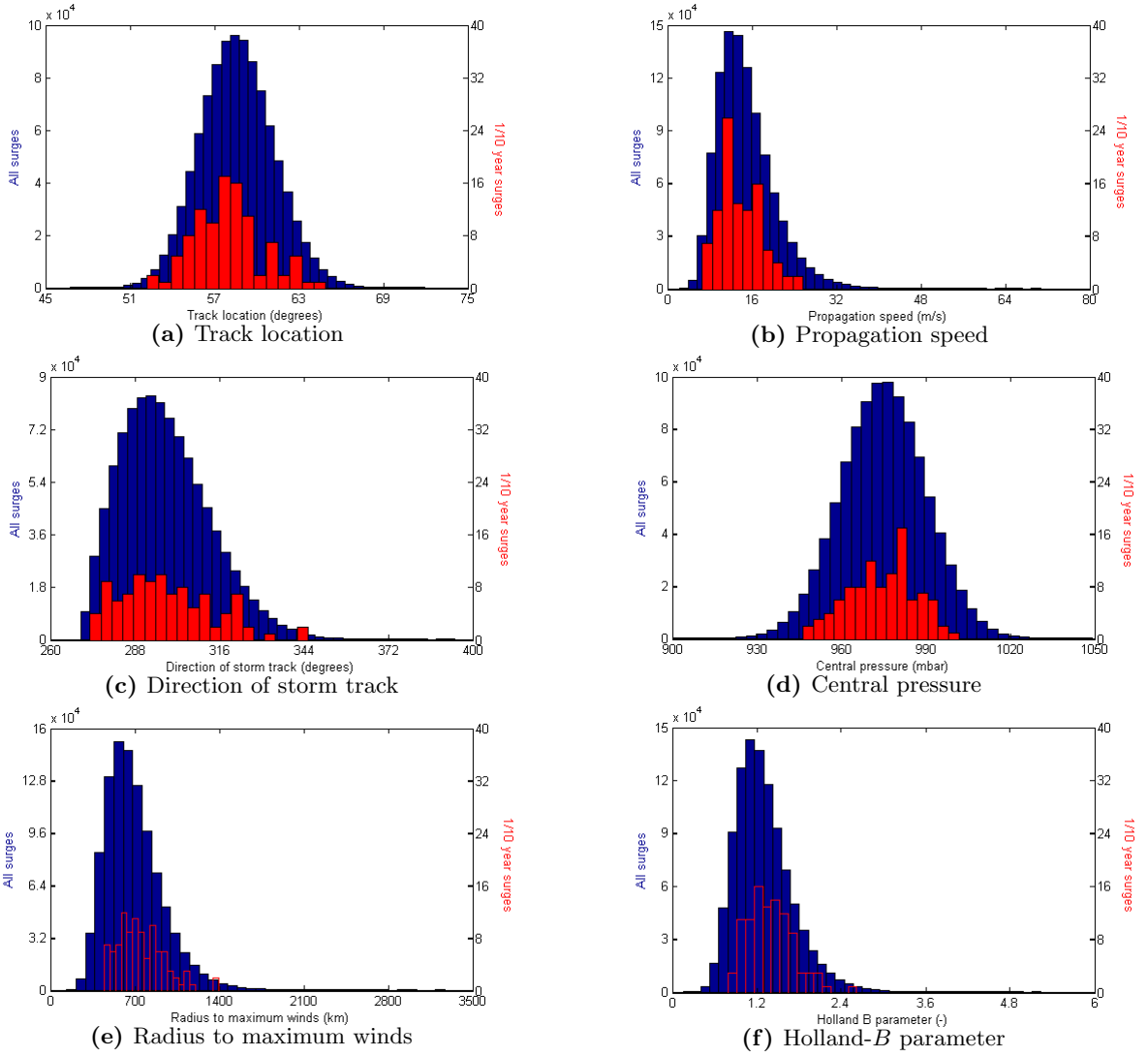

(a) Track location **(b)** Propagation speed **(c)** Direction of storm track **(d)** Central pressure **(e)** Radius to maximum winds **(f)** Holland-B parameter

Figure G.4: Distributions of storm parameter values of all surges (in blue) and surges with a return period of ±10 years (in red).

Appendix H

New storm parameter values

H.1 Method

Weather maps are obtained from an online database (Wetterzentrale, 2011). This database consists of, among other data, surface pressure from 1871 until today. One map per day is given. The maps are based on reanalysis of NCEP data (1948-current) and NOAA-CIRES data (1871-1947). In the reanalysis, observational data from the past are processed with modern analytical tools and interpolated to a grid. The coordinate system is north polar stereographic. For each storm, the weather map for which the depression is closest to the Netherlands is used to obtain the atmospheric pressure field. An example for storm 14 is given in Figure H.1. Contrary to De Jong (2012), data for all storms are obtained from one dataset (based upon only two datasets). In this way, input data are uniformly obtained.

The central pressure of the storms is obtained from the maps. Next, the storm parameters R_{max} and Holland-B are determined. Coordinates of the depression center and the isobars are determined using GIS software. Since the isobars are far from circular, the distance from the storm center to the isobars differs for each direction. The direction is chosen for which the distances are the shortest. The rationale behind this choice is that the shortest distances result in largest gradients, which result in the highest wind speeds. This working method is uniformly used for all storms. A possible overestimation of the wind speeds is thus valid for all storms. The distance from the storm center towards the isobars is determined using the Haversine formula (Robusto, 1957), which calculates the shortest distance between two points on a sphere. This way the distance from the storm center to each isobar and the associated atmospheric pressure is known. The Holland-B pressure model equation (3.1) is fitted to these data using non-linear regression techniques (iterative least squares estimation in MATLAB) in two ways: by minimizing differences in the pressure p (method 1) and the pressure gradient $\frac{\partial p}{\partial r}$ (method 2).

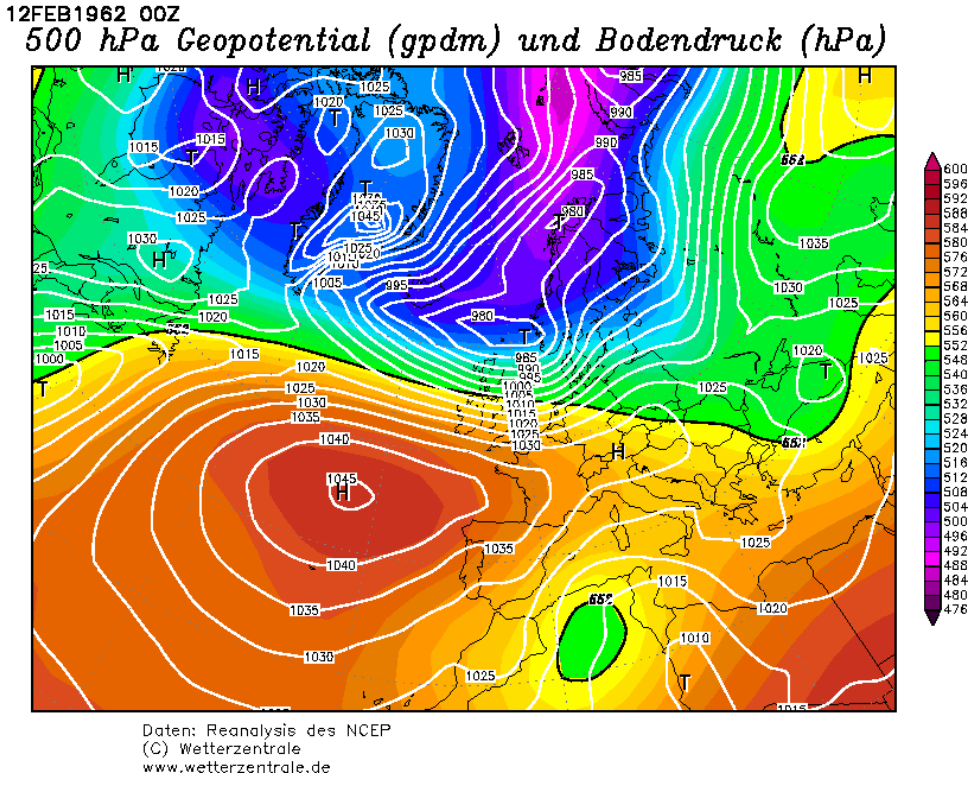

Figure H.1: Weather map of February 12, 1962 (Wetterzentrale, 2011).

H.2 Results

The results for storm 14 are shown in Figure H.2. Differences with the original data are clearly visible.

A complete overview is given in Table H.1. The storm parameters storm track location ψ, propagation speed C_{fm} and direction of storm track ϕ are not redetermined.

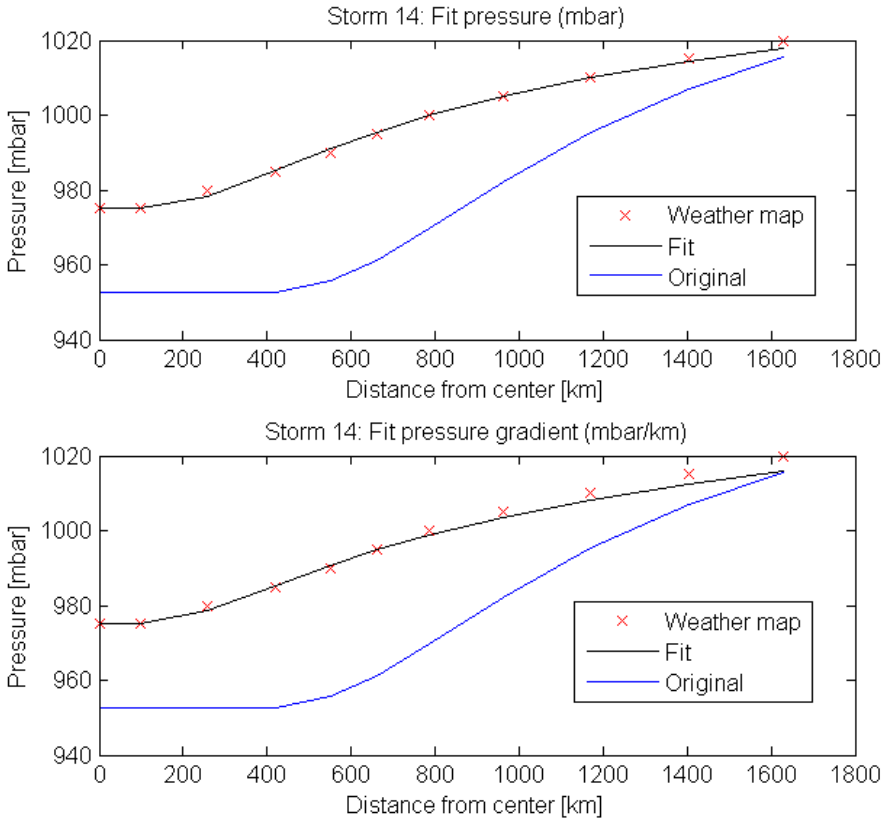

Figure H.2: Results of the reanalysis. The new fits are shown in black, the data obtained by De Jong (2012) are shown in blue. Results of method 1 are shown in the upper figure results of method 2 are shown in the lower figure.

H.3 Calibration

The model is calibrated again for both input datasets, using the method as described in section 4.3. Results are shown in Figure H.3. The model deviation is determined using equation (4.4) and is 18.4% for method 1 and 15.2% for method 2. This suggests that the second method is preferred over the first method. The model deviations are slightly less than the original model deviation of 19.2%. There is no clear under- or overestimation visible.

Storm number	Method 1 & 2	Method 1		Method 2		Original data		
	p_c (Pa)	R_{max} (km)	B (-)	R_{max} (km)	B (-)	p_c (Pa)	R_{max} (km)	B (-)
1	96000	1119	1.4	1310	1.4	96270	551	0.7
2	97500	877	0.9	921	0.9	95900	607	0.9
3	97500	870	1.5	965	1.5	97800	1158	2.3
4	98500	729	1.1	716	1.1	98270	669	1.0
5	98000	711	1.0	755	1.0	97700	578	1.4
6	96000	986	1.3	921	1.3	95600	954	1.2
7	97500	851	1.4	955	1.4	98470	883	1.3
8	98500	625	0.9	664	0.9	97800	577	1.0
9	98500	733	1.3	741	1.3	99000	664	1.1
10	97500	880	1.0	858	1.0	96930	1058	0.8
11	99000	591	1.1	599	1.1	98100	549	1.3
12	98500	678	1.5	653	1.5	96300	693	1.2
13	97000	680	1.2	828	1.2	97750	477	1.2
14	98000	686	1.2	728	1.2	95250	1055	1.9
15	96000	854	1.5	958	1.5	95250	861	2.2
16	97000	537	1.2	547	1.2	96750	341	0.9
17	98500	536	1.3	555	1.3	99000	463	1.4
18	97500	601	1.1	545	1.1	98200	523	0.9
19	98000	790	0.9	779	0.9	97000	363	0.7
20	98000	660	1.5	674	1.5	97900	569	1.3
21	96500	935	0.9	1039	0.9	96800	854	1.1

Table H.1: The redetermined storm parameter values for p_c, R_{max} and Holland-B using two methods and the original data from De Jong (2012).

H.4 Monte Carlo analysis

A Monte Carlo analysis is performed, as described in section 5.1. Probability distributions for the adjusted storm parameters are determined. The same type of distribution, given by De Jong (2012), are used. Only data of the second method are used, since it follows from calibration that these data are preferred over the data of the first method. Results are shown in Table H.2.

Storm parameter	**Probability distribution**	**Mean**	**Standard deviation**
p_c (mbar)	Normal	975	9.03
R_{max} (km)	Lognormal	775	1.26
B (-)	Lognormal	1.19	1.20

Table H.2: Adjusted input for the Monte Carlo analysis

Research shows that R_{max} depends on p_c, which is shown in Figure H.4. The following linear relation is found for R_{max} in km, with $R^2 = 0.49$:

$$R_{max} = (-0.1477 \cdot p_c + 15207) + \epsilon \tag{H.1}$$

where ϵ represents the uncertainty for values for B. The quantity ϵ has a normal distribution with $\mu = 0$ (km) and $\sigma = 191.13$ (km).

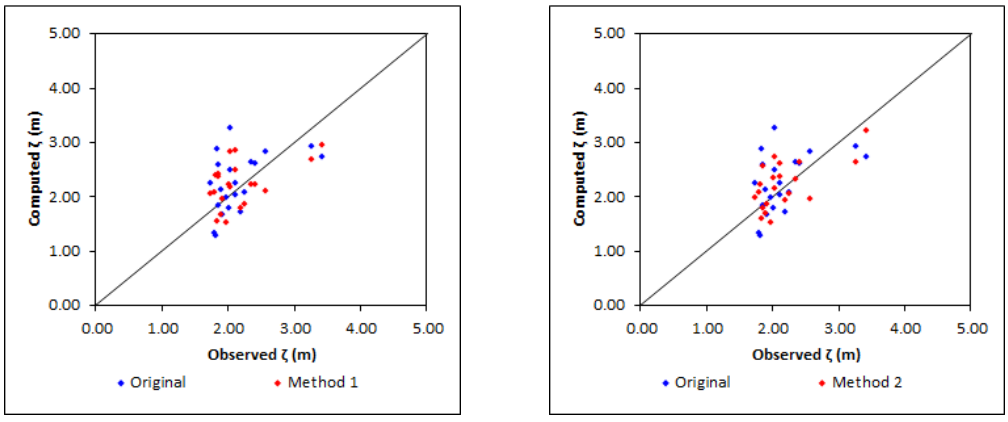

(a) Method 1 **(b)** Method 2

Figure H.3: Calibration results for the adjusted input datasets, compared to the original dataset.

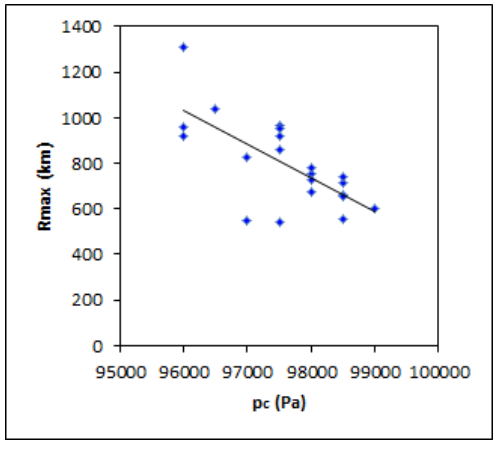

Figure H.4: Dependency between R_{max} and p_c with $R^2 = 0.49$.

For both datasets, without and with dependency between R_{max} and p_c, a Monte Carlo analysis is performed with 10,000 runs in total. Results are shown in Figure H.5. It can be seen that results for extreme return periods are lower than the original computations and that surge heights are about 6 m. Due to the relative low amount of runs, uncertainty is large for extreme return periods. Water levels for lower return periods of both methods are much closer to the observations which are used for calibration, compared to the original Gumbel plot. It turns out that results with dependency between R_{max} and p_c are slightly better.

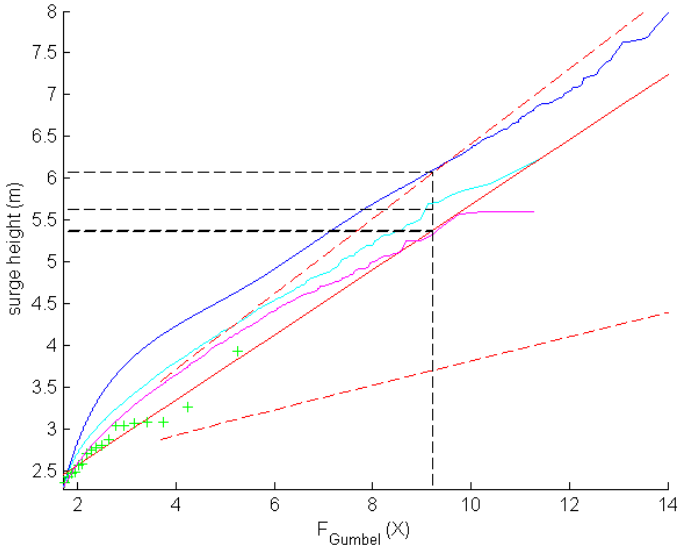

Figure H.5: Gumbel plots of Monte Carlo analysis. Results without dependency between R_{max} and p_c are shown in cyan, results with dependency are shown in magenta. The original Gumbel plot, as shown in Figure 5.1 is shown in blue.